Volume 2 Issue 2, June 2022

AGEING AND NEURODEGENERATIVE DISEASES

Wei-dong Le
Chief-in-Editor

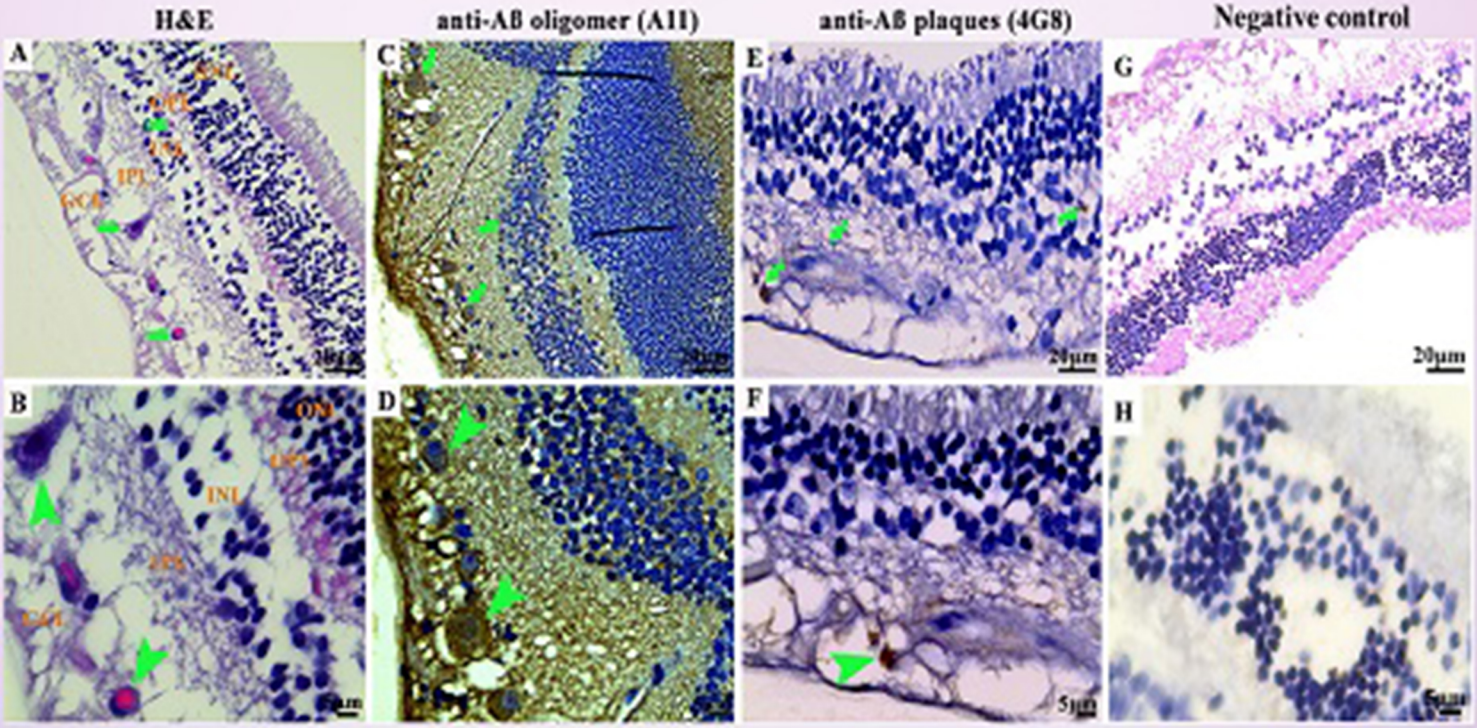

A sequential deposition of amyloid beta oligomers, plaques and phosphorylated tau occurs throughout life in the canine retina

Umma Habiba, John Morley, Mark Krockenberger, Brian A. Summers, Mourad Tayebi

Open Access
ISSN 2769-5301 (Online)
www.ageneudisjournal.com

Editor-in-Chief

Wei-Dong Le

Prof. Le is currently the deputy director of the Academic Committee and the director of the Institute of Neurology, Sichuan Academy of Medical Science-Sichuan Provincial People's Hospital. He is also a life-time Professor of Neurology and the director of Center for Translational Research on Neurological Diseases, the First Affiliated Hospital of Dalian Medical University. He has been engaged in clinical practice, teaching and research of neurology for almost 40 years, including 24 years of work in Baylor College of Medicine as a Professor of Neurology and Director of the Parkinson's Disease Research Center; and 10 years of working as a Professor of Neuroscience and Head of Neurogenomic Lab in the Institute of Health Science of Chinese Academy of Science jointed with Shanghai Jiao-Tong University School of Medicine.

Honorary Editors-in-Chief

Ted M. Dawson

David Rubinsztein

Journal Scope

High-quality original articles, reviews, case reports, commentaries are welcomed from ageing and neurodegenerative diseases, particularly on the basic mechanisms of ageing and their roles in the onset and progression of neurodegenerative diseases. The journal aims to report innovative research advances on the following topics:

1. The cellular and molecular mechanisms of ageing and the pathogenesis of neurodegenerative diseases;

2. The associations between neurodegenerative diseases and the biological bases of ageing with a focus on: genomic instability, epigenetic alterations, telomere attrition, protein degradation system failure, mitochondrial dysfunction, cellular senescence, nutrient sensing deregulation, stem cell exhaustion, intercellular communication impairment, etc.;

3. Translational research into prevention and treatment of age-related neurodegenerative diseases;

4. Mechanistic bases for epidemiological observations in aging-related neurodegenerative diseases.

Journal Homepage

EDITORIAL BOARD

GENERAL INFORMATION

About the Journal

AND is a peer-reviewed and open access multidisciplinary journal that publishes high-quality original articles, reviews, case reports, commentaries, letters to editor, etc. Ageing is a major risk factor for neurodegeneration, and the prevalence of ageing-related neurodegenerative diseases such as Alzheimer's disease, Parkinson's disease, amyotrophic lateral sclerosis, etc. continues to rise with the increased ageing population. Unfortunately, there are no effective treatments available for the age-related neurodegenerative diseases. Thus, to develop successful interventions, it is important to investigate the basic mechanisms of ageing and their roles in the onset and progression of neurodegenerative diseases. Therefore, we plan to launch this new journal, which is aimed to report innovative research advances on the following topics:

1. The cellular and molecular mechanisms of ageing and the pathogenesis of neurodegenerative diseases;
2. The associations between neurodegenerative diseases and the biological bases of ageing with a focus on: genomic instability, epigenetic alterations, telomere attrition, protein degradation system failure, mitochondrial dysfunction, cellular senescence, nutrient sensing deregulation, stem cell exhaustion, intercellular communication impairment, etc.;
3. Translational research into prevention and treatment of age-related neurodegenerative diseases;
4. Mechanistic bases for epidemiological observations in aging-related neurodegenerative diseases;
5. Psychology and Geriatric Mental Illness;
6. Neuropharmacology.

Information for Authors

Manuscripts should be prepared in accordance with Author Instructions.
Please check www.ageneudisjournal.com/pages/view/author_instructions for details.
All manuscripts should be submitted online at https://oaemesas.com/login?JournalId=and

Copyright

Permissions

Disclaimer

Publisher

OAE Publishing Inc.
245 E Main Street st112, Alhambra, CA 91801, USA
Website: www.oaepublish.com

Contacts

E-mail: editorialoffice@ageneudisjournal.com
Website: www.ageneudisjournal.com

Ageing and Neurodegenerative Diseases

CONTENTS

Volume 2, Issue 2

Zhang *et al. Ageing Neur Dis* 2022;2:5
DOI: 10.20517/and.2022.02

Ageing and Neurodegenerative Diseases

Letter to Editor

Open Access

Check for updates

Chronic intracerebroventricular administration is a reliable method in brain studies on monkeys

Lin-Heng Zhang[1,2], Hong-Yi Yang[3], Jing Wu[3], Yun Wu[3], Lu-Lu Wang[3], Hai-Yang Tong[3], Jin Zhang[3], Wen-Chao Wang[1], Rong-Yao Huang[1,4], Jiang-Lei Xu[1,4], Jing Su[1], Xun-Ran Luo[1], Yong Yin[5], Shi-Hao Wu[1], Xin-Tian Hu[1,6,7]

[1]Key Laboratory of Animal Models and Human Disease Mechanisms of the Chinese Academy of Sciences & Yunnan Province, Kunming Institute of Zoology, Chinese Academy of Sciences, Kunming 650223, Yunnan, China.
[2]School of medicine, Yunnan University, Kunming 650091, Yunnan, China
[3]High Magnetic Field Laboratory, Hefei Institutes of Physical Science, Chinese Academy of Sciences, Hefei 230031, Anhui, China.
[4]Kunming College of Life Science, University of Chinese Academy of Sciences, Kunming 650204, Yunnan, China.
[5]Department of Rehabilitation Medicine, Affiliated Hospital of Yunnan University, Kunming 650021, Yunnan, China.
[6]CAS Center for Excellence in Brain Science and Intelligence Technology, Chinese Academy of Sciences, Shanghai 200031, China.
[7]National Resource Center for Non-Human Primates, Kunming Primate Research Center, and National Research Facility for Phenotypic & Genetic Analysis of Model Animals (Primate Facility), Kunming Institute of Zoology, Chinese Academy of Sciences, Kunming 650107, Yunnan, China.

Correspondence to: Dr. Xin-Tian Hu, Key Laboratory of Animal Models and Human Disease Mechanisms of the Chinese Academy of Sciences & Yunnan Province, Kunming Institute of Zoology, Chinese Academy of Sciences, 32 East Jiaochang Road, Kunming 650223, Yunnan, China. E-mail: xthu@mail.kiz.ac.cn; Dr. Shi-Hao Wu, Key Laboratory of Animal Models and Human Disease Mechanisms of the Chinese Academy of Sciences & Yunnan Province, Kunming Institute of Zoology, Chinese Academy of Sciences, 32 East Jiaochang Road, Kunming 650223, Yunnan, China. E-mail: brad-315@163.com; Yong Yin, Department of Rehabilitation Medicine, Affiliated Hospital of Yunnan University, 176 Qingnian Road, Kunming 650021, Yunnan, China. E-mail: yyinpmr@126.com.

How to cite this article: Zhang LH, Yang HY, Wu J, Wu Y, Wang LL, Tong HY, Zhang J, Wang WC, Huang RY, Xu JL, Su J, Luo XR, Yin Y, Wu SH, Hu XT. Chronic intracerebroventricular administration is a reliable method in brain studies on monkeys. *Ageing Neur Dis* 2022;2:5. https://dx.doi.org/10.20517/and.2022.02

Received: 6 Jan 2022 **First Decision:** 9 Mar 2022 **Revised:** 28 Mar 2022 **Accepted:** 13 Apr 2022 **Published:** 18 Apr 2022

Academic Editor: Wei-Dong Le **Copy Editor:** Jia-Xin Zhang **Production Editor:** Jia-Xin Zhang

Abstract

Intracerebroventricular (ICV) administration through cannulas is a direct way to deliver large molecules and substances that are blocked by the blood-brain barrier into the central nervous system (CNS). It is widely used in brain studies on monkeys. However, this method is invasive, as it requires guide cannulas to be implanted into the brain. Whether the long-term implantation of the cannula and the administration of molecule-delivering vehicles,

usually saline, can affect the brain by inducing chronic CNS inflammation or even worse brain atrophy, remains an issue to be solved. To answer this question, we investigated inflammatory markers and brain structures on three vehicle-control monkeys who received cannula implantation and one-year ICV saline administration in another study. During the experiment, the monkeys' cerebrospinal fluid (CSF) samples were collected periodically, and the level of three classic inflammatory markers (IL-1β, IL-6, and TNF-α) were measured by electrochemiluminescence immunoassay. The monkeys' brain structures were imaged in vivo periodically by 9.4 Tesla magnetic resonance imaging, which can provide the best-resolution magnetic resonance images of living monkeys, and the volume of the hippocampus was measured to evaluate the brain atrophy. The data reveal that, during the administrating period, the long-term levels of the inflammatory markers in the CSF and the volumes of the hippocampus did not change significantly compared with the baseline. These results suggest that the long-term ICV administration of saline through cannulas did not induce chronic neuroinflammation or brain atrophy in these rhesus monkeys, suggesting chronic ICV administration via implanted cannulas is a reliable method in monkey brain research.

Keywords: Chronic ICV administration, neuroinflammation, brain atrophy

The central nervous system is protected by the blood-brain barrier (BBB), which is a semipermeable structure composed of tight endothelial junctions to provide a physical barrier for the entry of large molecules[1]. It restricts circulating toxic particles but facilitates nutrients to be delivered into the brain. Meanwhile, some therapeutic substances and test articles are also blocked by the BBB[2]. Intracerebroventricular (ICV) injection physically breaches the BBB and enables the direct administration of large molecules, including chemicals, virus vectors, and therapeutic substances, into the central nervous system (CNS) through pre-implanted guide cannulas. Studies on the distribution of injected large molecules revealed that large molecules including adenovirus vectors and proteins can spread into the subarachnoid space, meninges, and choroid plexus along with the flow of the CSF and diffuse into the brain parenchyma adjacent to these sites[3-5]. Although this method is an effective way to deliver molecules into the CNS, it is invasive and could affect the brain in many ways.

One major concern in chronic cannula-guided ICV administration comes from the implantation of the guide cannulas. To ease the repeated ICV injection, one or two guide cannulas must be implanted into the lateral ventricles. Drugs or test articles are injected into the lateral ventricles via the guide cannulas without repeated penetration of the brain parenchyma. The implantation of guide cannulas causes acute brain injury. It is well established that an acute brain injury induces acute inflammation in the brain, which is one important step in the repair of the injury. However, it is not clear if long-term implantation of cannulas can induce chronic neuroinflammation.

Chronic neuroinflammation is a persistently activated immune response in the CNS, which is always marked by sustained release of pro-inflammatory cytokines, including interleukins, tumor necrosis factor-α (TNF-α), transforming growth factor-β (TGF-β), and interferon-γ (IFN-γ)[6, 7]. Pro-inflammatory cytokines exert various functions in neuroinflammation, including induction of chemokines and adhesion molecules and recruitment of the peripheral immune cells into the CNS, leading to neuronal apoptosis and activation of the glial cells[6]. Increasing evidence suggests that cytokine-mediated neuroinflammation plays an important role in initiating or deteriorating neurodegenerative diseases[8-10]. Clinical evidence reveals that the pro-inflammatory cytokines are elevated in the body fluid of individuals with neurodegenerative diseases, including Alzheimer's disease, Parkinson's disease, and amyotrophic lateral sclerosis[11-13]. Therefore, if cannula-based ICV administration can induce chronic neuroinflammation, the results of studies on brain diseases and mechanisms would be seriously confounded, and the application of this method would be seriously limited.

Non-human primates are phylogenetically closer to humans than rodents. They share with humans many brain regions, circuits, and neural cells, which are critical for higher cognitive capacity. Thus, monkeys are widely used in the study of brain diseases and mechanisms, including in CNS disease modeling with ICV administration[14-16]. Unfortunately, no study on whether cannula-based ICV administration can induce chronic neuroinflammation in monkeys has been reported thus far.

To investigate if long-term cannula implantation and ICV saline administration can induce chronic neuroinflammation in monkeys, the levels of three most studied pro-inflammatory cytokines (IL-1β, IL-6, and TNF-α) in the CSF of three vehicle-control monkeys used as vehicle-control in another study were continuously monitored during one-year cannula-guide ICV saline administration [see Supplementary Materials for more method details]. The measurement of IL-1β, IL-6, and TNF-α in the CSF was carried out by an electrochemiluminescence immunoassay system, which has an extremely low detection limit in the measurement of biomarkers in body fluid.

The levels of CSF IL-1β, IL-6, and TNF-α were measured at 12 weeks before the administration (the baseline) and the 4, 9, 14, 19, 24, 29, 34, and 39 weeks after the administration [Figure 1A]. Kruskal-Wallis H test revealed the effect of ICV saline administration on the average levels of IL-1β and IL-6 was not significant ($P = 0.597$ for IL-1β, $P = 0.112$ for IL-6, Figure 1B and C). The levels of CSF TNF-α were around the low detection limit, and no meaningful statistics could be applied. The data for TNF-α are not shown. In summary, the results reveal that there was no elevated CSF IL-1β, IL-6, or TNF-α during the administration, which suggests there was no significant neuroinflammation during the ICV saline administration.

In addition, we also investigated whether there was any brain atrophy caused by long-term cannula implantation and ICV administration, considering reports on brain atrophy induced by traumatic brain injury and neuroinflammation[17-19]. The structures of the monkeys' brains were imaged periodically by magnetic resonance imaging (MRI) (see Supplementary Materials for more method details). To increase the accuracy in the measurement of hippocampus volumes, the monkeys' brains were scanned by a 9.4 Tesla MRI system, which provides the highest resolution structural images currently available on living monkeys.

The measurement was carried out one week before the administration (the baseline) and 4, 9, 14, 19, 25, 31, 37, 43, and 49 weeks after administration [Figure 2A]. First, longitudinal MR images from the same subject were realigned to examine general structural changes in the brain. No significant brain atrophy was observed on MR images from each time point compared with the baseline [Figure 2B]. Then, the volume of the hippocampus was calculated to evaluate the atrophy in the brain because it is one of the most vulnerable structures in the brain and has a clear contour on MR images. Kruskal-Wallis H test revealed that the effect of ICV saline administration on the average volumes of total hippocampus was not significant ($P = 0.775$, Figure 2C). We further compared the average volumes of the left and right hippocampus independently. Kruskal-Wallis H test also revealed that the difference between each time point in the volumes of the left and right hippocampus were both not significant ($P = 0.770$ for the left hippocampus, $P = 0.606$ for the right hippocampus, Figure 2D and E). In summary, the results from the ultra-high-resolution MRI scan revealed that there was no reduction in the volume of the hippocampus, which suggests there was no significant atrophy in the brain.

Here, we demonstrate that, compared with the baseline, there was no elevated IL-1β or IL-6 in the CSF of the three cannula implanted monkeys during 1-year ICV saline administration, suggesting that the cannula-guided long-term ICV administration technique did not induce chronic neuroinflammation in the monkeys. The other finding that there was no significant decrease in hippocampus volumes supports this

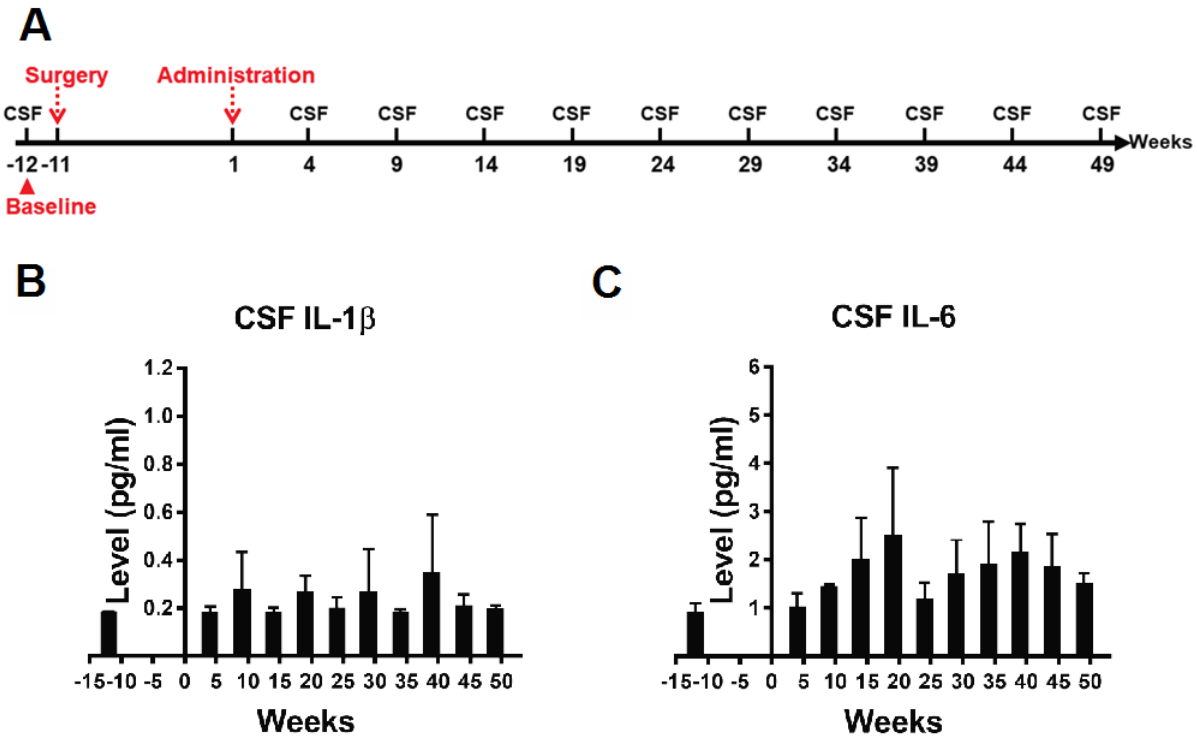

Figure 1. (A) The schedule of CSF sample collection. Cannula implantation was carried out in Week 11. ICV administration began in Week 1. CSF samples were collected in Weeks 12, 4, 9, 14, 19, 24, 29, 34, 39, 44, and 49. CSF sample collected at Week -12 was taken as the baseline. (B,C) Kruskal-Wallis H test revealed no significant difference between different time points in the average levels of CSF IL-1 β (P = 0.597) and IL-6 (P = 0.112). Data are presented as mean ± standard deviation (SD). CSF: Cerebrospinal fluid; ICV: intracerebroventricular.

conclusion.

To increase the accuracy of the measurement of inflammatory cytokines in the body fluid, an advanced detection method was employed in this study. Inflammatory cytokines in the body fluid exert their physiological functions at low levels, and many of them are usually below the low detection threshold under physiological conditions using common enzyme-linked immunosorbent assay kits[20]. Advanced techniques are developed to detect the cytokines in the body fluids, with much higher detection sensitivity and smaller specimen volumes. Among the newly developed assay techniques, the MSD multiplex immunoassay platform represents a combination of electrochemiluminescence and patterned arrays with an ultra-low detection limit, which is also one of the most used methods in the measurement of cytokines in body fluids nowadays. The detection sensitivity can reach 0.1 pg/mL for some cytokines using this method. The reliability of this method was validated in three recent studies, which proved that this method had a high detection rate for most of the cytokines and displayed a moderate-to-excellent intra-individual variability[21-23]. In our experiment, the detection rate was 100% for IL-1β and IL-6, but only 60% for the TNF-α, which indicates that the level of TNF-α in the CSF of monkeys under physiological conditions was extremely low.

The hippocampus is one of the most vulnerable structures in the brain under many conditions such as injury, aging, and neurodegenerative diseases[24], and it is lying in the inferior horn of the lateral ventricle, directly affected by ICV administration. Due to the vulnerability and clear contour in MR images, the hippocampus volume was taken as an indicator of brain atrophy in this study. To investigate if ICV saline

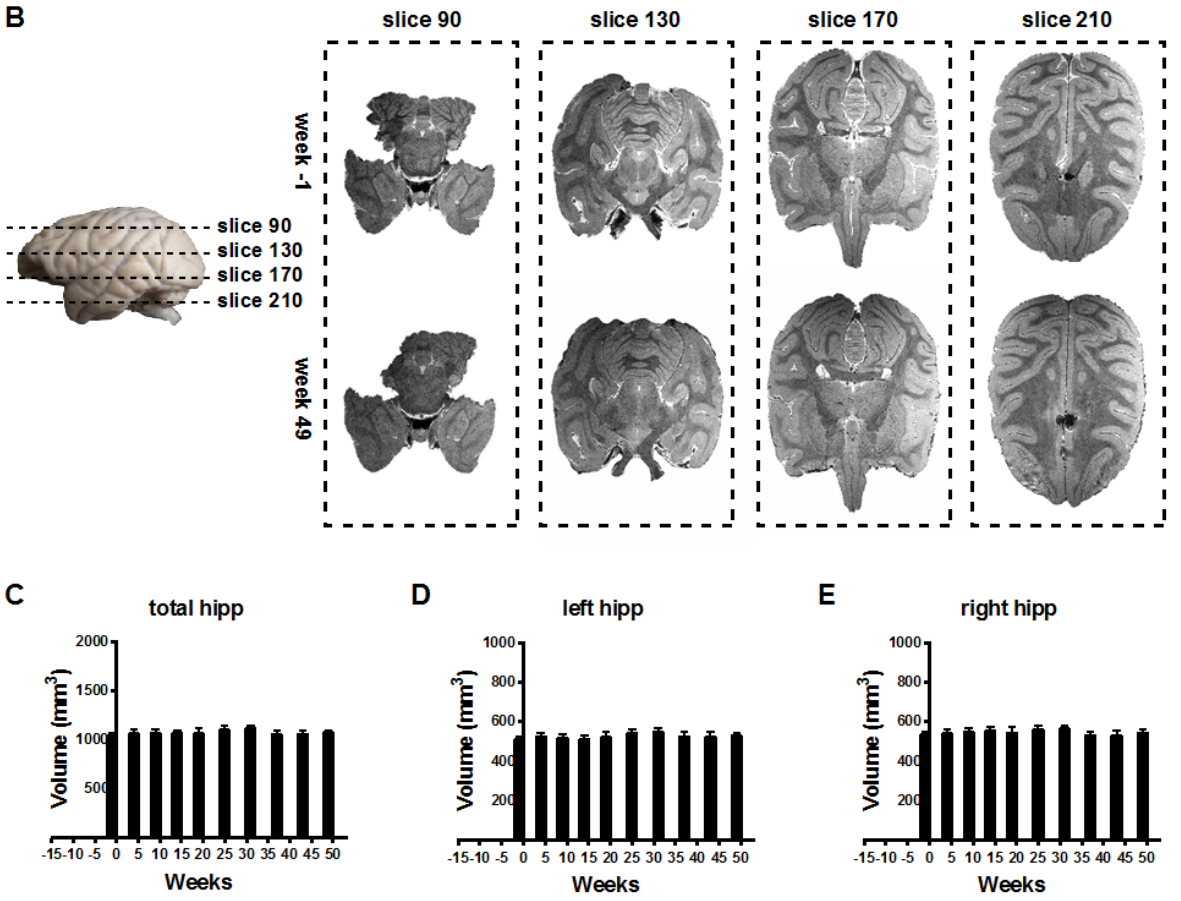

Figure 2. (A) Schedule of MRI scans. Cannula implantation was carried out in Week -11. ICV administration began in Week 1. MR images were acquired in Weeks 1, 4, 9, 14, 19, 25, 31, 37, 43, and 49. MR images acquired in Week -1 were taken as the baseline. (B) Representative MR images show there was no significant brain atrophy in Week 49 when compared with the baseline (Week 11). (C-E) Kruskal-Wallis H test revealed no significant difference between different time points in the average total hippocampus volumes (P = 0.775), the average left hippocampus volumes (P = 0.770), and the average right hippocampus volumes (P = 0.606). Data are presented as mean ± standard deviation (SD). MRI: Magnetic resonance imaging; ICV: intracerebroventricular.

administration can induce atrophy, ultra-high magnetic field MRI was employed to image the brain. The fact that we did not find any decrease in the hippocampus volumes strongly suggests no brain atrophy in the monkeys' brains, which also supported the conclusion that there was no significant inflammation in the brain.

Taken together, our results reveal that long-term cannula implantation and ICV administration of drug-vehicle do not induce chronic neuroinflammation and brain atrophy in rhesus monkeys, which suggests that chronic ICV administration is a reliable method for brain studies on monkeys.

DECLARATIONS

Acknowledgments

We thank Professor Zhong Kai's (High Magnetic Field Laboratory, Chinese Academy of Science) great help in MRI scanning and MRI data analysis. Thank Jing Wu for providing technical help in the cannula implantation surgery. Thank Hong-yi Yang, Yun Wu, and Lu-lu Wang for providing great endeavor in the MRI scanning, including the development of the head coil, and optimizing the sequence of the MRI

scanning.

Author's contributions

Designed the experiment: Hu XT, Yin Y, Wu SH, and Zhang LH
Carried out the cannula implantation surgery: Wu J, Wang WC, Huang RY, Xu JL, and Zhang LH
Carried out the MRI scanning: Yang HY, Wu Y, Wang LL, and Zhang LH
Carried out the CSF sample collection: Tong HY, Zhang J, Zhang LH, Su J, and Luo XR
Carried out the data analysis: Zhang LH
Wrote the manuscript: Zhang LH
Revised the manuscript: Hu XT and Yin Y
All authors read and approved the final version of the manuscript.

Availability of Data and Materials

Not applicable.

Financial Supports and Sponsorship

This work was supported by the National Program for National Key R&D Program of China (2018YFA0801403), Key Realm R&D Program of Guangdong Province (2019B030335001), the Strategic Priority Research Program of the Chinese Academy of Sciences (XDB32060200), the National Natural Science Foundation of China (81941014, 81771387, 31700897), the Applied Basic Research Programs of Science and Technology Commission Foundation of Yunnan Province (2019FA007), China Postdoctoral Science Foundation (2018M631105) and CAS "Light of West China" Program.

Conflicts of Interest

All authors declared that there are no conflicts of interests.

Ethical Approval and Consent to Participate

All experimental procedures were carried out following "Guide for the Care and Use of Laboratory Animals"[20] and approved by the Animal Care and Use Committee (IACUC) of the Kunming Institute of Zoology, Chinese Academy of Sciences (IACUC No.: IACUC19001).

Consent for Publication

Not applicable.

REFERENCES

1. Rustenhoven J, Kipnis J. Bypassing the blood-brain barrier. *Science* 2019;366:1448-9. DOI PubMed
2. Bauer HC, Krizbai IA, Bauer H, Traweger A. "You Shall Not Pass"-tight junctions of the blood brain barrier. *Front Neurosci* 2014;8:392. DOI PubMed PMC
3. Vuillemenot BR, Kennedy D, Reed RP, et al. Recombinant human tripeptidyl peptidase-1 infusion to the monkey CNS: safety, pharmacokinetics, and distribution. *Toxicol Appl Pharmacol* 2014;277:49-57. DOI PubMed
4. Kawasaki H, Kosugi I, Sakao-Suzuki M, Meguro S, Tsutsui Y, Iwashita T. Intracerebroventricular and intravascular injection of viral particles and fluorescent microbeads into the neonatal brain. *J Vis Exp* 2016. DOI PubMed PMC
5. Driesse MJ, Kros JM, Avezaat CJ, et al. Distribution of recombinant adenovirus in the cerebrospinal fluid of nonhuman primates. *Hum Gene Ther* 1999;10:2347-54. DOI PubMed
6. Lucas SM, Rothwell NJ, Gibson RM. The role of inflammation in CNS injury and disease. *Br J Pharmacol* 2006;147 Suppl 1:S232-40. DOI PubMed PMC
7. Heppner FL, Ransohoff RM, Becher B. Immune attack: the role of inflammation in Alzheimer disease. *Nat Rev Neurosci* 2015;16:358-72. DOI PubMed

8. Sankowski R, Mader S, Valdés-Ferrer SI. Systemic inflammation and the brain: novel roles of genetic, molecular, and environmental cues as drivers of neurodegeneration. *Front Cell Neurosci* 2015;9:28. DOI PubMed PMC
9. Ransohoff RM. How neuroinflammation contributes to neurodegeneration. *Science* 2016;353:777-83. DOI PubMed
10. Galimberti D, Fenoglio C, Scarpini E. Inflammation in neurodegenerative disorders: friend or foe? *Curr Aging Sci* 2008;1:30-41. DOI PubMed
11. Mitchell RM, Freeman WM, Randazzo WT, et al. A CSF biomarker panel for identification of patients with amyotrophic lateral sclerosis. *Neurology* 2009;72:14-9. DOI PubMed
12. Lindqvist D, Hall S, Surova Y, et al. Cerebrospinal fluid inflammatory markers in Parkinson's disease - associations with depression, fatigue, and cognitive impairment. *Brain Behav Immun* 2013;33:183-9. DOI PubMed
13. Darweesh SKL, Wolters FJ, Ikram MA, de Wolf F, Bos D, Hofman A. Inflammatory markers and the risk of dementia and Alzheimer's disease: a meta-analysis. *Alzheimers Dement* 2018;14:1450-9. DOI PubMed
14. Zhai R, Rizak J, Zheng N, et al. Alzheimer's Disease-like pathologies and cognitive impairments induced by formaldehyde in non-human primates. *Curr Alzheimer Res* 2018;15:1304-21. DOI PubMed
15. Li H, Lei X, Huang B, et al. A quantitative approach to developing Parkinsonian monkeys (Macaca fascicularis) with intracerebroventricular 1-methyl-4-phenylpyridinium injections. *J Neurosci Methods* 2015;251:99-107. DOI PubMed
16. Erratum: Forny-Germano et al. , "Alzheimer's Disease-like pathology induced by amyloid-β oligomers in nonhuman primates". *J Neurosci* 2020;40:8204. DOI PubMed PMC
17. Tate DF, Bigler ED. Fornix and hippocampal atrophy in traumatic brain injury. *Learn Mem* 2000;7:442-6. DOI PubMed
18. Tomaiuolo F, Carlesimo GA, Di Paola M, et al. Gross morphology and morphometric sequelae in the hippocampus, fornix, and corpus callosum of patients with severe non-missile traumatic brain injury without macroscopically detectable lesions: a T1 weighted MRI study. *J Neurol Neurosurg Psychiatry* 2004;75:1314-22. DOI PubMed PMC
19. Tsai SY, Gildengers AG, Hsu JL, Chung KH, Chen PH, Huang YJ. Inflammation associated with volume reduction in the gray matter and hippocampus of older patients with bipolar disorder. *J Affect Disord* 2019;244:60-6. DOI PubMed
20. Aziz N. Measurement of circulating cytokines and immune-activation markers by multiplex technology in the clinical setting: what are we really measuring? *For Immunopathol Dis Therap* 2015;6:19-22. DOI PubMed PMC
21. Koelman L, Pivovarova-Ramich O, Pfeiffer AFH, Grune T, Aleksandrova K. Cytokines for evaluation of chronic inflammatory status in ageing research: reliability and phenotypic characterisation. *Immun Ageing* 2019;16:11. DOI PubMed PMC
22. Belzeaux R, Lefebvre MN, Lazzari A, et al. How to: measuring blood cytokines in biological psychiatry using commercially available multiplex immunoassays. *Psychoneuroendocrinology* 2017;75:72-82. DOI PubMed
23. McKay HS, Margolick JB, Martínez-Maza O, et al. Multiplex assay reliability and long-term intra-individual variation of serologic inflammatory biomarkers. *Cytokine* 2017;90:185-92. DOI PubMed PMC
24. McEwen BS. Possible mechanisms for atrophy of the human hippocampus. *Mol Psychiatry* 1997;2:255-62. DOI PubMed

Yu *et al. Ageing Neur Dis* 2022;2:6
DOI: 10.20517/and.2022.07

Ageing and Neurodegenerative Diseases

Original Article

Open Access

Selective expression of neurodegenerative diseases-related mutant p150^{Glued} in midbrain dopaminergic neurons causes progressive degeneration of nigrostriatal pathway

Jia Yu[1,2], Carmelo Sgobio[2,3], Xuan Yang[1], Yu Peng[1], Xi Chen[2], Lixin Sun[2], Hoon Shim[2], Huaibin Cai[2]

[1]Basic Research Center, Institute for Geriatrics and Rehabilitation, Beijing Geriatric Hospital, Beijing 100095, China.
[2]Transgenic Section, Laboratory of Neurogenetics, National Institute on Aging, National Institutes of Health, Bethesda, MD 20892, USA.
[3]Center for Neuropathology and Prion Research, Ludwig-Maximilians University Munich, Munich 81377, Germany.

Correspondence to: Dr. Huaibin Cai, Transgenic Section, Laboratory of Neurogenetics, National Institute on Aging, National Institutes of Health, Building 35, Room 1A112, MSC 3707, 35 Convent Drive, Bethesda, MD 20892, USA. E-mail: caih@mail.nih.gov; Dr. Jia Yu, Basic Research Center, Institute for Geriatrics and Rehabilitation, Beijing Geriatric Hospital, 118 Wenquan Road, Haidian District, Beijing 100095, China. E-mail: jyu319@163.com

How to cite this article: Yu J, Sgobio C, Yang X, Peng Y, Chen X, Sun L, Shim H, Cai H. Selective expression of neurodegenerative diseases-related mutant p150^{Glued} in midbrain dopaminergic neurons causes progressive degeneration of nigrostriatal pathway. *Ageing Neur Dis* 2022;2:6. https://dx.doi.org/10.20517/and.2022.07

Received: 4 Mar 2022 **First Decision:** 2 Apr 2022 **Revised:** 2 Apr 2022 **Accepted:** 25 Apr 2022 **Published:** 28 Apr 2022

Academic Editor: Wei-dong Le **Copy Editor:** Tiantian Shi **Production Editor:** Tiantian Shi

Abstract

Aim: Missense mutations of dynactin subunit p150^{Glued} have been associated with multiple neurodegenerative diseases, including Perry syndrome, characterized by inherited parkinsonism, depression, weight loss, and hypoventilation. The current study investigated how the pathogenic mutant p150^{Glued} affects the integrity and function of the nigrostriatal dopaminergic (DA) pathway *in vivo*.

Methods: Using a tetracycline-controlled transcriptional regulation system, transgenic mouse models were generated with selective overexpression of wild-type, motor neuron disease-related G59S mutant, or Perry syndrome-related G71R mutant human p150^{Glued} in midbrain DA neurons. A series of behavioral, neuropathological, neurochemical, electrochemical, and biochemical studies were performed on the mice to examine and compare the pathogenic impact of the two mutant p150^{Glued} on the survival and function of midbrain DA neurons.

Results: Compared with non-transgenic control mice, transgenic mice overexpressing wild-type human p150^{Glued} showed neither motor phenotypes nor pathological, functional, or biochemical abnormalities of the nigrostriatal DA pathway. Transgenic mice overexpressing G59S mutant p150^{Glued} displayed weight loss, motor deficits, early-onset defects in dopamine transmission, and early-onset loss of DA neurons and axons. Transgenic mice overexpressing G71R p150^{Glued} mutant exhibited hyperactivities, impaired motor coordination, early-onset dysfunction of dopamine uptake, and late-onset loss of DA neurons and axons. In addition, overexpression of either G59S or G71R mutant p150^{Glued} in midbrain DA neurons preferentially downregulated the expression of dopamine transporter at dopaminergic axon terminals. Furthermore, G59S mutant p150^{Glued} rather than G71R mutant p150^{Glued} formed aggregates in midbrain DA neurons *in vivo*, and the aggregates trapped dynein/dynactin, co-localized with lysosomes, and upregulated ubiquitination.

Conclusion: These findings demonstrate that selective expression of either G59S or G71R mutant p150^{Glued} in mouse midbrain DA neurons leads to progressive degeneration of the nigrostriatal DA pathway and indicate that G59S and G71R mutant p150^{Glued} exhibit differential pathogenic impact on the survival and function of midbrain DA neurons *in vivo*.

Keywords: Perry syndrome, motor neuron disease, *DCTN1* gene, dynactin subunit p150^{Glued}, missense mutation, nigrostriatal pathway, midbrain dopaminergic neuron, neurodegeneration

INTRODUCTION

Cytoplasmic dynein and its cofactor dynactin mediate microtubule minus-end-directed trafficking, performing critical roles in mitosis, intracellular positioning and movement of organelles, retrograde axonal transport, and synapse formation and stability[1-3]. Dynactin is a macromolecular protein complex consisting of more than ten types of subunits, with the largest subunit p150^{Glued} binding directly with dynein and microtubule[4]. Missense mutations of *DCTN1*, the gene encoding p150^{Glued}, have been linked to different neurodegenerative diseases, in which the G59S missense mutation was linked to autosomal dominant motor neuron disease, and 13 more mutations (F52L, K56R, G67D, K68E, G71A/R/E/V, T72P, Q74P, Y78C/H, and Q93H) were associated with Perry syndrome[5-8]. Perry syndrome is an autosomal dominant neurodegenerative disorder characterized by a series of symptoms (parkinsonism, depression, central hypoventilation, and weight loss) and pathology of severe neuronal loss in the *substantia nigra* and *locus coeruleus*[9,10]. However, the underlying pathogenic mechanism and potential therapeutic target of neurodegeneration in Perry syndrome remain elusive.

P150^{Glued} contains two microtubule-binding domains (MTBDs) at its N-terminus: the cytoskeleton-associated protein and glycine-rich (CAP-Gly) domain, which interacts with both tubulin and microtubule end binding proteins, and the adjacent serine-rich basic domain, which has an affinity for tubulin[11,12]. The MTBDs of p150^{Glued} are required to initiate retrograde transport and maintain microtubule stability in axons[13-15]. Deleting the MTBDs in p150^{Glued} upregulates microtubule acetylation, increases the surface level of ionotropic glutamate receptors, disrupts neuromuscular junctions, and leads to selective degeneration of spinal motor neurons[16]. Motor neuron disease-related G59S mutation of p150^{Glued} and all the Perry syndrome-related mutations are point mutations clustered within or close to the CAP-Gly domain, resulting in loss-of-function of the MTBD[6-8]. Furthermore, G59S mutant p150^{Glued}, as well as G71A, G71E, G71R, T72P, Q74P, and F52L mutant p150^{Glued}, form cytoplasmic aggregates *in vitro* in a time- and concentration-dependent manner[17-19], suggesting both loss-of-function and toxic-gain-of-function mechanisms might be involved in *DCTN1* mutation-induced neurodegeneration. Additionally, G59S mutant p150^{Glued} is less stable[20], and both G59S and Perry syndrome-related mutant p150^{Glued} compromise normal functions of dynactin p150^{Glued} in a dominant-negative fashion when overexpressed[13,14,21], suggesting

a dominant-negative mechanism for *DCTN1* mutation-induced neurodegeneration. Movement disorder and the underlying neuropathology, including loss of spinal motor neurons and degeneration of axon and neuromuscular junctions, have been reported in G59S mutant p150^{Glued} knock-in and transgenic mice[20-22]. Behavioral defects have also been found in G71A mutant p150^{Glued} knock-in and transgenic mice[23,24]. However, how the pathogenic mutant p150^{Glued} affects the integrity and function of the nigrostriatal DA pathway has not been critically examined in animal models.

Here, we investigated and compared the pathogenic impact of two different neurodegenerative diseases-related mutant p150^{Glued} in the survival and function of midbrain DA neurons *in vivo*. Transgenic mouse models with selective overexpression of wild-type, G59S mutant, or G71R mutant human p150^{Glued} in midbrain DA neurons were generated using a tetracycline-controlled transcriptional regulation system. A series of experiments were performed to identify any behavioral, neuropathological, neurochemical, electrochemical, and biochemical abnormalities in the transgenic mice. Our findings highlight the importance of p150^{Glued} and its MTBDs in maintaining the survival and function of midbrain DA neurons and reveal the pathogenic similarity and difference between G59S and G71R mutant 150^{Glued}.

METHODS

Animals

The *tetO*-human *DCTN1* WT transgenic mice (for simplicity, referred to as tetO-WT) carrying the wild-type (WT) human p150^{Glued} gene (*DCTN1*) under the control of tetracycline operator (*tetO*) were generated as described previously[25,26]. The tetO-WT mice were mated with *Pitx3-IRE2-tTA* mice (referred to as tTA, a "Tet-Off" tool, JAX stock #021962), which predominantly express tetracycline-controlled transactivator protein (tTA) in midbrain DA neurons[27]. This breeding strategy produced *Pitx3-IRE2-tTA/tetO*-human *DCTN1* WT transgenic mice (referred to as WT Tg), which had the selective expression of wild-type human p150^{Glued} in midbrain DA neurons, and littermate controls [non-transgenic (nTg), tetO-WT, and *tTA* mice].

Following the same protocol, *Pitx3-IRE2-tTA/tetO*-human *DCTN1* G59S transgenic mice (referred to as G59S Tg), which had the selective expression of G59S mutant human p150^{Glued} in midbrain DA neurons, and littermate controls (nTg, tetO-G59S, and *tTA* mice) were obtained.

Following the same protocol, *Pitx3-IRE2-tTA/tetO*-human *DCTN1* G71R transgenic mice (referred to as G71R Tg), which had the selective expression of G71R mutant human p150^{Glued} in midbrain DA neurons, and littermate controls (nTg, tetO-G71R, and tTA mice) were obtained.

The mice were housed in a 12 h light/dark cycle and fed a regular diet *ad libitum*. All mouse work followed the guidelines approved by the Institutional Animal Care and Use Committees of National Institute on Aging, NIH.

Genotyping

Genomic DNA was extracted from tail biopsy using DirectPCR Lysis Reagent (Viagen Biotech) and used for PCR amplification. Genotyping was performed with specific sets of PCR primers for *Pitx3-IRES2-tTA* transgene (GACTGGCTTGCCCTCGTCCCA and GTGCACCGAGGCCCCAGATCA)[27] and *tetO*-human *DCTN1* transgene (AGGAGATGGCTGATACTGCTGATG and TTCATCGCTTCCAAGTCTCCCACA).

Behavior tests

Cohorts of *WT Tg* mice and littermate controls [nTg (n = 10), tTA (n = 10), tetO-WT (n = 10), and WT Tg (n = 10)] were repeatedly weighed and assessed for motor function at 1, 6, 12, and 18 months of age.

Cohorts of *G59S Tg* mice and littermate controls [nTg (n = 10), tTA (n = 11), tetO-G59S (n = 10), and G59S Tg (n = 10)] were repeatedly weighed and assessed for motor function at 1, 6, 12, and 18 months of age.

Cohorts of *G71R Tg* mice and littermate controls [nTg (n = 11), tTA (n = 10), tetO-G71R (n = 10), and G71R Tg (n = 10)] were repeatedly weighed and assessed for motor function at 1, 6, 12, and 18 months of age.

Open-field test. Mice were placed in the open-field apparatus of the Flex-Field Activity System (San Diego Instruments). Ambulatory, rearing, and fine movements of mice were traced and quantified with infrared photobeams sensors and Flex-Field software in the unit as the number of beam breaks per 30 min.

Rotarod test. Mice were placed onto a rotating rod with auto-acceleration from 0 to 40 rpm within 1 min (San Diego Instruments). The time length that each mouse stayed on the rotating rod was measured across three trials.

Histology, immunostaining, and light microscopy

Mice were sacrificed and perfused with 4% paraformaldehyde (PFA) in phosphate-buffered saline (PBS). Mouse brains were dissected, post-fixed in 4% PFA/PBS solution overnight, and submerged in 30% sucrose in PBS for at least 72 h. The 40 μm-thick brain sections were prepared using CM1950 cryostat (Leica) and stained with antibodies specific to human and mouse $p150^{Glued}$ (amino acid 3-202 at the N-terminus of $p150^{Glued}$, 1:200, BD Biosciences, Catalog # 610474, recognizing wild-type $p150^{Glued}$ but not G59S mutant $p150^{Glued}$, G71R mutant $p150^{Glued}$, or p135+), human and mouse $p150^{Glued}$ and p135+ (amino acid 1266-1278 at the C-terminus of $p150^{Glued}$ and p135+, 1:500, Abcam, Catalog # ab11806, recognizing wild-type, G59S mutant and G71R mutant $p150^{Glued}$, and p135+), tyrosine hydroxylase (TH, 1:2500, Pel-freez, Catalog # P40101-150; 1:500, ImmunoStar, Catalog # 22941), dynactin subunit p50 (1:1000, Millipore, Catalog # AB5869P), dynactin subunit actin-related protein 1 (ARP1, 1:1000, Millipore, Catalog # AB6058), cytoplasmic dynein light intermediate chain (DLIC, 1:500, Abcam, Catalog # ab123901), lysosomal associated membrane protein 2 (LAMP2, 1:500, Abcam, Catalog # ab13524), and ubiquitin (1:500, Enzo Life Sciences, Catalog # BML-PW0930), as suggested by manufacturers. Fluorescent signals were visualized with Alex Fluor-conjugated secondary antibody (1:500, Invitrogen, Catalog # A-11055, A-21202, A-21206, A-21208, A-21447, A10036, and A10040) and examined using LSM 880 laser-scanning confocal microscope (Zeiss). The paired images in all figures were collected using identical gain and offset settings, processed uniformly, and displayed as either a single optic layer or the maximum-intensity projections of the z-series confocal stack at 1.0 μm intervals.

Stereology

The number of midbrain dopaminergic neurons was estimated by unbiased stereology, as described previously[27,28]. According to Paxinos and Franklin's The Mouse Brain in Stereotaxic Coordinates (4th edition), a series of coronal sections (40 μm thick) across the midbrain (every fourth section from Bregma -2.54 to -4.24 mm, 10 sections per animal) were stained with an antibody specific to TH (1:2500, Pel-Freez, Catalog # P40101-150). After subsequent staining with Vectastain Elite ABC Kit, sections were visualized with DAB Kit (Vector Laboratories). Bright-field images were captured, and the number of TH-positive neurons was assessed using the optical fractionator function of Stereo Investigator 10 (MicroBrightField) under the Axio microscope Imager A1 (Zeiss). Counters were blinded to the genotypes of mice, and the sampling scheme was designed to have a coefficient of error less than 10% for the reliability of results.

Image analysis

Quantitative analysis of images was performed with ImageJ (NIH). After converting image type to 8-bit, areas of interest were selected with Freehand tools, and then mean optical intensities or area fractions were measured. The mean intensity for the background area was subtracted from the selected area to determine the net mean intensity. For quantitative analysis of DA neurite dystrophy, 5 tile images per animal (5 sections per animal and 1 tile image per section) from the *substantia nigra pars reticulata* (SNr) were taken with a 20× lens. Dystrophic DA neurites were defined as neuritic varicosity ≥ 25 μm^2. The area of dystrophic TH-positive DA neurites and the area of the SNr were quantified with ImageJ (NIH). For quantitative analysis of DA axon degeneration, 50 images per animal (10 sections per animal and 5 images per section) from the dorsal striatum were taken with a 63× lens. The area fraction of TH-positive DA axon terminals in each image was quantified with ImageJ (NIH). For quantitative analysis of G59S mutation-induced p150^{Glued} aggregates, aggregates were defined as puncta ≥ 1 μm^2.

High-performance liquid chromatography (HPLC)

The dorsal striatum of mice was dissected, weighed, and homogenized by sonication in 0.1 N perchloric acid containing 100 μM EDTA (500 μl buffer per 100 mg tissue). After centrifugation, the supernatant was collected and assayed for dopamine and DOPAC content by HPLC with electrochemical detection, as described previously[27,28]. Briefly, the mobile-phase solution containing octanesulfonic acid was used as an ion-pairing agent and pumped isocratically through a reversed-phase liquid chromatographic column. DA and DOPAC were measured by the current produced after exposure of the eluate to a flow-through electrode set to oxidizing and then reducing potentials in series, with recordings from the last electrode reflecting reversibly oxidized species.

Fast-scan cyclic voltammetry (FSCV)

The kinetics of striatal dopamine release evoked by electrical stimulation was measured using FSCV, as described previously[27,28]. The 400 μm-thick slices of dorsal striatum were prepared and transferred into 32 °C oxygenated artificial cerebrospinal fluid (aCSF: 126 mM NaCl, 2.5 mM KCl, 1.2 mM NaH_2PO_4, 2.4 mM $CaCl_2$, 1.2 mM $MgCl_2$, 25 mM $NaHCO_3$, 11 mM glucose, 20 mM 4-(2-hydroxyethyl)-1-piperazineethanesulfonic acid, and 0.4 mM L-ascorbic acid). Cylindrical carbon-fiber microelectrode prepared with T650 fibers (Goodfellow) was held at -0.4 V, and the potential was increased to 1.2 V and back at 400 V/s every 100 ms using a triangle waveform. Dopamine release in striatal slices was evoked by rectangular, electrical pulse stimulation (100-400 μA, 0.6 ms per phase, biphasic) applied every 5 min. Data were collected and analyzed with the Demon Voltammetry and Analysis software suite[29]. Ten cyclic voltammograms of charging currents were recorded as background before stimulation, and the average of these responses was subtracted from data obtained during and after stimulation. Maximum amplitudes of extracellular dopamine transients were calculated from input/output function (I/O) curves. I/O curves were plotted with stimulus current against the concentration of dopamine response amplitude over a range of stimulus intensities. The time constant of the slope decay (τ) was used as an uptake kinetic indicator of evoked dopamine release. Following experiments, electrodes were calibrated using 1 and 10 μM dopamine solutions in aCSF.

Western blot analysis

Mouse brain tissues were homogenized and sonicated in 1% SDS lysis buffer (50 mM Tris-HCl, 150 mM NaCl, 2 mM EDTA, pH 7.5, and 1% SDS) supplemented with Protease/Phosphatase Inhibitor Cocktails (ThermoFisher Scientific). Lysates were centrifuged at 15,000 *g* for 15 min at 4 °C. Supernatants were collected, and protein content was quantified with the bicinchoninic acid (BCA) assay kit (ThermoFisher Scientific). Equal amounts of total proteins were size-fractioned with NuPage 4%-12% Bis-Tris gel in MES or MOPS running buffer (ThermoFisher Scientific). After transferring to nitrocellulose membranes with the

Trans-Blot Turbo Transfer System (Bio-Rad), proteins were immunoblotted with specific primary antibodies to human p150^{Glued} (1:1000, Covance, custom-made), human and mouse p150^{Glued} and p135+ (1:1000, Abcam, Catalog # ab11806), dynactin subunit DCTN4 (1:1000, Abcam, Catalog # ab170107), dynactin subunit p50 (1:1000, BD Biosciences, Catalog # 611002), dynactin subunit actin-related protein 1 (ARP1, 1:1000, Sigma-Aldrich, Catalog # A5601), tyrosine hydroxylase (TH, 1:1000, Sigma-Aldrich, Catalog # T1299), dopamine transporter (DAT, 1:1000, Millipore, Catalog # MAB369), and β-actin (1:5000, Sigma-Aldrich, Catalog # A1978). Protein signals were visualized using the Odyssey System with IRDye secondary antibodies (LI-COR Biosciences, Catalog # 926-32212, 926-32219, 926-3221, 926-32411, and 926-68023) and quantified with NIH ImageJ software.

Statistical analysis

Statistical analysis was performed using GraphPad Prism 9 (GraphPad Software). Data are presented as mean ± SEM. Statistical significance was determined by comparing means of different groups using unpaired t-test, one-way, and two-way ANOVA with post hoc analysis. $^{*}P < 0.05$, $^{**}P < 0.01$, $^{***}P < 0.001$, $^{****}P < 0.0001$.

RESULTS

Generation of mouse models with selective expression of wild-type or mutant human p150^{Glued} in midbrain DA neurons

To investigate the involvement and mechanism of p150^{Glued} in neurodegeneration *in vivo*, three lines of *tetO*-human *DCTN1* mice (tetO-WT, tetO-G59S, or tetO-G71R) with inducible expression of wild-type or mutant human p150^{Glued} under the transcriptional control of tetracycline operator (*tetO*) were generated. The *tetO*-human *DCTN1* mice were then crossed with *Pitx3-IRE2-tTA* knock-in mice to obtain *Pitx3-IRE2-tTA/tetO*-human *DCTN1* WT (WT Tg), *Pitx3-IRE2-tTA/tetO*-human *DCTN1* G59S (G59S Tg), or *Pitx3-IRE2-tTA/tetO*-human *DCTN1* G71R (G71R Tg) bigenic mice [Figure 1A]. Since the tetracycline transactivator (tTA) is specifically expressed in midbrain DA neurons under the endogenous *Pitx3* promoter[27], it turned on the expression of human wild-type or mutant p150^{Glued} selectively in midbrain DA neurons [Figure 1A]. The target overexpression of human p150^{Glued} in midbrain DA neurons of one-month-old WT mice was visualized by immunostaining [Figure 1B]. Using a human p150^{Glued}-specific antibody, Western blot confirmed the expression of human p150^{Glued} in the midbrain homogenates of one-month-old *WT Tg*, *G59S Tg*, and *G71R Tg* mice but not *nTg* mice [Figure 1C and D]. The steady level of G59S human p150^{Glued} was significantly less (approximately 30%) compared with WT or G71R human p150^{Glued}. Western blot further revealed substantially increased levels of total (human and mouse) p150^{Glued} (approximately two-fold) and other dynactin subunits, including DCTN4, p50, and ARP1, but markedly reduced level of p135+ (alternative splicing isoforms of *Dctn1* lacking the N-terminus) in the midbrain homogenates of *WT Tg*, *G59S Tg*, and *G71R Tg* mice compared to the *nTg* mice [Figure 1C and D].

G59S Tg and *G71R Tg* mice exhibit profound motor abnormalities.

As motor symptoms and weight loss are the main clinical manifestations in familial motor neuron disease and Perry syndrome cases with *DCTN1* mutation[5], *WT Tg*, *G59S Tg*, *G71R Tg* mice, and their littermate controls were weighed, tested for locomotion activity in the open-field test, and examined for motor coordination in the rotarod test at 1, 6, 12, and 18 months of age. *WT Tg* mice developed normally and exhibited comparable body weight and motor function with littermate single- or non-transgenic mice in the open field test and the rotarod test [Figure 2A-D]. *G59S Tg* mice displayed substantial weight loss starting at 12 months of age, normal ambulatory movement, dramatic reduction of rearing movement at 18 months of age, and significant impairment in rotarod test starting at six months of age [Figure 2E-H]. *G71R Tg* mice showed normal body weight, significant hyperactivities of ambulatory movement and rearing, and substantially impaired rotarod performance starting at six months of age [Figure 2I-L]. Together, these

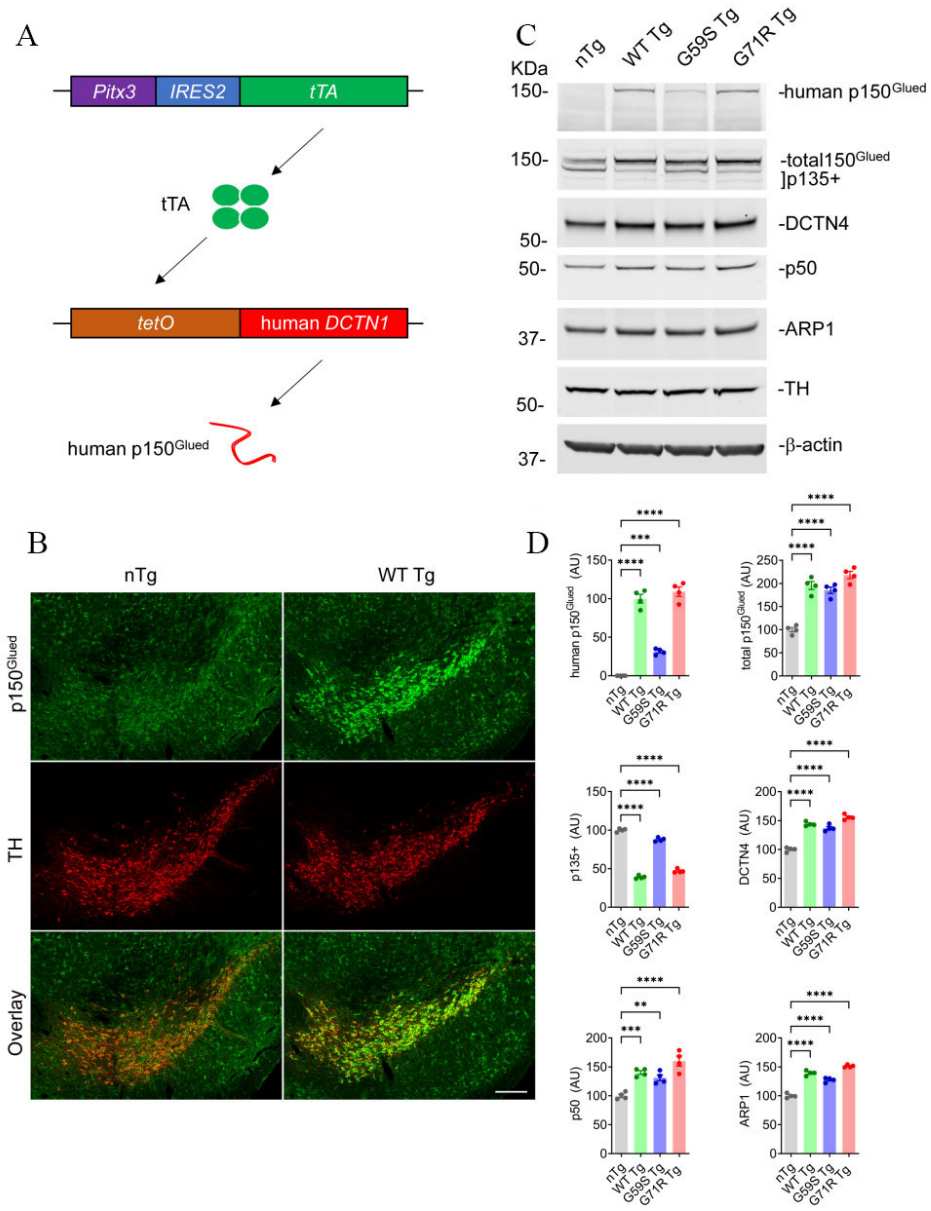

Figure 1. Selective expression of wild-type or mutant human p150^{Glued} in mouse midbrain DA neurons. (A) The schematic diagram depicts the generation of transgenic mice with target expression of human p150^{Glued} in midbrain DA neurons by crossing *Pitx3-IRE2-tTA* and *tetO*-human *DCTN1* mice. (B) Immunofluorescent images show the staining of p150^{Glued} (green) and TH (red) in the coronal midbrain sections of one-month-old *nTg* and *WT Tg* mice. DA neurons were visualized by TH staining. Scale bar: 200 μm. (C, D) Western blots show the expression of human p150^{Glued}, total (human and mouse) p150^{Glued}, p135+, DCTN4, p50, and ARP1 in the midbrain homogenates of one-month-old *nTg*, *WT Tg*, *G59S Tg*, and *G71R Tg* mice. β-actin and TH were used as the loading control. The bar graph estimates the protein level of dynactin subunits normalized with β-actin (n = 4 per genotype). Data are presented as mean ± SEM. One-way ANOVA with Dunnett's multiple comparisons test was used for statistical analysis (the mean of each genotype was compared with the mean of nTg). $^{**}P < 0.01$, $^{***}P < 0.001$, $^{****}P < 0.0001$.

findings demonstrate that selective expression of either G59S or G71R mutant p150^{Glued} in midbrain DA neurons causes profound motor abnormalities in mice and suggest that both G59S and G71R mutant p150^{Glued} may impair the function and survival of midbrain DA neurons.

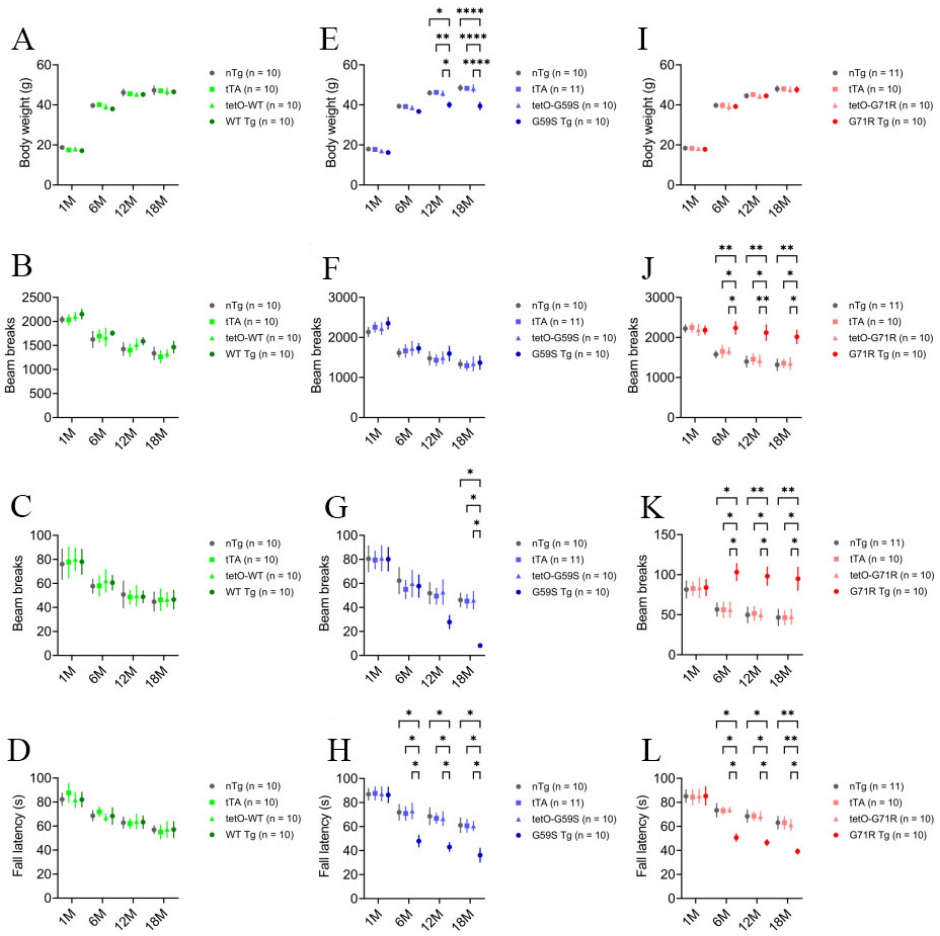

Figure 2. Profound motor abnormalities of *G59S Tg* and *G71R Tg* mice. (A-D) At 1, 6, 12, and 18 months of age, cohorts of male *nTg*, *tTA*, *tetO-WT*, and *WT Tg* mice (n = 10 per genotype) were repeatedly weighed (A); tested for ambulatory movement (B) and rearing (C) in the open-field test; and examined for the latency to fall in the rotarod test (D). (E-H) At 1, 6, 12, and 18 months of age, cohorts of male *nTg* (n = 10), *tTA* (n = 11), *tetO-G59S* (n = 10), and *G59S Tg* (n = 10) mice were repeatedly weighed (E); tested for ambulatory movement (F) and rearing (G) in the open-field test; and examined for the latency to fall in the rotarod test (H). (I-L) At 1, 6, 12, and 18 months of age, cohorts of male *nTg* (n = 11), *tTA* (n = 10), *tetO-G71R* (n = 10), and *G71R Tg* (n = 10) mice were repeatedly weighed (I); tested for ambulatory movement (J) and rearing (K) in the open-field test; and examined for the latency to fall in the rotarod test (L). Data are presented as mean ± SEM. Two-way ANOVA with Tukey's multiple comparisons test was used for statistical analysis (at each time point, the mean of each genotype was compared with the mean of every other genotype). $^{*}P < 0.05$, $^{**}P < 0.01$, $^{****}P < 0.0001$.

G59S Tg and *G71R Tg* mice develop progressive degeneration of midbrain DA neurons

Since neuronal loss in *substantia nigra* is a pathological hallmark of Perry syndrome[9,10], the numbers of TH-positive midbrain DA neurons in the *substantia nigra pars compacta* (SNc) and ventral tegmental area (VTA) of *WT Tg*, *G59S Tg*, *G71R Tg* mice, and their control mice were counted using an unbiased stereological approach. *WT Tg* mice presented with no apparent loss of DA neurons in either the SNc or VTA at 1, 6, 12, and 24 months of age compared with control mice [Figure 3A-D]. *G59S Tg* mice displayed severe and early-onset degeneration of DA neurons in the midbrain, with approximately 13%, 28%, and 57% neuronal loss in the SNc at 6, 12, and 24 months of age, respectively, and 50% of neuronal loss in the VTA at 24 months of age [Figure 3A-D]. *G71R Tg* mice exhibited mild and late-onset degeneration of DA neurons in the midbrain, with approximately 25% neuronal loss in the SNc as well as the VTA at 24 months of age [Figure 3A-D]. Interestingly, besides neuronal loss, *G59S Tg* and *G71R Tg* mice showed remarked and progressive dystrophy of DA neurites in the *substantia nigra pars reticulata* (SNr) starting at two months of age [Figure 3A and E]. Therefore, expression of either G59S or G71R mutant $p150^{Glued}$ in midbrain DA

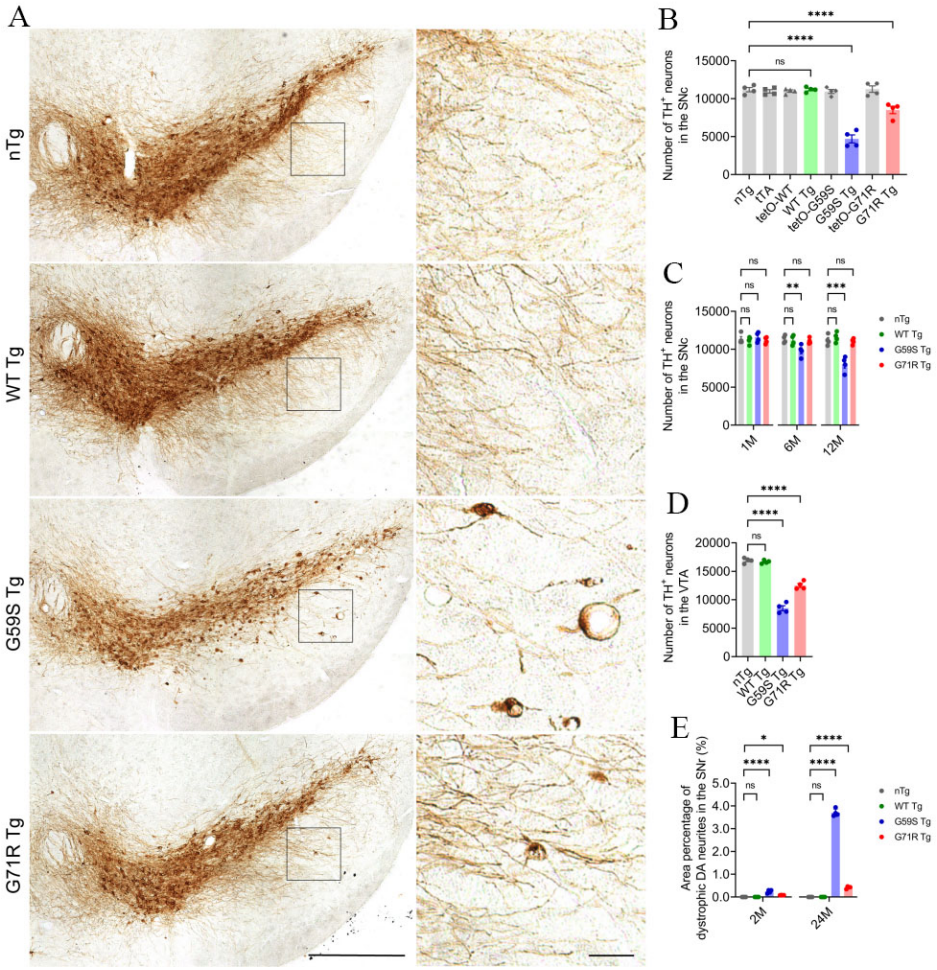

Figure 3. Progressive degeneration of DA neurons in the midbrain of *G59S Tg* and *G71R Tg* mice. (A) Immunohistochemical images show TH staining in the coronal midbrain sections of 24-month-old *nTg*, *WT Tg*, *G59S Tg*, and G71R Tg mice. Scale bar: (left) 500 μm (low-magnification images) and (right) 50 μm (high-magnification images). Note the dystrophic TH-positive DA neurites in the SNr of *G59S Tg* and *G71R Tg* mice. (B) Bar graphs depict the unbiased stereological estimation of the number of TH-positive DA neurons in the SNc of 24-month-old *nTg*, *tTA*, *tetO-WT*, *WT Tg*, *tetO-G59S*, *G59S Tg*, *tetO-G71R*, *and G71R Tg* mice (n = 4 per genotype). Data are presented as mean ± SEM. One-way ANOVA with Dunnett's multiple comparisons test was used for statistical analysis (the mean of each genotype was compared with the mean of nTg). $^{****}P < 0.0001$. ns: Not significant. (C) Bar graphs depict the unbiased stereological estimation of the number of TH-positive DA neurons in the SNc of 1-, 6-, and 12-month-old *nTg*, *WT Tg*, *G59S Tg*, and *G71R Tg* mice (n = 4 per genotype per time point). Data are presented as mean ± SEM. At each time point, one-way ANOVA with Dunnett's multiple comparisons test was used for statistical analysis (the mean of each genotype was compared with the mean of nTg). $^{**}P = 0.0099$, $^{***}P = 0.0001$. (D) Bar graphs depict the unbiased stereological estimation of the number of TH-positive DA neurons in the VTA of 24-month-old *nTg*, *WT Tg*, *G59S Tg*, *and G71R Tg* mice (n = 4 per genotype). Data are presented as mean ± SEM. One-way ANOVA with Dunnett's multiple comparisons test was used for statistical analysis (the mean of each genotype was compared with the mean of nTg). $^{****}P < 0.0001$. (E) Bar graphs quantify the area percentage of dystrophic TH-positive DA neurites in the SNr of 2- and 24-month-old *nTg*, *WT Tg*, *G59S Tg*, *and G71R Tg* mice (at each time point, n = 4 animals per genotype and 5 sections per animal). Dystrophic DA neurites were defined as neuritic varicosity ≥ 25 μm^2. Data are presented as mean ± SEM. At each time point, one-way ANOVA with Dunnett's multiple comparisons test was used for statistical analysis (the mean of each genotype was compared with the mean of nTg). $^{*}P = 0.0259$, $^{****}P < 0.0001$. TH: Tyrosine hydroxylase.

neurons leads to substantial and progressive neurodegeneration.

G59S Tg and *G71R Tg* mice display robust degeneration of DA axon terminals

As axon dystrophy was reported in the striatum of patients with Perry syndrome[30,31], the density and morphology of DA axon terminals in the dorsal striatum of *nTg*, *WT Tg*, *G59S Tg*, and *G71R Tg* mice were

examined. Compared with age-matched nTg controls, 2-, 12-, and 24-months old *WT Tg* mice had no apparent alteration of TH-positive DA axon terminals [Figure 4A and B]. However, *G59S Tg* and *G71R Tg* mice displayed substantial loss of DA axon terminals, with approximately 15%, 33%, and 55% of axonal loss in 6-, 12- and 24-month-old *G59S Tg* mice, respectively, and 35% of axonal loss in 24-month-old *G71R Tg* mice [Figure 4A and B]. Furthermore, TH staining also revealed abnormally enlarged DA axon terminals in the striatum of *G59S Tg* and *G71R Tg* mice [Figure 4A, arrow]. These data demonstrate that expression of either G59S or G71R mutant $p150^{Glued}$ in midbrain DA neurons causes robust degeneration of DA axon terminals and suggest dysfunctional DA transmission in *G59S Tg* and *G71R Tg* mice.

G59S Tg and G71R Tg mice show alteration of dopamine transmission

Considering the pathological findings, the steady-state level of dopamine in the dorsal striatum of *nTg*, *WT Tg*, *G59S Tg*, and *G71R Tg* mice was assessed with HPLC. At 18 months of age, *WT Tg* and *G71R Tg* mice showed no apparent change in dopamine level compared with nTg controls, while *G59S Tg* mice displayed a significant reduction of dopamine content, with an approximately 53% of decrease [Figure 5A]. Regarding the primary dopamine metabolite 3,4-dihydroxyphenylacetic acid (DOPAC), neither its content nor the DOPAC/dopamine ratio in 18-month-old *WT Tg*, *G59S Tg*, and *G71R Tg* mice was significantly different with age-matched nTg controls [Figure 5A]. These data reveal dopamine deficiency in the striatum of *G59S Tg* mice, which might be the functional consequence of robust degeneration of midbrain DA neurons and the pathophysiological basis for the motor deficits observed in *G59S Tg* mice. By contrast, at 18 months of age, *G71R Tg* mice developed neither loss of midbrain DA neurons nor reduced dopamine content, further supporting the late-onset DA neuronal loss in *G71R Tg* mice.

Next, dopamine release kinetics in the dorsal striatum of *nTg*, *WT Tg*, *G59S Tg*, and *G71R Tg* mice was evaluated using fast-scan cyclic voltammetry (FSCV). At six months of age, *WT Tg* mice showed comparable evoked dopamine release and dopamine uptake in response to single-pulse stimulation compared with nTg controls [Figure 5B and C]. However, *G59S Tg* mice displayed significantly decreased dopamine release and slower dopamine uptake, while *G71R Tg* mice exhibited substantially increased dopamine release and slower dopamine uptake [Figure 5B and C]. Similarly, 18-month-old *WT Tg* mice showed comparable evoked dopamine release and dopamine uptake in response to burst-pulse stimulation compared with age-matched nTg controls [Figure 5D and E]. However, *G59S Tg* mice displayed significantly decreased dopamine release and slower dopamine uptake, while *G71R Tg* mice exhibited substantially increased dopamine release and slower dopamine uptake [Figure 5D and E]. Taken together, *G59S Tg* mice showed early-onset defects in striatal dopamine transmission, consistent with the early-onset loss of DA neurons and axons. In contrast, *G71R Tg* mice showed early-onset dysfunction of dopamine release and uptake long before the substantial loss of DA neurons and axons occurred. Thus, these data indicate that expression of either G59S or G71R mutant $p150^{Glued}$ in midbrain DA neurons profoundly compromises the dopamine transmission of the nigrostriatal DA pathway, contributing to the motor phenotypes developed in these transgenic mice.

G59S Tg and G71R Tg mice exhibit an age-dependent reduction of DA proteins

Tyrosine hydrolase (TH) is the rate-limiting enzyme in dopamine synthesis, and dopamine transporter (DAT) mediates dopamine uptake[32,33]. Since TH and DAT play critical roles in the nigrostriatal DA pathway, the protein levels of TH and DAT in the striatal homogenates of 1- and 24-month-old *nTg*, *WT Tg* , *G59S Tg*, and *G71R Tg* mice were examined. At one month of age, *nTg*, *WT Tg*, *G59S Tg*, and *G71R Tg* mice had comparable levels of TH and DAT in the striatum [Figure 6A and B]. At 24 months of age, *WT Tg* mice showed no marked change in TH and DAT protein expression compared with nTg controls, while both *G59S Tg* and *G71R Tg* mice displayed substantial loss of TH and DAT [Figure 6A and B]. Interestingly, the percentages of DAT loss in the striatum of 24-month-old *G59S Tg* and *G71R Tg* mice (approximately

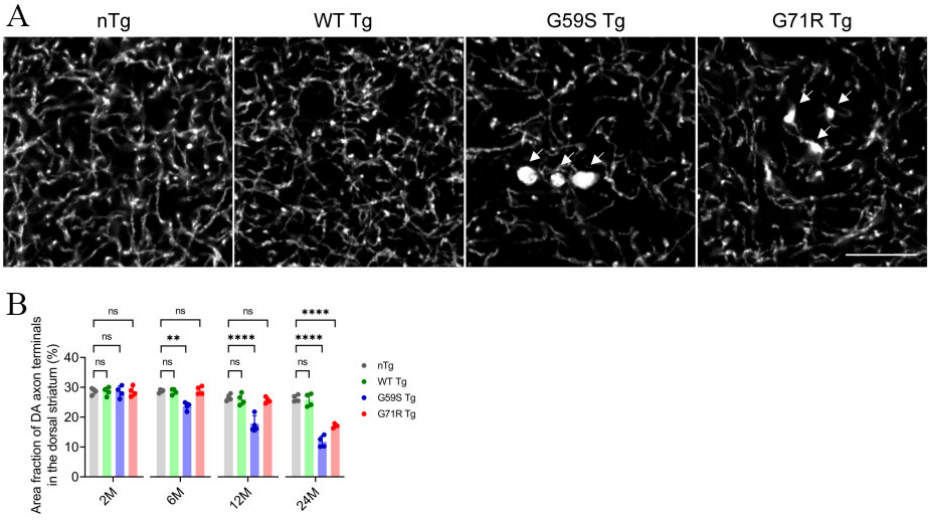

Figure 4. Robust degeneration of DA axon terminals in the striatum of *G59S Tg* and *G71R Tg* mice. (A) Representative images show TH staining in the dorsal striatum coronal sections of 24-month-old *nTg*, *WT Tg*, *G59S Tg*, and *G71R Tg* mice. Scale bar: 10 μm. Arrows point to swellings of TH-positive DA axon terminals in the striatum of *G59S Tg* and *G71R Tg* mice. (B) Bar graph estimates the area fraction of TH-positive DA axon terminals in the dorsal striatum of 2-, 6-, 12-, and 24-month-old *nTg*, *WT Tg*, *G59S Tg*, and *G71R Tg* mice (at each time point, n = 4 animals per genotype and 10 sections per animal). Data are presented as mean ± SEM. At each time point, one-way ANOVA with Dunnett's multiple comparisons test was used for statistical analysis (the mean of each genotype was compared with the mean of nTg). $^{**}P = 0.0018$, $^{****}P < 0.0001$. ns: Not significant. TH: Tyrosine hydroxylase.

70% and 42%, respectively) were more severe than the TH loss (about 53% and 29%, respectively) [Figure 6A and B]. These data suggest expression of either G59S or G71R mutant p150^{Glued} in midbrain DA neurons may preferentially downregulate the expression and function of DAT protein at DA axon terminals.

G59S Tg mice display age-dependent accumulation of p150^{Glued} aggregates in midbrain dopaminergic neurons

As both G59S and G71R mutant p150^{Glued} were found aggregation-prone *in vitro*[17-19], the subcellular distribution pattern of p150^{Glued} in the midbrain DA neurons of 2-, 6-, 12-, and 24-month-old *nTg*, *WT Tg*, *G59S Tg*, and *G71R Tg* mice was examined. TH and p150^{Glued} co-staining revealed diffuse cytoplasmic localization of p150^{Glued} without apparent aggregate formation in the soma and neurites of midbrain DA neurons from both young and aged *nTg*, *WT Tg*, and *G71R Tg* mice [Figure 7A and B]. By contrast, *G59S Tg* mice presented with p150^{Glued}-positive cytoplasmic aggregates, mainly in the soma and in the neurites of midbrain DA neurons [Figure 7A]. Furthermore, the percentage of DA neurons with p150^{Glued} aggregate in *G59S Tg* mice increased in an age-dependent manner, approximately 0%, 10.54%, 19.66%, and 82.17% at 2, 6, 12, and 24 months of age, respectively [Figure 7B]. Immunostaining further revealed the co-aggregation of dynactin subunit p50 and ARP1, as well as dynein subunit DLIC, with p150^{Glued} aggregates inside the dystrophic DA neurites in the SNr of six-month-old *G59S Tg* mice [Figure 8A-C]. In addition, co-staining of coronal midbrain sections showed co-localization of lysosomes with p150^{Glued} aggregates and a substantial increase of ubiquitin immunoreactivities within the dystrophic DA neurites in the SNr of six-month-old *G59S Tg* mice, compared with nTg controls [Figure 9A and B]. Thus, G59S mutation rather than G71R mutation induces mutant p150^{Glued} to form cytoplasmic aggregates in midbrain DA neurons *in vivo*. Moreover, the aggregates trap dynein/dynactin, co-localize with lysosomes, and upregulate ubiquitination, implying detrimental effects of G59S mutant p150^{Glued} on dynein/dynactin function and the degradative pathway in the midbrain DA neurons. These findings may explain why *G59S Tg* mice developed severe and early-onset degeneration of midbrain DA neurons, while *G71R Tg* mice showed milder and more slowly progressive neurodegeneration.

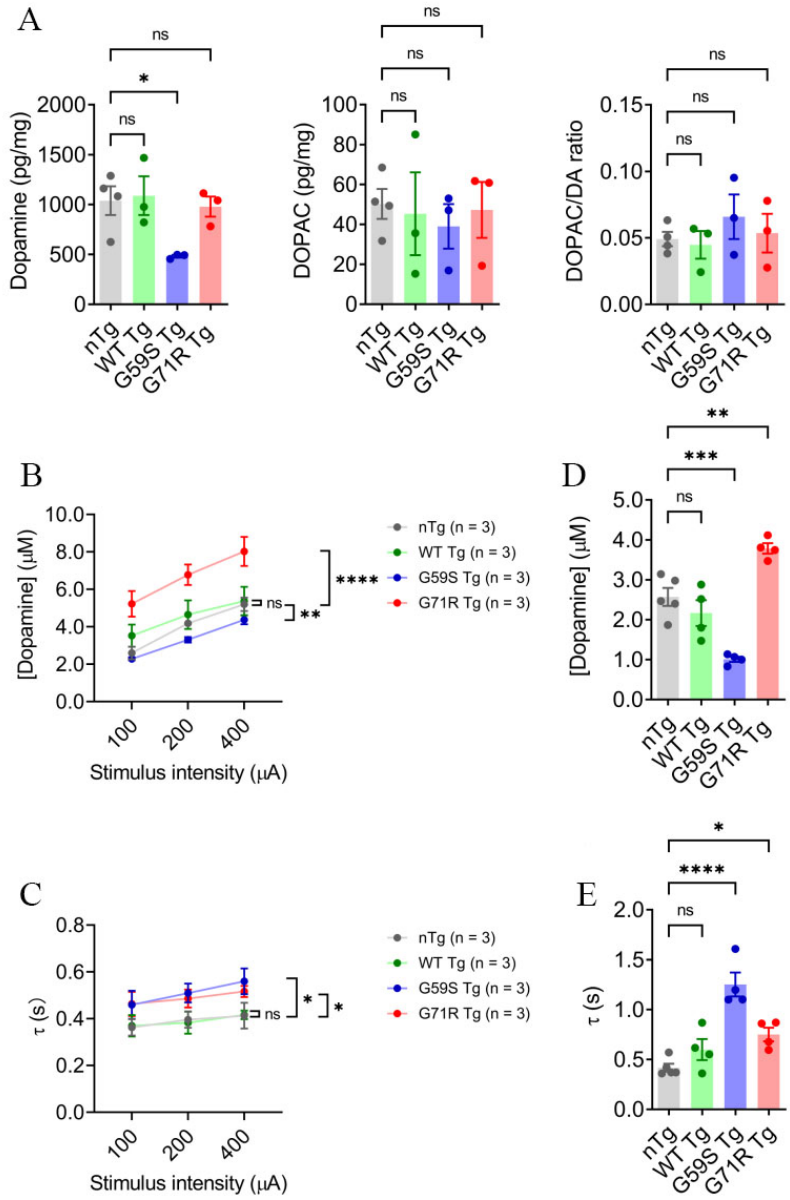

Figure 5. Alteration of dopamine content and release in the striatum of *G59S Tg* and *G71R Tg* mice. (A) HPLC measures the content of dopamine and DOPAC in the dorsal striatum of 18-month-old *nTg*, *WT Tg*, *G59S Tg*, and *G71R Tg* mice (n = 3 or 4 per genotype). Data are presented as mean ± SEM. One-way ANOVA with Dunnett's multiple comparisons test was used for statistical analysis (the mean of each genotype was compared with the mean of nTg). $^{*}P$ = 0.0397. ns: Not significant. (B, C) FSCV quantifies the peak evoked dopamine release (B) and time constant of slope decay (C) following single-pulse electrical stimulation of different stimulus intensity in the dorsal striatum of six-month-old *nTg*, *WT Tg*, *G59S Tg*, *and G71R Tg* mice (n = 3 animals per genotype and 3 sections per animal). Data are presented as mean ± SEM. Two-way ANOVA genotype factor: nTg *vs.* G59S Tg, $F_{(1,12)}$ = 25.11, $^{**}P$ = 0.0044; nTg *vs.* G71R Tg, $F_{(1,12)}$ = 40.19, $^{****}P$ < 0.0001 (B). Two-way ANOVA genotype factor: nTg *vs.* G59S Tg, $F_{(1,12)}$ = 9.285, $^{*}P$ = 0.0101; nTg *vs.* G71R Tg, $F_{(1,12)}$ = 8.491, $^{*}P$ = 0.0130 (C). (D,E) FSCV quantifies the peak evoked dopamine release (D) and time constant of slope decay (E) in response to burst electrical stimulation (200 μA, 50 Hz, 5 pulses) in the dorsal striatum of 18-month-old *nTg*, *WT Tg*, *G59S Tg*, and *G71R Tg* mice (n = 4 or 5 animals per genotype and 3 sections per animal). Data are presented as mean ± SEM. One-way ANOVA with Dunnett's multiple comparisons test was used for statistical analysis (the mean of each genotype was compared with the mean of nTg). nTg *vs.* G59S Tg, $^{***}P$ = 0.0004; nTg *vs.* G71R Tg, $^{**}P$ = 0.0034 (D). nTg *vs.* G59S Tg, $^{****}P$ < 0.0001; nTg *vs.* G71R Tg, $^{*}P$ = 0.0357 (E).

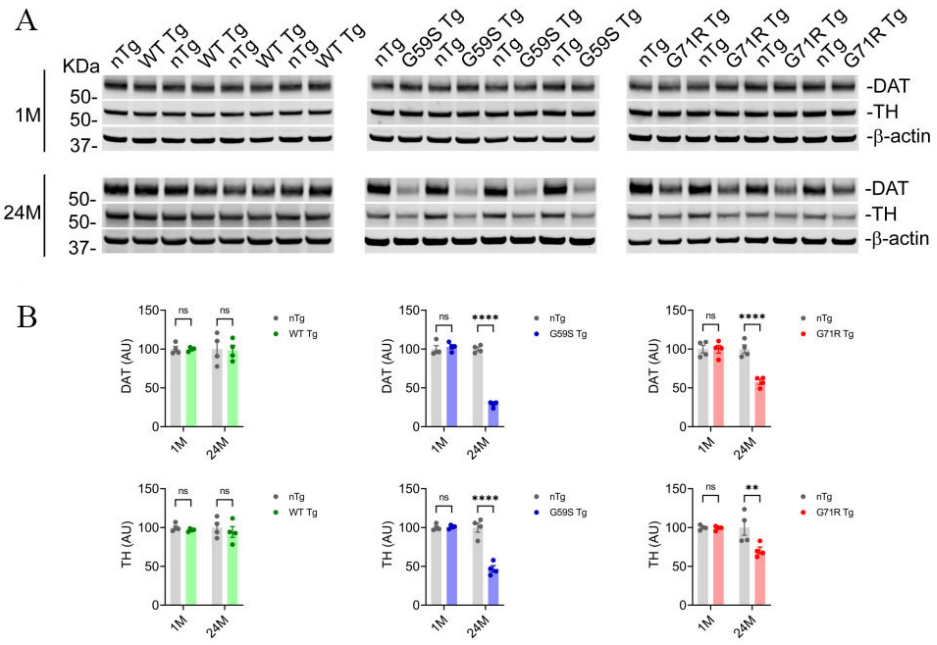

Figure 6. Reduction of dopaminergic proteins in the striatum of *G59S Tg* and *G71R Tg* mice. (A, B) Western blots show the expression of DAT and TH in the striatum homogenates of 1- and 24-month-old *nTg*, *WT Tg*, *G59S Tg*, and *G71R Tg* mice. Actin was used as the loading control. The bar graph estimates the levels of DAT and TH expression normalized against β-actin (n = 4 per genotype). Data are presented as mean ± SEM. Two-way ANOVA with Sidak's multiple comparisons test was used for statistical analysis. $^{**}P$ = 0.0054, $^{****}P < 0.0001$. ns: Not significant.

DISCUSSION

In this study, transgenic mouse lines with selective overexpression of wild-type human p150^{Glued}, motor neuron disease-related G59S mutant p150^{Glued}, or Perry syndrome-related G71R mutant p150^{Glued} in midbrain DA neurons were generated and characterized. The *WT Tg* mice did not develop any overt motor phenotypes or midbrain DA neurodegeneration compared with age-matched *nTg* mice. The *G59S Tg* mice displayed weight loss, motor deficits, early-onset decreased dopamine transmission, and early-onset progressive loss of DA neurons and axons. The *G71R Tg* mice exhibited hyperactivities, impaired motor coordination, early-onset increased dopamine release and slower dopamine uptake, and late-onset loss of DA neurons and axons. Furthermore, both *G59S Tg* and *G71R Tg* mice showed an age-dependent reduction of DA proteins in the striatum, with a more severe loss of DAT than TH. Finally, G59S mutant p150^{Glued} rather than G71R mutant p150^{Glued} was found to form aggregates in mouse midbrain DA neurons in an age-dependent manner, and the aggregates trapped dynein/dynactin, co-localized with lysosomes, and upregulated ubiquitination.

Since the initial identification of motor neuron disease- and Perry syndrome-causative mutations in p150^{Glued}, several mouse strains of mutant p150^{Glued} have been generated to study their effects on selective degeneration of specific types of neurons. Motor neuron disease-like motor phenotypes and degeneration of spinal motor neurons have been reported in G59S p150^{Glued} transgenic and knock-in mouse models[20-22]. Decreased exploratory activity and impaired motor coordination were observed in the transgenic mice overexpressing G71A p150^{Glued} under the control of the *Thy1* promotor[23]. However, either the expression of G71A p150^{Glued} in midbrain DA neurons or neuronal loss in the brain tissue was detected in the transgenic mice[23]. Recently, G71A p150^{Glued} knock-in mouse models were created[24]. Increased immobility time in the tail suspension test, impaired motor coordination in the beam-walking test, and decreased TH staining

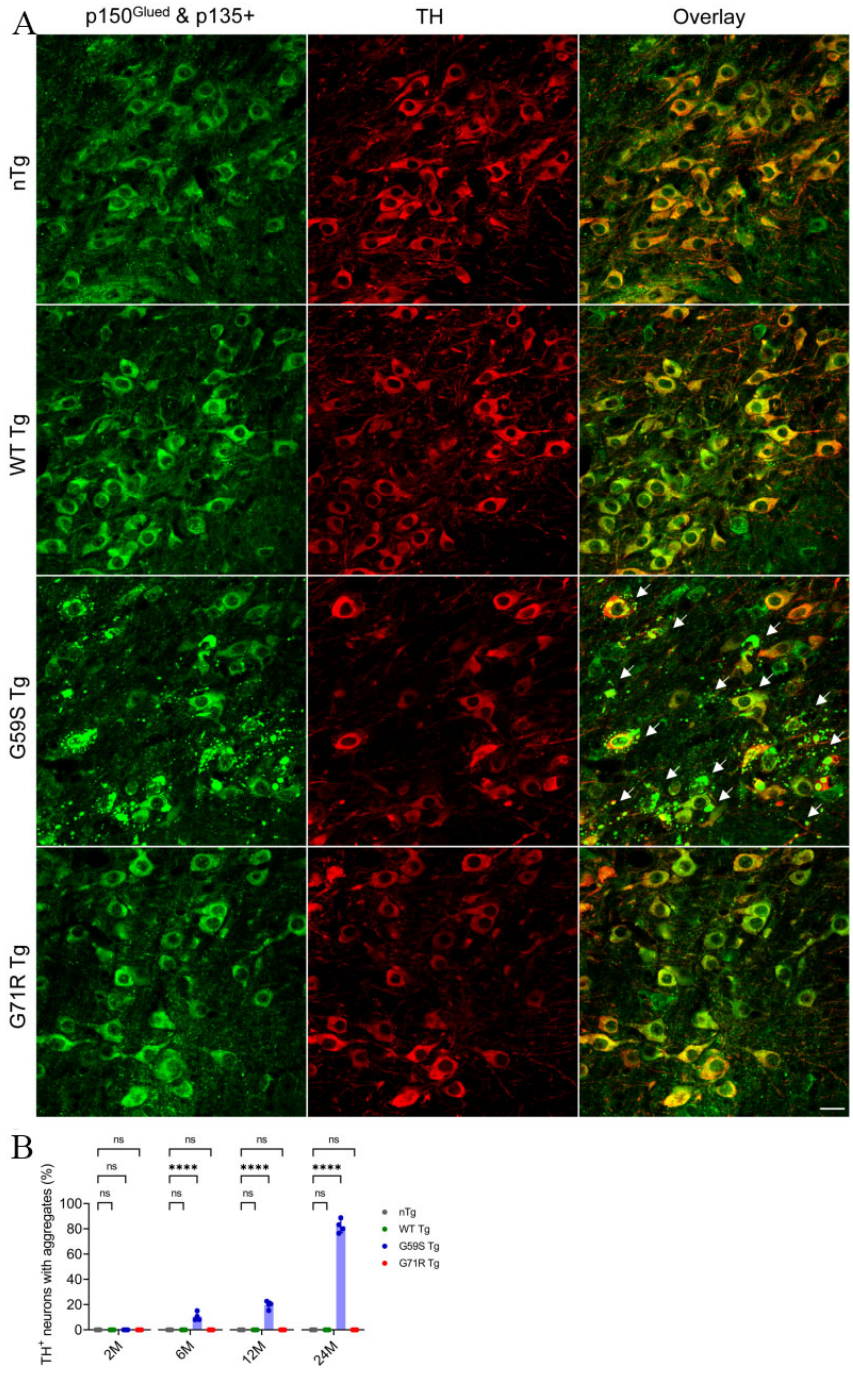

Figure 7. Formation of p150^{Glued}-positive protein aggregates in midbrain DA neurons of *G59S Tg* mice. (A) Immunofluorescent images show the staining of p150^{Glued} and p135+ (green) and TH (red) in midbrain coronal sections of 24-month-old *nTg*, *WT Tg*, *G59S Tg*, and *G71R Tg* mice. Scale bar: 20 μm. Arrows point to proteins aggregates of p150^{Glued} and p135+ in the soma and neurites of DA neurons from *G59S Tg* mice. (B) Bar graph estimates the percentage of TH-positive neurons with proteins aggregates of p150^{Glued} and p135+ in the midbrain of 2-, 6-, 12-, and 24-month-old *nTg*, *WT Tg*, *G59S Tg*, and *G71R Tg* mice (at each time point, n = 4 animals per genotype and 5 sections per animal). Aggregates were defined as puncta ≥ 1 μm^2. Data are presented as mean ± SEM. At each time point, one-way ANOVA with Dunnett's multiple comparisons test was used for statistical analysis (the mean of each genotype was compared with the mean of nTg). $^{****}P < 0.0001$. ns: Not significant. TH: Tyrosine hydroxylase.

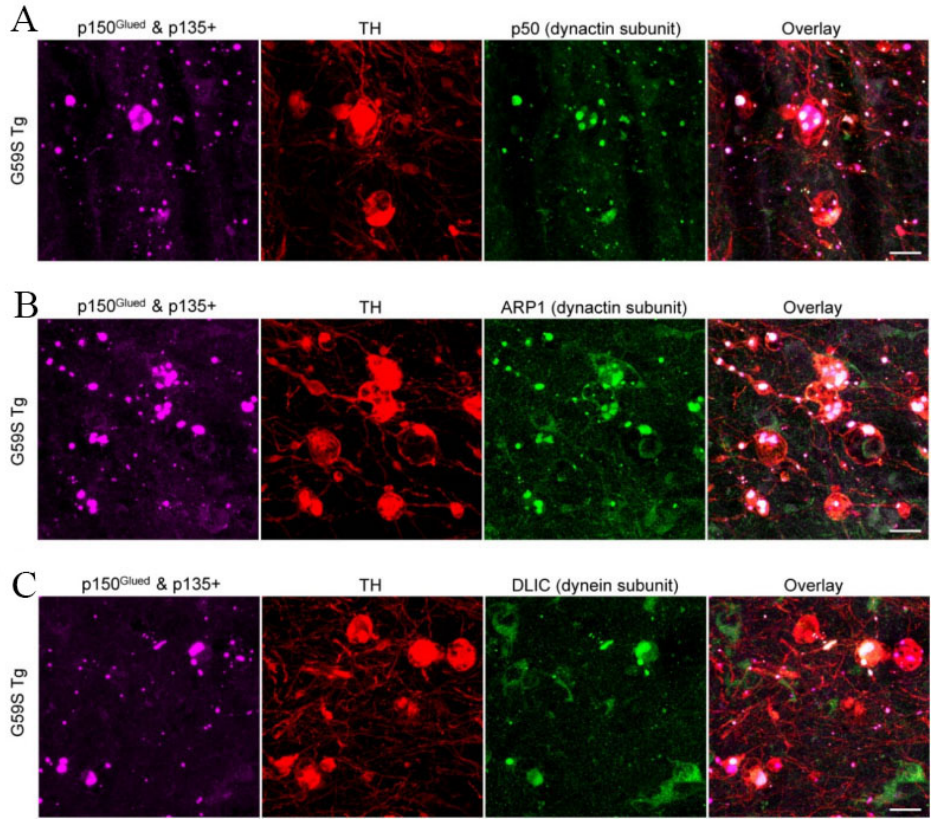

Figure 8. Co-aggregation of dynactin and dynein subunits with G59S mutation-induced p150^{Glued} aggregates in the dystrophic DA neurites of *G59S Tg* mice. (A) Immunofluorescent images show the staining of p150^{Glued} and p135+ (purple), TH (red), and dynactin subunit p50 (green) in the SNr of six-month-old *G59S Tg* mice. Scale bar: 20 μm. (B) Immunofluorescent images show the staining of p150^{Glued} and p135+ (purple), TH (red), and dynactin subunit ARP1 (green) in the SNr of six-month-old *G59S Tg* mice. Scale bar: 20 μm. (C) Immunofluorescent images show the staining of p150^{Glued} and p135+ (purple), TH (red), and dynein subunit DLIC (green) in the SNr of six-month-old *G59S Tg* mice. Scale bar: 20 μm.

intensity in the substantia nigra neurons were found in the heterozygous G71A p150^{Glued} knock-in mice[24], recapitulating some of the clinical features of Perry syndrome. However, the pathogenic effects of mutant p150^{Glued} on Perry syndrome-related degeneration of the nigrostriatal DA pathway remain to be determined. New lines of transgenic mice (*WT Tg*, *G59S Tg*, and *G71R Tg*) with selective overexpression of wild-type, G59S mutant, or G71R mutant human p150^{Glued} in midbrain DA neurons were generated in the current study, allowing us to systematically evaluate the impact of mutant p150^{Glued} on survival and function of midbrain DA neurons. *WT Tg* mice showed neither motor phenotypes nor pathological, functional, or biochemical abnormalities of the nigrostriatal DA pathway. *G59S Tg* mice displayed substantial weight loss, dramatic reduction of rearing movement in the open field test, and significant impairment of motor coordination in the rotarod test. The pathophysiological basis for the motor phenotypes in *G59S Tg* mice is the early-onset and severe loss of DA neurons and axon terminals and the resultant deficiency of dopamine content and transmission. *G71R Tg* mice exhibited significant hyperactivities in ambulatory and rearing movements and substantially impaired rotarod performance through 6-18 months of age. In contrast to the severe and early-onset degeneration of nigrostriatal DA pathway in *G59S Tg* mice, the neurodegeneration in *G71R* mice was much milder and more slowly progressive, with no significant loss of DA neurons and axon terminals occurring before 18 months of age. Despite no early-onset DA neuron degeneration, *G71R Tg* mice showed an early-onset increase of dopamine release and slower dopamine uptake in the striatum, which may elevate the extracellular dopamine level and contribute to hyper-dopamine motor phenotypes.

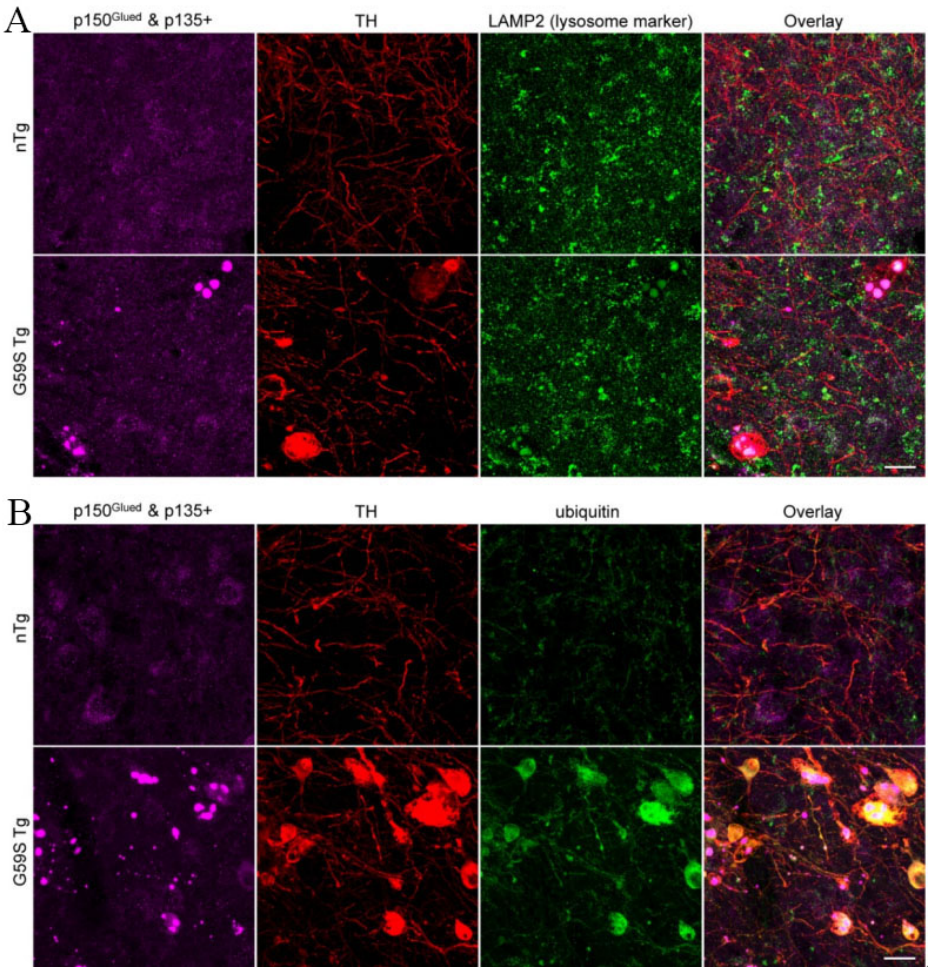

Figure 9. Co-localization of lysosomes with G59S mutation-induced p150^{Glued} aggregates and upregulated ubiquitination in the dystrophic DA neurites of *G59S Tg* mice. (A) Immunofluorescent images show the staining of p150^{Glued} and p135+ (purple), TH (red), and LAMP2 (green) in the SNr of six-month-old nTg and *G59S Tg* mice. Scale bar: 20 μm. (B) Immunofluorescent images show the staining of p150^{Glued} and p135+ (purple), TH (red), and ubiquitin (green) in the SNr of six-month-old *nTg* and *G59S Tg* mice. Scale bar: 20 μm.

Thus, our data demonstrate that both G59S and G71R mutant p150^{Glued} are pathogenic to the nigrostriatal DA pathway *in vivo*, but differentially impair the survival and functions of midbrain DA neurons. The finding on G59S mutation is unexpected since the mutation was particularly linked to a slowly progressive autosomal dominant form of lower motor neuron disease, the distal hereditary motor neuropathy 7B (HMN7B)[6]. Our previous study showed that both homozygous *Dctn1* knock-out mice and homozygous *DCTN1* G59S knock-in mice died during early embryogenesis, indicating the loss-of-function nature of G59S mutation[20]. Furthermore, we found that the G59S mutation disrupts the stability of p150^{Glued} protein, so we could not detect any expression and accumulation of p150^{Glued} protein in the tissues of homozygous *DCTN1* G59S knock-in embryos[20]. By contrast, in the *G59S Tg* mice, an artificial overexpression of G59S mutation in DA neurons led to an extensive accumulation of misfolded p150^{Glued} proteins, which may overwhelm the protein degradation system in the DA neurons and eventually induce cell death. Therefore, the overexpression data in either cell or animal models must be interpreted with caution.

Microtubule-binding domains in p150^{Glued} are required for the initiation of retrograde axonal transport, stability of axonal microtubules, and integrity of axon terminals[13-16]. Accordingly, degeneration of ventral root axons and disruption of neuromuscular junctions have been observed in G59S mutant p150^{Glued} transgenic mice[21,22]. In line with these earlier findings, the current study revealed that expression of either G59S or G71R mutant p150^{Glued} in midbrain DA neurons resulted in substantial dysfunction and degeneration of DA axon terminals in the striatum. Additionally, our study showed expression of either G59S or G71R mutant p150^{Glued} in midbrain DA neurons led to the dystrophy of DA neurites in the SNr, indicating an essential role of p150^{Glued} in maintaining the structural integrity of both axons and dendrites of DA neurons. Future studies will be needed to determine the underlying mechanism of how mutant p150^{Glued} triggers the structural and functional changes of distal and proximal DA neurites.

Several mechanisms have been hypothesized to address the selective degeneration of motor neurons caused by G59S mutant p150^{Glued}, including impaired retrograde axonal transport of trophic signaling, defects of vesicular trafficking in the ER-Golgi secretory pathway, aberrant autophagosome-lysosome degradative pathway, and cytotoxicity of mutant p150^{Glued} aggregates[17,21,22]. However, due to the lack of appropriate animal models, mechanisms for the selective degeneration of DA neurons in Perry syndrome have been poorly understood. Until recently, *DCTN1* G71A knock-in mice were generated, and homozygous knock-in mice died prenatally, suggesting a potential loss-of-function nature of the mutation[24]. In the heterozygous *DCTN1* G71A knock-in mice, a reduction of TH immunoreactivity in DA neurons was reported[24]. However, the effect of mutant p150^{Glued} on dopamine transmission and the related regulating proteins remains to be determined. Our HPLC and FSCV studies revealed that overexpression of human G71R p150^{Glued} in midbrain DA neurons led to substantial dopamine deficiency, significantly decreased dopamine release, and slower dopamine uptake, reflecting the severe and early-onset loss of DA neurons and axons. In contrast, overexpression of human G71R p150^{Glued} in midbrain DA neurons resulted in early-onset substantially increased dopamine release and slower dopamine uptake long before the loss of DA axons and the deficiency of dopamine content in the striatum occurred, indicating the early-onset dysfunction of DAT. Correlatively, Western blot analysis demonstrated that overexpression of either G59S or G71R mutant p150^{Glued} in midbrain DA neurons preferentially downregulated the expression of DAT at DA axon terminals. Further investigation will be required to unmask the specific cellular mechanisms leading to the DAT dysfunction and the selective cell death of DA neurons in Perry syndrome.

G59S mutation, as well as all the Perry syndrome-causative mutations, occurs within or close to the CAP-Gly domain of p150^{Glued}, causing loss of function of the MTBDs[6-8]. G59S mutant p150^{Glued} is prone to misfold and form cytoplasmic aggregates leading to enhanced cell death both *in vitro* and *in vivo*, suggesting both loss-of-function and toxic-gain-of-function mechanisms are involved in G59S mutation-induced neurodegeneration[17,21]. Perry syndrome-related G71A mutant p150^{Glued} has been reported to aggregate less than G59S mutant p150^{Glued} when overexpressed in HeLa cells[18]. Moreover, no evident p150^{Glued} aggregates are observed in G71A transgenic mice[23]. In line with these earlier findings, our study revealed that neither wild-type nor G71R mutant p150^{Glued} formed aggregates *in vivo* when overexpressed in midbrain DA neurons. In contrast, G59S mutant p150^{Glued} formed aggregates in an age-dependent way when overexpressed in mouse midbrain DA neurons. Moreover, co-aggregation of dynactin and dynein subunits with G59S mutation-induced p150^{Glued} aggregates was observed inside the dystrophic DA neurites of *G59S Tg* mice. The data suggest the sequestration of active motors in aggregates; the restricted accessibility of adaptors, cargoes, and regulatory proteins to dynein/dynactin; and thus the impairment of normal functions of dynein/dynactin in the midbrain DA neurons. In addition, co-localization of lysosomes with G59S mutation-induced p150^{Glued} aggregates and upregulated ubiquitination were found within the dystrophic DA neurites of *G59S Tg* mice, implying the disruption of the degradative pathway in the midbrain DA neurons.

These observations may explain why the degeneration of the nigrostriatal DA pathway in *G59S Tg* mice is more early-onset and severe than in *G71R Tg* mice in our study. Future studies will explore whether overexpression of exogenous G59S or G71R mutant p150^{Glued} compromises the normal functions of endogenous dynactin p150^{Glued} in the midbrain DA neurons to test if there is a dominant-negative mechanism for *DCTN1* mutation-induced degeneration of nigrostriatal DA pathway.

While the present study focused on the role of mutant p150^{Glued} in Perry syndrome-related parkinsonism and the underlying degeneration of midbrain DA neurons, the pathophysiological basis and pathogenic mechanisms of other Perry syndrome-related symptoms remain to be delineated in detail, including apathy/depression and central hypoventilation[9,10]. Except for the loss of midbrain DA neurons, Perry syndrome patients also display marked degeneration of norepinephrine neurons in *locus coeruleus* and serotonergic neurons in the medullary raphe and ventrolateral medulla[34,35]. Future studies will be needed to crossbreed our tetO-human *DCTN1* with suitable tTA lines and determine the pathogenic significance of mutant p150^{Glued} on norepinephrine neurons and serotonergic neurons.

In summary, our findings show selective expression of either G59S or G71R mutant p150^{Glued} in mouse midbrain DA neurons leads to parkinsonism-like motor abnormalities and degeneration of the nigrostriatal DA pathway, recapitulating some key clinical and pathological features of Perry syndrome. Moreover, G59S and G71R mutant p150^{Glued} exhibit differential pathogenic impact on the survival and function of midbrain DA neurons *in vivo*. The p150^{Glued} transgenic moue models provide valuable tools for mechanistic insights and therapeutic targets of DA neuron degeneration in Perry syndrome.

DECLARATIONS

Acknowledgments

The authors thank Dr. David M Lovinger of National Institute on Alcohol Abuse and Alcoholism for assisting the FSCV recording, members of Cai and Yu Labs for various supports, and Beijing Hospital Authority for the Science & Technology Innovation Program and High-level Talents Program.

Authors' contributions

Designed the study, analyzed the data, and wrote the manuscript: Cai H, Yu J, Sgobio C
Performed the experiments: Yu J, Sgobio C, Yang X, Peng Y, Chen X, Sun L, Shim H
Read and approved the final version of the manuscript: all authors

Availability of data and materials

Data and materials of the current study will be available upon reasonable request.

Financial support and sponsorship

This work was supported by the intramural research programs of National Institute on Aging (AG000946), National Natural Science Foundation of China (No. 82071438 and 81601117), Beijing Natural Science Foundation (No. 7202077), Beijing BaiQianWan Talents Project (No. 2017002), and Beijing Nova Program (No. xx2018099).

Conflicts of interest

All authors declared that there are no conflicts of interest.

Ethical approval and consent to participate

All animal procedures conformed to the NIH (13-040) guide for the ethical care and use of laboratory animals. Animal protocols were approved by the Institutional Animal Care and Use Committee of National

Institute on Aging and Beijing Geriatric Hospital.

Consent for publication

Not applicable.

Copyright

REFERENCES

1. Reck-Peterson SL, Redwine WB, Vale RD, Carter AP. The cytoplasmic dynein transport machinery and its many cargoes. *Nat Rev Mol Cell Biol* 2018;19:382-98. DOI PubMed PMC
2. Cianfrocco MA, DeSantis ME, Leschziner AE, Reck-Peterson SL. Mechanism and regulation of cytoplasmic dynein. *Annu Rev Cell Dev Biol* 2015;31:83-108. DOI PubMed PMC
3. Bercier V, Hubbard JM, Fidelin K, et al. Dynactin1 depletion leads to neuromuscular synapse instability and functional abnormalities. *Mol Neurodegener* 2019;14:27. DOI PubMed PMC
4. Schroer TA. Dynactin. *Annu Rev Cell Dev Biol* 2004;20:759-79. DOI PubMed
5. Konno T, Ross OA, Teive HAG, Sławek J, Dickson DW, Wszolek ZK. DCTN1-related neurodegeneration: Perry syndrome and beyond. *Parkinsonism Relat Disord* 2017;41:14-24. DOI PubMed PMC
6. Puls I, Jonnakuty C, LaMonte BH, et al. Mutant dynactin in motor neuron disease. *Nat Genet* 2003;33:455-6. DOI PubMed
7. Farrer MJ, Hulihan MM, Kachergus JM, et al. DCTN1 mutations in Perry syndrome. *Nat Genet* 2009;41:163-5. DOI PubMed PMC
8. Zhang J, Wang H, Liu W, et al. A novel Q93H missense mutation in DCTN1 caused distal hereditary motor neuropathy type 7B and Perry syndrome from a Chinese family. *Neurol Sci* 2021;42:3695-705. DOI PubMed
9. Dulski J, Cerquera-Cleves C, Milanowski L, et al. Clinical, pathological and genetic characteristics of Perry disease-new cases and literature review. *Eur J Neurol* 2021;28:4010-21. DOI PubMed
10. Tsuboi Y, Mishima T, Fujioka S. Perry disease: concept of a new disease and clinical diagnostic criteria. *J Mov Disord* 2021;14:1-9. DOI PubMed PMC
11. Dixit R, Levy JR, Tokito M, Ligon LA, Holzbaur EL. Regulation of dynactin through the differential expression of p150Glued isoforms. *J Biol Chem* 2008;283:33611-9. DOI PubMed PMC
12. Zhapparova ON, Bryantseva SA, Dergunova LV, et al. Dynactin subunit p150Glued isoforms notable for differential interaction with microtubules. *Traffic* 2009;10:1635-46. DOI PubMed
13. Lloyd TE, Machamer J, O'Hara K, et al. The p150(Glued) CAP-Gly domain regulates initiation of retrograde transport at synaptic termini. *Neuron* 2012;74:344-60. DOI PubMed PMC
14. Moughamian AJ, Holzbaur EL. Dynactin is required for transport initiation from the distal axon. *Neuron* 2012;74:331-43. DOI PubMed PMC
15. Lazarus JE, Moughamian AJ, Tokito MK, Holzbaur EL. Dynactin subunit p150(Glued) is a neuron-specific anti-catastrophe factor. *PLoS Biol* 2013;11:e1001611. DOI PubMed PMC
16. Yu J, Lai C, Shim H, et al. Genetic ablation of dynactin $p150^{Glued}$ in postnatal neurons causes preferential degeneration of spinal motor neurons in aged mice. *Mol Neurodegener* 2018;13:10. DOI PubMed PMC
17. Levy JR, Sumner CJ, Caviston JP, et al. A motor neuron disease-associated mutation in p150Glued perturbs dynactin function and induces protein aggregation. *J Cell Biol* 2006;172:733-45. DOI PubMed PMC
18. Ishikawa K, Saiki S, Furuya N, et al. P150glued-associated disorders are caused by activation of intrinsic apoptotic pathway. *PLoS One* 2014;9:e94645. DOI PubMed PMC
19. Mishima T, Ishikawa T, Imamura K, et al. Cytoplasmic aggregates of dynactin in iPSC-derived tyrosine hydroxylase-positive neurons from a patient with Perry syndrome. *Parkinsonism Relat Disord* 2016;30:67-72. DOI PubMed
20. Lai C, Lin X, Chandran J, Shim H, Yang WJ, Cai H. The G59S mutation in p150(glued) causes dysfunction of dynactin in mice. *J Neurosci* 2007;27:13982-90. DOI PubMed PMC
21. Laird FM, Farah MH, Ackerley S, et al. Motor neuron disease occurring in a mutant dynactin mouse model is characterized by defects in vesicular trafficking. *J Neurosci* 2008;28:1997-2005. DOI PubMed PMC
22. Chevalier-Larsen ES, Wallace KE, Pennise CR, Holzbaur EL. Lysosomal proliferation and distal degeneration in motor neurons expressing the G59S mutation in the p150Glued subunit of dynactin. *Hum Mol Genet* 2008;17:1946-55. DOI PubMed PMC
23. Mishima T, Deshimaru M, Watanabe T, et al. Behavioral defects in a $DCTN1^{G71A}$ transgenic mouse model of Perry syndrome. *Neurosci Lett* 2018;666:98-103. DOI PubMed
24. Deshimaru M, Mishima T, Watanabe T, et al. Behavioral profile in a $Dctn1^{G71A}$ knock-in mouse model of Perry disease. *Neurosci Lett* 2021;764:136234. DOI PubMed
25. Wang L, Xie C, Greggio E, et al. The chaperone activity of heat shock protein 90 is critical for maintaining the stability of leucine-rich repeat kinase 2. *J Neurosci* 2008;28:3384-91. DOI PubMed PMC
26. Lin X, Parisiadou L, Gu XL, et al. Leucine-rich repeat kinase 2 regulates the progression of neuropathology induced by Parkinson's-

disease-related mutant alpha-synuclein. *Neuron* 2009;64:807-27. DOI PubMed PMC

27. Schmoldt A, Benthe HF, Haberland G. Digitoxin metabolism by rat liver microsomes. *Biochem Pharmacol* 1975;24:1639-41. PubMed
28. Liu G, Sgobio C, Gu X, et al. Selective expression of Parkinson's disease-related Leucine-rich repeat kinase 2 G2019S missense mutation in midbrain dopaminergic neurons impairs dopamine release and dopaminergic gene expression. *Hum Mol Genet* 2015;24:5299-312. DOI PubMed PMC
29. Yorgason JT, España RA, Jones SR. Demon voltammetry and analysis software: analysis of cocaine-induced alterations in dopamine signaling using multiple kinetic measures. *J Neurosci Methods* 2011;202:158-64. DOI PubMed PMC
30. Felicio AC, Dinelle K, Agarwal PA, et al. In vivo dopaminergic and serotonergic dysfunction in DCTN1 gene mutation carriers. *Mov Disord* 2014;29:1197-201. DOI PubMed PMC
31. Chung EJ, Hwang JH, Lee MJ, et al. Expansion of the clinicopathological and mutational spectrum of Perry syndrome. *Parkinsonism Relat Disord* 2014;20:388-93. DOI PubMed
32. Nagatsu T, Nakashima A, Ichinose H, Kobayashi K. Human tyrosine hydroxylase in Parkinson's disease and in related disorders. *J Neural Transm (Vienna)* 2019;126:397-409. DOI PubMed
33. Mulvihill KG. Presynaptic regulation of dopamine release: role of the DAT and VMAT2 transporters. *Neurochem Int* 2019;122:94-105. DOI PubMed
34. Wider C, Dickson DW, Stoessl AJ, et al. Pallidonigral TDP-43 pathology in Perry syndrome. *Parkinsonism Relat Disord* 2009;15:281-6. DOI PubMed PMC
35. Tsuboi Y, Dickson DW, Nabeshima K, et al. Neurodegeneration involving putative respiratory neurons in Perry syndrome. *Acta Neuropathol* 2008;115:263-8. DOI PubMed

Habiba *et al. Ageing Neur Dis* 2022;2:7
DOI: 10.20517/and.2022.06

Ageing and Neurodegenerative Diseases

Original Article

Open Access

A sequential deposition of amyloid beta oligomers, plaques and phosphorylated tau occurs throughout life in the canine retina

Umma Habiba[1], John Morley[1], Mark Krockenberger[2], Brian A. Summers[3], Mourad Tayebi[1]

[1]School of Medicine, Western Sydney University, Campbelltown, NSW 2560, Australia.
[2]Faculty of Science, University of Sydney, Camperdown, NSW 2050, Australia.
[3]School of Veterinary Medicine, Melbourne University, Victoria, Werribee 3030, Australia.

Correspondence to: Dr. Mourad Tayebi, School of Medicine, Western Sydney University, Campbelltown, NSW 2560, Australia. E-mail: m.tayebi@westernsydney.edu.au

How to cite this article: Habiba U, Morley J, Krockenberger M, Summers BA, Tayebi M. A sequential deposition of amyloid beta oligomers, plaques and phosphorylated tau occurs throughout life in the canine retina. *Ageing Neur Dis* 2022;2:7. https://dx.doi.org/10.20517/and.2022.06

Received: 25 Feb 2022 **First Decision:** 21 Mar 2022 **Revised:** 25 Apr 2022 **Accepted:** 18 May 2022 **Published:** 25 May 2022

Academic Editor: Wei-Dong Le **Copy Editor:** Peng-Juan Wen **Production Editor:** Peng-Juan Wen

Abstract

Aims: Cerebral amyloid burdens may be found in otherwise cognitively intact adults, often not showing worsening deficits with passing years. Alzheimer's transgenic rodents have been widely used to investigate this phenomenon, but a spontaneous disorder in other animals, such as dogs that cohabit with humans and thus may have some shared environmental risks, may contribute and offer opportunities not possible in the smaller laboratory animals. In animals, the spontaneous disorder most comparable to Alzheimer's disease (AD) affects mature to aged dogs and is designated canine cognitive dysfunction. Motivated by AD, many studies have revealed that amyloid progressively accumulates in the canine central nervous system, including the retina. Here, we investigated whether deposits of amyloid and/or tau can be found in the canine retina of neurologically normal animals from the first year of life to the elderly. Suppose canine ocular amyloid and tau are present from early life. In that case, that raises the question of whether similar patterns of accumulation occur in man, whether as part of aging, AD, or other.

Methods: This study used eye tissues from 30 dogs with a variety of ophthalmic or other orbital disorders, of which 7/30 were 1-2 years old. Tissues were subdivided into dogs of three different age groups: young (1-5 years old), middle (6-10 years old), and old (≥ 11 years old).

Results: Following immunostaining of tissue sections with nanobodies against retinal $A\beta_{1-40}$ and $A\beta_{1-42}$ oligomers, and antibodies against Aβ plaques (Aβp) and hyperphosphorylated Tau (p-Tau), our investigations revealed that accumulation of $A\beta_{1-40}$ and $A\beta_{1-42}$ oligomers were widespread in the retina in all age groups. In contrast, Aβp were detected in the middle and old age groups but not in the young age group. Furthermore, p-Tau staining was observed in four old dogs only, while other dogs were p-Tau free. Interestingly, both Aβo and Aβp co-localized in the middle and old age groups of dogs. Moreover, diffuse granular p-Tau co-localized with intracellular Aβo in the old age group. Finally, we also observed co-localization of Aβo and Aβp in the retinal vasculature which might be similar to cerebral amyloid angiopathy associated with AD.

Conclusion: As far as we know, the presence of amyloid and tau in the canine retina is hitherto unreported. If similar, early-in-life subclinical retinal deposits occur in a human cohort perhaps identified by AD genetic risk factors, following this group may offer the prospect of preclinical therapeutic intervention in imminent dementia, a strategy recognized as likely necessary to impact this burgeoning disorder.

Keywords: Alzheimer's disease, canine cognitive dysfunction, retina, early diagnosis, Aβo, Aβp, p-Tau

INTRODUCTION

The principal neuropathological lesions in Alzheimer's disease (AD) brains include extracellular neuritic and/or diffuse plaques containing amyloid-beta (Aβ), intracellular tau protein (p-Tau) in the form of neurofibrillary tangles (NFTs) in addition to cerebral amyloid angiopathy (CAA), ubiquitin, severe synaptic loss, neuronal death, and brain atrophy[1-4]. While the deposition of Aβ in the human brain has traditionally been accepted as a major hallmark of AD[5], its accumulation is also observed in about 20% of cognitively unimpaired, aged individuals[6,7]. For decades, the association of Aβ with AD has been demonstrated, but the significance and impact of Aβ accumulation in healthy individuals are both poorly understood[8] and a source of confusion. For example, previous studies did not establish a clear correlation with memory loss in the aging brain[9-11]. Previous reports documented the progressive accumulation of both Aβ plaques (Aβp) in the brain[12,13] and Aβ oligomers (Aβo) in the brain and periphery of cognitively unimpaired individuals[14,15]. A study by Lesne *et al.* measured the levels of three Aβo "species", including Aβ trimers, Aβ*56 and Aβ dimers, in brain tissues from 75 cognitively unimpaired individuals, including young children and adolescents[14]. The authors showed that Aβ trimers were present in the central nervous system (CNS) of children and adolescents, and their levels increased progressively with age, suggesting that this particular Aβo could be used to track the potential progression into AD from a very young age. Another study investigated the relationship between amyloid levels and memory performance[15]. This study, which included 147 participants divided into three groups of adults 30-49, 50-69, and 70-89 years of age, established a clear relationship between episodic memory performance and amyloid accumulation in the youngest group[15]. A longitudinal study by Hanseeuw *et al.* demonstrated a correlation between Aβ/p-Tau and declining cognition in 60 clinically normal individuals aged between 65-85 years[16]. The authors concluded that there was a positive correlation between Aβ/p-Tau positron emission tomography (PET) and cognition, where participants with high Aβ and tau were at higher risk of developing mild cognitive impairment (MCI)[16]. These studies highlighted the importance of investigating and characterizing normal aging in cognitively unimpaired younger individuals to identify those at risk of progressive increase of AD-associated neuropathology changes and cognitive impairment and establish a time frame for early diagnostic and therapeutic intervention. However, such studies are difficult to implement in human subjects and will take decades to deliver any meaningful outcome[8,17].

Currently available transgenic animal models of AD do not replicate the subtle clinical and pathological features of the disease, as demonstrated by their lack of reproducible therapeutic outcomes[18,19]. As to the dog's age, there is an anatomically defined accumulation of Aβ peptides in the CNS, while less is known about cerebral p-Tau deposition. Some animals will develop a progressive cognitive decline with loss of learned behaviors and memory, a syndrome named canine cognitive dysfunction (CCD)[20-24], with CNS changes similar to the neuropathological hallmarks characteristic of AD[25-28]. In those destined to develop AD, amyloid precursor protein (APP) is sequentially cleaved by β and γ secretase leading to the production of Aβ peptide fragments (36-43 amino acids), which then aggregate and deposit as plaques[4,5,29]. The canine APP and Aβ peptides are 98% and 100% identical to their human counterparts[24]. In older dogs and others affected with CCD, Aβ deposits as diffuse plaques, while the dense core of humans' mature plaques is very rare or absent[20,21,27,30].

There are two major isoforms of Aβ, $Aβ_{1-40}$ (~80%-90%) and $Aβ_{1-42}$ (~5%-10%) and three major assemblies[31-34] recognized in man and animals/dogs, including monomeric Aβ, Aβo containing 12-24 monomers which become elongated to form protofibrils and finally insoluble fibrils[35]. Among these three stages, Aβo is thought to be the most toxic to neurons and responsible for the structural and functional pathologic changes associated with AD[36-39]. Likewise, a previous study reported that cognitive decline occurs before the accumulation of Aβp in CCD, supporting the premise that earlier assembly states of Aβ may be the toxic species[23]. In addition, CAA, ubiquitin, and severe synaptic loss have also been reported in CCD[20,40-43]. Another cardinal pathological hallmark of AD is the accumulation of p-Tau[3,4]. Several phosphorylation sites were identified on tau in aged dogs including Thr181[42], Ser422[43], Ser202/Thr205[40,43], Ser396[30,40,43], Ser189, and Ser207[44]; however, demonstrating the presence of NFTs has been infrequent compared to the consistent demonstration of amyloid oligomers and diffuse plaques. A study by Schmidt and colleagues using anti-pT205, AT8, AT100, PHF-1, and anti-pT422 antibodies seeking the presence of tau pathology in 24 dogs aged between two and nineteen years, showed that three 13-15-year-old dogs displayed p-Tau and only one 15-year-old Pekingese dog displayed NFT-like appearance[43].

In AD, visual disturbances are one of the early complaints and include loss of color vision, impairment of peripheral vision and object recognition, contrast sensitivity, and decreased visual memory and perception[45-47]. A recent longitudinal study of 1349 older adults showed that poor visual acuity paralleled the development of dementia[48], suggesting the possibility that ocular disturbances can be used as an early predictor of dementia risk in the older population[48]. Moreover, post-mortem studies of AD and animal models of AD demonstrated a strong association between retinal accumulation of Aβo[49,50]. Aβ plaques[51,52], p-Tau[53,54] and brain depositions and cognitive decline, where retinal Aβo was shown to deposit earlier than the brain and before deficits in cognition. Although, to our knowledge, age-dependent retinal deposition of Aβo and/or Aβp has not been investigated in AD and cognitively unimpaired individuals, including children and adolescents, our recent studies in AD mice models confirmed the conversion of cerebral and retinal Aβ o to Aβp in an age-dependent manner, where retinal Aβo was detected as early as 3-month old APP/PS1 mice, before brain pathology and cognitive decline were observed[49,55].

In this study, we investigated the retinal accumulation of Aβo, Aβp, and p-Tau in three age groups of genetically diverse and neurologically intact populations of dogs. Here, following immunohistochemistry and immunofluorescence analysis, we confirmed the presence of retinal $Aβ_{40}$ and $Aβ_{42}$ oligomers, Aβp, and p-Tau. Retinal $Aβ_{40}$ and $Aβ_{42}$ oligomers deposition was conspicuous and widespread and observed in all age groups, including the young 1-5-year-old neurologically intact group. Moreover, retinal co-localization of

$A\beta_{40}/A\beta_{42}$ oligomers and Aβp was observed in few middle-aged dogs and most dogs in the old neurologically intact age group, while retinal co-localization of $A\beta_{40}/A\beta_{42}$ oligomers and p-Tau was only seen in the old neurologically intact age group of dogs. Morphologically, extracellular Aβp deposits appeared as small, dot-like rounded deposits, while intracellular p-Tau deposits adopted a diffuse appearance in the retinal layers[54]. No NFTs or neuropil threads were observed in these dogs. Taken together, these results highlight the importance of further investigations of AD-related pathology in the retina of presymptomatic children and adolescents to gain insight into disease progression and potentially identify early at-risk individuals to help implement speedy therapeutic interventions.

METHODS

Dog eye samples and animal ethics

Sections of eyes used in this study were prepared from archived cases in the Comparative Ocular Pathology Laboratory of Wisconsin (COPLOW) at the Department of Pathobiological Sciences, School of Veterinary Medicine, University of Wisconsin, Madison. Surgical enucleations had been submitted by practicing veterinarians to COPLOW for routine pathological diagnosis. These canine eyes came from 30 random, genetically diverse dogs (15 different breeds) ranging from 1 to 16 years of age with a broad variety of ocular disorders [Tables 1 and 2]. Such tissues, historically submitted for disease investigation purposes, are not subject to approval by institutional animal ethical regulations.

Tissue preparation

Enucleated eyes were submitted to the laboratory fixed in 10% neutral buffered formalin. On receipt, they were examined for gross abnormalities before trimming, followed by processing overnight using a Leica ASP300S tissue processor (Leica biosystem, Wetzlar, Germany). Tissues were then embedded in paraffin blocks and sectioned at 4μm thickness using a Leica RM2235 microtome (Leica biosystem, Wetzlar, Germany) and placed on charged slides. Sections were then stained with hematoxylin and eosin (H&E) and Congo red (CR). Further sections were used for immunohistochemistry (IHC) and immunofluorescence (IF) staining, and both upper and lower parts of the retina were assessed.

Hematoxylin and eosin staining

Paraffin sections were dewaxed by two changes of absolute xylene for 5 min each. Sections were rehydrated using two changes of 100% ethanol for 2 min each, 95% ethanol for 3 min, 70% ethanol for 2 min, and finally rinsed in deionized water for 2 min. H&E stain was then performed by adding Gill ll Haematoxylin solution (Leica Biosystems, Wetzlar, Germany), followed by 1% acid alcohol and subsequently eosin stain (Leica Biosystems, Wetzlar, Germany). Finally, the sections were dehydrated with increasing concentrations of ethanol, from 70%, 95% to 100%, then dewaxed by two changes of xylene and finally mounted with xylene-based mounting media (Sigma Aldrich, Missouri, United States)[56]. H&E staining was used to assess retinal morphology, the neuronal population within the eye.

Congo red staining

Initially, the CR working solution was prepared by mixing 50 ml Congo red solution and 0.5 ml potassium hydroxide solution supplied in the Congo red amyloid special stain kit (Leica Biosystems, Wetzlar, Germany). Retinal sections were placed in the working solution for 20 min and then rinsed in 5-8 changes of deionized water. This was followed by staining with Gill ll Haematoxylin (Leica Biosystems, Wetzlar, Germany) for 1-3 min and rinsing in 3 changes of deionized water. Sections were then dehydrated in two changes of 95% alcohol followed by three changes of absolute alcohol for one minute each. Finally, the sections were cleared in two changes of xylene and mounted in a xylene miscible medium. Amyloid fibrils appeared as dull to red brick under light microscopy (Olympus CX 43, Shinjuku, Tokyo, Japan) and apple green birefringent under polarized light (Olympus CX 43, Shinjuku, Tokyo, Japan).

Table 1. Signalment for 30 dogs and their retinal Aβ oligomers and plaques IHC scores

Age groups	Age (year)	Sex	Breed	Size	Pathological Aβ IHC findings in the dog retina	
					A11 - Aβ oligomers	4G8 - Aβ plaques
Young (1-5 years)	1	SF	Staffordshire terrier	Medium	+	-
	1.4	M	Siberian husky	Medium	-	-
	1.8	SF	Mixed breed	ND*	+++	-
	1.10	SF	Siberian husky	Medium	++	-
	2	F	Chihuahua mix	Toy	+++	-
	2	M	Bichon frise mix	Small	+	-
	2	NM	Shih Tzu	Small	+	-
	3	NM	German shepherd	Large	+++	-
	3	F	Giant schnauzer	Large	+	-
	3.6	M	Siberian husky	Medium	+	-
Middle age (6-10 years)	7	NM	Hound mixed	Medium	-	-
	8	SF	Bedlington terrier	Small	-	-
	8	SF	Cocker spaniel	Medium	-	-
	8	M	Mixed breed	ND*	-	-
	8	M	Cocker spaniel	Medium	+	-
	8	F	German shepherd mix	Large	-	-
	8	SF	Great dane dog	Giant	-	-
	9	M	Jack Russell terrier dog	Small	-	-
	9.5	SF	Boxer dog	Large	-	-
	9.9	SF	Cocker spaniel	Medium	-	-
Elderly (11-16 years)	11	NM	Mixed breed	ND*	-	-
	11	NM	Beagle	Small	-	-
	11.9	SF	Bouvier des flanders	Large	+	-
	12	SF	German shepherd	Large	-	++
	12	SF	German shepherd mix	Large	-	-
	12	NM	Husky mix	Medium	-	-
	12.8	NM	Shih-tzu	Small	-	++
	13	NM	Border collie	Medium	-	-
	15	SF	Basset hound	Medium	-	+
	16	SF	Shih Tzu	Small	-	-

Sizes were determined according to the American Kennel Club (AKC)[76]. Size range between 34 - ≥ 54 kg is considered "giant", 24-38 kg is considered "large", 15-29 kg is considered "medium", 3-15 kg is considered "small", and 0.9-4 kg is considered "toy". Aβ oligomers and Aβ plaques staining intensity were semi-quantitatively analyzed and scored across the retinal layers under the brightfield microscope (Olympus CX 43, Shinjuku, Tokyo, Japan). The total area was examined at 40 magnification and categorized into no immunostaining "-"; low immunoreactivity found only in limited areas of the retinal layers "+", moderate immunoreactivity where Aβ deposits were more apparent "++"; and finally strong immunoreactivity with widespread A11 and 4G8 positive Aβ labeling were exhibited "+++". ND*: Not determined; SF: spayed female; F: female; NM: neutered male; M: male; IHC: immunohistochemical.

Immunohistochemical staining of amyloid-beta plaques and amyloid-beta oligomers

Eye sections that contained the retina were pre-treated using the 2100 antigen retriever (Aptum Biologics Ltd, Southampton, United Kingdom) to expose the target epitopes. The sections were then treated with 90% formic acid for 5 min at room temperature (RT) followed by cell membrane permeabilization, achieved by using 0.1% Triton X for 1 min before the addition of 0.3% H_2O_2 for 15 min to inactivate endogenous peroxidases. Sections were then blocked with protein block serum-free (Agilent, City, Country) for 15 min. The sections were then stained for 1 h with the following primary antibodies in phosphate-buffered saline (PBS): mouse purified 4G8 anti-$A\beta_{17-24}$ (1:500; Bio legend, San Diego, CA, USA) or A11 rabbit anti-Aβo (1:250; Merck Millipore, Burlington, MA, USA) antibodies. After washing with PBS, sections were

Table 2. Signalment for 30 dogs, their ophthalmological disorders, and retinal Aβ and p-Tau IF scores

Age groups	Age (year)	Sex	Breed	Size	Ophthalmological disorders which resulted in enucleation	Pathological IF findings in the dog retina			
						$A\beta_{40}$ oligomers	$A\beta_{42}$ oligomers	Aβ	p-Tau
Young (1-5 years)	1	SF	Staffordshire terrier	Medium	Anterior segment dysgenesis	+	+	-	-
	1.4	M	Siberian husky	Medium	Anterior segment dysgenesis	-	-	-	-
	1.8	SF	Mixed breed	ND*	Anterior segment dysgenesis	+++	+++	-	-
	1.10	SF	Siberian husky	Medium	Anterior segment dysgenesis	+++	+++	-	-
	2	F	Chihuahua mix	Toy	Anterior segment dysgenesis	+++	+++	-	-
	2	M	Bichon frise mix	Small	Proptosis	+++	+++	-	-
	2	NM	Shih Tzu	Small	Melanoma limbal	++	++	-	-
	3	NM	German shepherd	Large	Rhabdomyosarcoma orbital	+++	+++	-	-
	3	F	Giant schnauzer	Large	Phthisis bulbi	++	++	-	-
	3.6	M	Siberian husky	Medium	Anterior segment dysgenesis	++	++	-	-
Middle age (6-10 years)	7	NM	Hound mixed	Medium	Hemangiosarcoma	-	-	-	-
	8	SF	Bedlington terrier	Small	Neoplasia	-	-	-	-
	8	SF	Cocker spaniel	Medium	Conjunctivitis	+++	+++	+	-
	8	M	Mixed breed	ND*	Conjunctival melanoma	+++	+++	+	-
	8	M	Cocker spaniel	Medium	Pre glaucoma	+++	+++	+++	-
	8	F	German shepherd mix	Large	Mast cell tumor	++	++	+	-
	8	SF	Great dane dog	Giant	Complex apocrine adenocarcinoma	+	+	-	-
	9	M	Jack Russell terrier dog	Small	Sialoadenitis	++	++	-	-
	9.5	SF	Boxer dog	Large	Hemangioma	+	+	-	-
	9.9	SF	Cocker spaniel	Medium	Adenocarcinoma a orbital	+++	+++	+++	-
Elderly (11-16 years)	11	NM	Mixed breed	ND*	Squamous cell carcinoma	-	-	-	-
	11	NM	Beagle	Small	Melanoma conjunctival	+++	+++	+++	-
	11.9	SF	Bouvier des flanders	Large	Melanoma eyelid	+	+	-	-
	12	SF	German shepherd	Large	Melanoma eyelid	+++	+++	+++	+++
	12	SF	German shepherd mix	Large	Melanoma conjunctival	+++	+++	+++	-
	12	NM	Husky mix	Medium	Orbital carcinoma	+++	+++	++	+++
	12.8	NM	Shih-tzu	Small	Glaucoma	+++	+++	++	+++
	13	NM	Border collie	Medium	Melanoma skin	+++	+++	+++	+++
	15	SF	Basset hound	Medium	Conjunctival hemangiosarcoma	+++	+++	+++	-
	16	SF	Shih Tzu	Small	Squamous cell carcinoma	+	+	-	-

Existing ophthalmological conditions of the 30 neurologically intact unimpaired dogs were determined from the clinical report. Sizes were determined according to the American Kennel Club (AKC). Size range between 34 - ≥ 54 kg is considered "giant", 24-38 kg is considered "large", 15-29 kg is considered "medium", 3-15 kg is considered "small", and 0.9-4 kg is considered "toy". Aβ oligomers Aβ plaques and p-Tau staining intensity were semi-quantitatively analyzed and scored across the retinal layers under the confocal microscope (LSM800, Zeiss, Oberkochen, Germany). The total area was examined at 40 magnification and categorized into no immunostaining "-"; low immunoreactivity found only in limited areas of the retinal layers "+", moderate immunoreactivity where deposits were more apparent "++"; and finally strong immunoreactivity with widespread Aβo, Aβp, and p-Tau labeling was exhibited "+++". ND*: Not determined; SF: spayed female; F: Female; NM: neutered male; M: male; IF: immunofluorescence.

incubated for 1 h at RT with the following secondary antibodies in PBS: HRP-conjugated anti-mouse IgG (Sigma-Aldrich, Missouri, United States) or anti-rabbit IgG (Sigma-Aldrich, Missouri, United States). The

sections were then washed three times with PBS before the addition of the 3,3'-Diaminobenzidine substrate chromogen system and incubated for 5-10 min. The sections were then counterstained with hematoxylin for 1 min before mounting. Sections were finally imaged using Olympus CX 43 light microscopy (Shinjuku, Tokyo, Japan).

The staining intensity was semi-quantitatively analyzed and scored across the retinal layers. Each bright field was examined at 40× magnification and categorized into no immunostaining "-"; low immunoreactivity, found in limited areas of the retinal layers "+"; moderate immunoreactivity where Aβ deposits were numerous "++"; and finally strong immunoreactivity with widespread A11 and 4G8 positive Aβ labeling "+++" [Table 1].

Immunofluorescence detection and co-localization studies

To investigate whether Aβo co-localized with Aβp or with p-Tau, we performed immunofluorescence double labeling using camelid-derived single domain anti-A_{40} (PRIOAD12) or anti-A_{42} (PRIOAD13) oligomer antibodies with 4G8 anti-Aβp antibody (Bio legend, San Diego, California, United States) or anti-phosphorylated tau AT8 antibody targeting amino acid residues Ser202/Thr205 (Thermo-fisher Scientific, Massachusetts, United States). Slides were processed as described above for IHC before adding the primary antibodies. The sections were double-stained with either PRIOAD 12 (1:500) or PRIOAD 13 (1:500)[57] and 4G8 antibody overnight (1:500) or AT8 (1:500) and either PRIOAD 12 (1:500) or PRIOAD 13 (1:500). Sections were then washed in Tris-buffered saline with 0.05% Tween 20 (TBST) and incubated with secondary antibodies at a dilution of 1:500, including goat anti-llama IgG conjugated to FITC (Bethyl Laboratories, Inc, Texas, USA) or donkey-anti-mouse IgG conjugated to Texas red (Sigma-Aldrich, Missouri, United States) for 2 hours at room temperature. Other sections were used as negative control and stained with secondary antibodies with the omission of the primary antibodies. Retinal sections derived from an APP/PS1 and TAU58/2 transgenic mice models[58,59] were used as positive control and stained with anti-Aβ and anti-P-Tau antibodies, respectively. The sections were covered, slipped with paramount aqueous mounting medium (Dako, Agilent, Santa Clara, California, United States), sealed, and dried overnight. Finally, the sections were visualized with LSM800 confocal microscope with a standard FITC/Texas Red double band-pass filter set (Zeiss, Oberkochen, Germany).

RESULTS

Histological assessment of the retina in 30 dogs

We performed H&E staining of the canine eye sections and examined the retinal layers to assess their general morphological appearance and identify pathological changes such as vacuolation, neuronal death, and eosinophilic deposits[49,55]. No specific lesions were observed in the retinal layers of the young and middle age groups (data not shown). However, scattered eosinophilic deposits in the ganglion cell layer (GCL) and inner nuclear layer (INL) of the retina were noticeable in 5/10 dogs in the older age group (11-16 years old), including an 11-year-old Beagle, a 12-year-old German shepherd, a 12-year-old Husky mix, a 12.8-year-old Shih Tzu, and a 15-year-old Basset hound [Figure 1A and B]. Furthermore, CR staining used to detect any amyloid fibrils and CAA in eye sections of the dogs did not display any staining in the retina tissues from all age groups (data not shown).

Immunohistochemical detection of Aβ oligomers and plaques in the retina of 30 dogs

While demonstrated in the CNS of aged animals including cats and bears[24,60], dogs have been more comprehensively studied and shown to develop human type Aβ deposition at a very young age. Retinal tissues stained with A11 exhibited intracellular Aβo depositions in the outer nuclear layer (ONL), INL, and GCL [Figure 1C and D]. The intraneuronal Aβo intensity following A11 staining ranged from low (+), moderate (++) to strong (+++) in all dogs in the young age group except a 1.4 years old male Siberian husky

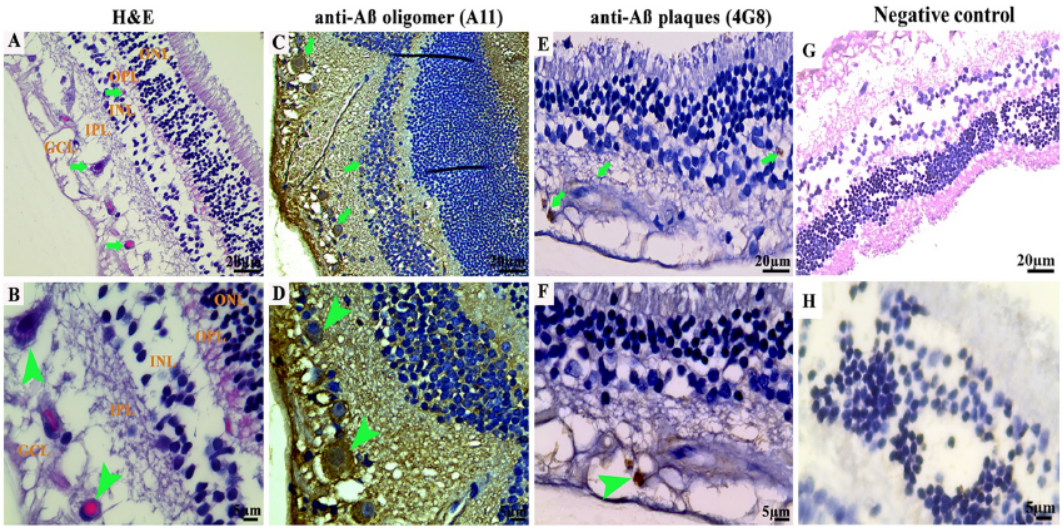

Figure 1. Photomicrographs of the microscopic lesions in the canine retina. The retina in a 12-year-old German shepherd dog. Eosinophilic deposits (green arrows) were observed in the ganglion cell layer (GCL) and inner nuclear layer (INL). Representative of 10 cases of old-aged dogs. Hematoxylin and eosin (H&E) 40×. (B) Higher magnification of the deposits in image (A) (green arrowhead) in the GCL. H&E 100×. (C) Retina of a 3-year-old German shepherd dog. Immunohistochemical staining with A11 anti-Aβo IgG antibody exhibited cytoplasmic Aβo depositions in the GCL and INL (green arrows). Representative of 10 cases of young age group. IHC 40×. (D) Higher magnification of deposits from image (C) in the GCL (green arrowheads). IHC 100×. (E) Retina of a 12-year-old German shepherd mix dog. Immunohistochemical staining with 4G8 anti-Aβp IgG antibody exhibited extracellular Aβ aggregates in the GCL and INL (green arrows). IHC 40×. (F) Higher magnification of deposit from image (E) in the GCL (green arrowhead). (G and H) Representative retinal sections derived from dogs of all age groups stained with secondary antibodies with the omission of the primary antibody did not show any depositions (40× and 100×, respectively). The photomicrographs were taken from the peripheral region of the retina - away from the optic disc. Representative of all 30 dogs examined. IHC 100×. IHC: Immunohistochemistry.

that did not display any A11 positive stain [Supplementary Figure 1A]. Of note, retinal sections derived from wild-type mice were used as negative control following immunofluorescence staining [Supplementary Figure 1B and C].

A spayed female mixed breed aged 1.8 years, a female Chihuahua aged 2 years, and a neutered male German shepherd aged 3 years showed strong (+++) accumulation of A11 positive Aβo [Figure 1C and D]. Two dogs displayed a low amount (+) of A11 positive Aβo in the retinal layers in the middle and old age groups, including an 8-year-old male Cocker spaniel and an 11.9-year-old spayed female Bouvier des Flanders [Table 1]. In addition, 4G8-positive small rounded and dot-like extracellular Aβp deposits were observed in the INL, inner plexiform layer (IPL), and GCL [Figure 1E and F] of the retina. They were structurally different from the typical large diffuse plaques normally observed in dog brains with CCD[21,30,61]. The extracellular Aβp intensity following 4G8 staining ranged from low (+) to moderate (++) in some dogs in the old age group, including a 15-year-old spayed female Basset hound, a 12.8-year-old neutered male Shih Tzu, and a 12-year-old spayed female German shepherd. Other dogs in this age group were all negative for 4G8 staining [Table 1, Figure 1E and F]. Representative retinal sections derived from dogs of all age groups stained with secondary antibodies with the omission of the primary antibody did not show any depositions [Figure 1G and H].

Immunofluorescence detection and co-localization of retinal $A\beta_{40}$, $A\beta_{42}$ oligomers, and Aβ plaques in the retina of 30 dogs

To confirm the presence of retinal $A\beta_{40}$ and $A\beta_{42}$ oligomers and to determine whether $A\beta_{40}$ and/or $A\beta_{42}$ oligomers co-localized with Aβp in the retinas of different age groups and breeds of neurologically intact dogs, we performed immunofluorescence double staining using PRIOAD12 ($A\beta_{40}$ oligomers), PRIOAD13

($A\beta_{42}$ oligomers) camelid-derived single domain anti-Aβ oligomer and 4G8 anti-Aβp antibodies. Morphologically, Aβo appeared as globular and annular in shape[55,62] and deposited intracellularly in the ONL, INL, and GCL [Figures 2-4]. 4G8 positive Aβ plaques appeared morphologically as dot-like and small rounded extracellular deposits[50,54] in the outer plexiform layer (OPL), IPL, and GCL [Figures 2-4]. We found that both $A\beta_{40}$ and $A\beta_{42}$ oligomers staining was widespread in the majority of the dogs in young [Table 2, Figure 2A and B], middle [Table 2, Figure 3A and B], and old age groups [Table 2, Figure 4A and B] except four dogs including a 1.4-years-old male Siberian husky, a 7-years-old neutered male Hound mixed, an 8-years-old spayed female Bedlington terrier and an 11-years-old mixed breed. In comparison, Aβp was absent in young dogs [Table 2, Figure 2C and D], but its presence in the middle age group was moderate [Table 2, Figure 3D and E] and conspicuous in the old age group [Table 2, Figure 4D and E]. Therefore, no co-localization of Aβo and Aβp was noticed in the retinal layers of the young age group [Figure 2E-H]. However, retinal Aβp was shown to co-localize with $A\beta_{40}$ or $A\beta_{42}$ in the GCL, IPL & INL of the middle [Figure 3G, H, J and K] and old [Figure 4G, H, J and K] neurologically intact age groups. Co-localization of Aβ oligomers and 4G8 positive Aβ plaques were also exhibited in the retinal vessel wall, where young dogs didn't exhibit any co-localization, the middle age group showed scarce co-localization [Figure 3I and L], and the older age group exhibited conspicuous co-localization in the vessel wall [Figure 4I and L]. In the middle age group, two Cocker spaniels aged 8 years male and 9.9 years female respectively exhibited widespread co-localization of Aβo and Aβp, and in the old age group, a neutered male Beagle aged 11 years, two spayed female German shepherds aged 12 years, a neutered male Border collie aged 13 years, and a spayed female Basset hound aged 15 years displayed strong and widespread co-localization of Aβo and Aβp. This co-localization study revealed an age-dependent distribution and co-accumulation of Aβo and Aβp in the retina of the neurologically intact dogs. We found that the young dogs exhibited widespread accumulation of $A\beta_{40}$ and $A\beta_{42}$ oligomers without any plaque deposits; in the middle age group, $A\beta_{40}$ and $A\beta_{42}$ oligomers accumulation was less conspicuous and, in some cases, co-localized with Aβp; and at the old age group, there was widespread and strong co-localization of Aβo and Aβp strongly distributed in most dogs [Supplementary Figures 2 and 3]. Representative retinal sections derived from dogs of all age groups stained with secondary antibodies with the omission of the primary antibody did not show any co-localization [Supplementary Figure 4A-F]. Retinal sections derived from an APP/PS1 mouse were used as positive control and confirmed the presence of $A\beta_{40}$ and $A\beta_{42}$ oligomers [Supplementary Figure 5A and B] and Aβp [Supplementary Figure 5C][49,55].

Immunofluorescence co-localization of retinal Aβ oligomers and phosphorylated tau in the retina of 30 dogs

To confirm the presence of p-Tau and to investigate whether p-Tau co-localizes with Aβo, we performed double fluorescence staining of Aβo and p-Tau using PRIOAD 12 ($A\beta_{40}$) or PRIOAD 13 ($A\beta_{42}$) anti-oligomer[57] and AT8 anti-p-Tau antibody, targeting Ser202/Thr205[54]. Aβo appeared as globular and annular in shape[55,62] [Figure 5A and B] and AT8 positive p-Tau appeared morphologically as diffuse and granular intracellular deposits[54] in the OPL, INL, IPL, and GCL [Figure 5C and D]. Overall, Aβo and p-Tau did not display consistent co-localization in all age groups, as P-tau was only detected in the old age group and $A\beta_{40}$ or $A\beta_{42}$ oligomers were identified in all age groups. Among ten dogs in the old age group, only four dogs have displayed the presence of p-Tau including a spayed female German shepherd and a neutered male Husky aged 12 years, a neutered male Shih Tzu aged 12.8 years, and a neutered male Border collie aged 13 years, and they exhibited strong co-localization with $A\beta_{40}$ or $A\beta_{42}$ oligomers [Figure 5E-H]. Representative retinal sections derived from Tau 58/2 mouse were used as positive control and confirmed the presence of AT8 positive p-Tau [Supplementary Figure 5D][58]. Representative retinal sections derived from dogs of all age groups stained with secondary antibodies with the omission of the primary antibody did not show any co-localization [Supplementary Figure 6A and B].

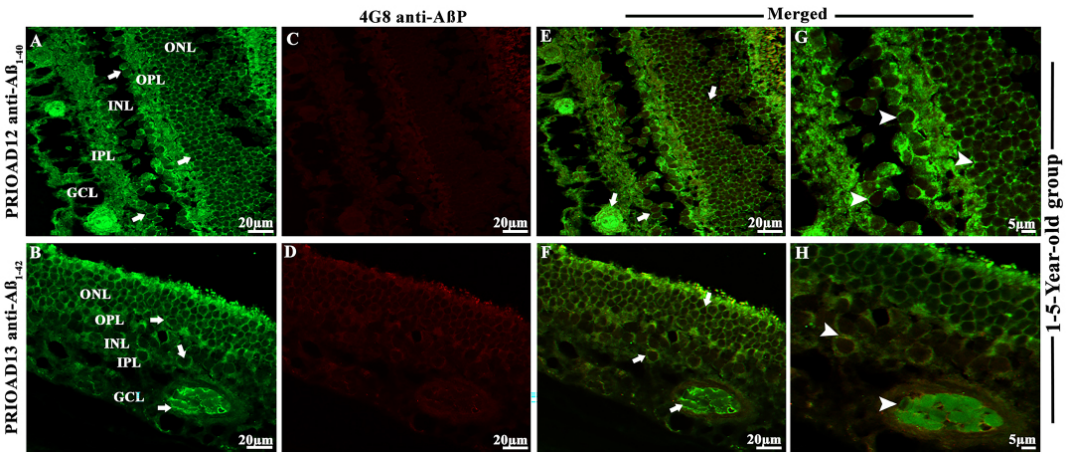

Figure 2. Immunofluorescence (IF) detection and co-localization of retinal amyloid-beta oligomers and amyloid-beta plaques in the dogs of the 1-5-year-old group. Retinal co-staining of oligomers with anti-$A\beta_{40}$ (PRIOAD12) or anti-$A\beta_{42}$ (PRIOAD 13) camelid-derived single domain antibodies (green) and plaques with anti-Aβ (4G8) antibody (red) of a 3-year-old German shepherd dog (A-H). A and B show widespread accumulation of $A\beta_{40}$ and $A\beta_{42}$oligomers in the GCL, INL, and ONL (white arrows) and retinal vasculature, respectively. IF 40×. (C and D) No Aβp was detected in the retinal layers. IF 40×. (E and F) Co-localization of Aβo and Aβp was not observed in the retinal layers of this animal (Aβo was present - white arrows). G and H are higher magnification 100× of images (A and B) in the GCL and INL, ONL and retinal vasculature. Representative of 10 dogs in the younger age group (1-5 years). GCL: Ganglion cell layer; INL: inner nuclear layer; ONL: outer nuclear layer.

Influence of demographic factors on the retinal deposition of Aβ oligomers, Aβ plaques, and phosphorylated tau in 30 dogs

To investigate the influence of the demographic factors on retinal Aβ and p-Tau deposition, staining intensity was compared with the age, breed, size, and sex of the neurologically intact dogs [Table 2]. $A\beta_{40}$ and $A\beta_{42}$ oligomers, Aβp and p-Tau fluorescence intensity, were assessed at 40× magnification. Immunoreactivity throughout the retinal layers was semi-quantified and categorized into no immunostaining "-"; low immunoreactivity, exhibited in limited areas of the retinal layers "+"; moderate immunoreactivity where deposits were more apparent "++" and finally strong immunoreactivity with widespread Aβo, Aβp and p-Tau labeling "+++" [Table 2]. After comparing the age of the dogs and immunofluorescence staining scores, we found that both $A\beta_{40}$ and $A\beta_{42}$ oligomers staining was high in young dogs, which slightly decreased in the middle age group, then finally, an upward trend was noticed in older dogs [Table 2, Figure 6]. In comparison, Aβp was absent in young dogs, but its presence in the middle age group was moderate and high in the old age group [Table 2, Figure 6]. Finally, p-Tau deposits were not observed in the young and middle age groups, whereas old dogs exhibited widespread staining for p-Tau [Table 2, Figure 6]. However, when the size of the dog was compared with the pathological outcome, we found that six medium-sized dogs displayed strong Aβo staining and only two dogs exhibited strong p-Tau staining [Table 2, Figure 7]. In addition, seven dogs revealed strong Aβp staining, of which four were medium size [Table 2, Figure 7].

Influence of eye pathology on the retinal deposition of Aβ oligomers, Aβ plaques, and phosphorylated tau in 30 dogs

Further, to understand whether the presence of pre-existing underlying eye pathology in the dogs may influence retinal Aβ and p-Tau depositions, we compared their staining intensity with the reported underlying clinical eye conditions [Table 2]. We found that four young dogs aged 1-5 years affected with anterior segment dysgenesis, a spectrum of disorders that affect the development of the anterior segment, including the cornea, iris, ciliary body, and lens[63-65], displayed "moderate" to "strong" intensity staining for $A\beta_{40}$ and $A\beta_{42}$ oligomers [Table 2]. However, another two dogs in this age group and affected with anterior segment dysgenesis showed little to no deposition of $A\beta_{40}$ and $A\beta_{42}$ oligomers [Table 2]. Eighteen out of

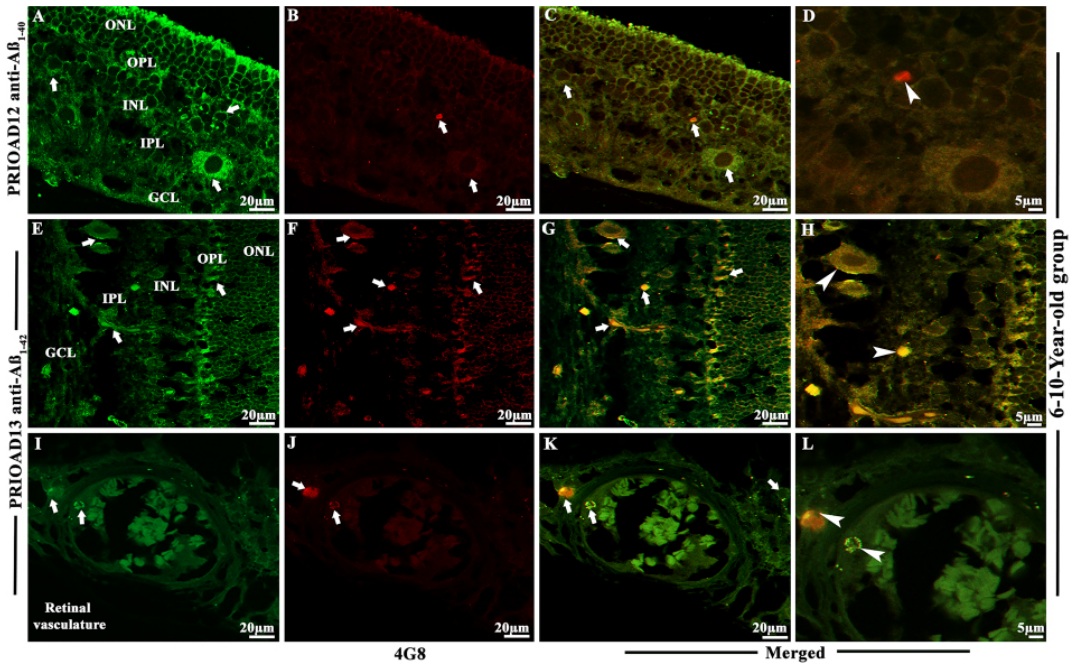

Figure 3. Immunofluorescence detection and co-localization of retinal amyloid-beta oligomers and amyloid-beta plaques in dogs of the 6-10-year-old group. Retinal co-staining with anti-$A\beta_{40}$ (PRIOAD 12) and anti-$A\beta_{42}$ (PRIOAD 13) camelid-derived single domain antibody (green) and 4G8 antibody (red) of a 9-year-old Cocker spaniel dog (A-L). (A) A large number of $A\beta_{40}$ and (B) $A\beta_{42}$ oligomers were found in the GCL, INL, and ONL (white arrows, 40×). (C) Detection of $A\beta_{42}$ oligomers in the vasculature. 4G8 positive Aβ plaque-like deposits were observed in the (D and E) GCL, IPL, INL, and OPL of the retina (white arrows, 40×). Widespread co-localization was observed in the (G and H) retinal layers (white arrows, 40×). Co-localization of 4G8 positive Aβ plaque with (J) $A\beta_{40}$ and (K) $A\beta_{42}$ depositions (white arrowhead) showed with higher magnification (100×) in the GCL and INL of the same 9-year-old Cocker spaniel dog retinal section. (C) Aβ oligomers and (F) 4G8 positive Aβ plaques were observed in the retinal vasculature (white arrows). (I and L) Co-localization of Aβ oligomers and 4G8 positive Aβ plaques were exhibited with 40× and with higher 100× magnification in the retinal vessel wall, respectively (white arrowhead). The photomicrograph was derived from the peripheral region of the retina - away from the optic disc. Representative of 10 dogs examined from middle age group (6-10 years). GCL: Ganglion cell layer; IPL: inner plexiform layer; INL: inner nuclear layer; OPL: outer plexiform layer; ONL: outer nuclear layer.

thirty dogs presented with eye neoplasms, including two in the young age group, seven in the middle age group, and nine in the old age group [Table 2]. There was no clear relation between neoplasms and the intensity of Aβ or p-Tau [Table 2]. Interestingly, eye inflammation (proptosis/ phthisis bulbi in young dogs and conjunctivitis in a middle-aged dog) corresponded to $A\beta_{40}$ and $A\beta_{42}$ oligomers intensity that ranged from "moderate" to "strong" [Table 2]. Finally, a case of pre-glaucoma in the middle age group and a case of glaucoma in the old age group also matched well with $A\beta_{40}$ and $A\beta_{42}$ oligomers as well as Aβp intensity. Overall, this analysis appears to indicate that no direct influence of pre-existing eye disorders on Aβ and p-Tau intensity exists; however, the small size of the cohorts used in this study did not allow to reach a substantive conclusion, and studies with much larger cohorts are needed.

DISCUSSION

Eye imaging can provide an opportunity to develop an easily accessible and point-of-care routine diagnostic testing to help predict MCI/AD early[66,67]. A study by Ko and colleagues examined the retinal NFL thickness and cognitive status of individuals aged 40 to 69 years over three years[68]. The authors found that individuals with thinner NFL showed a higher incidence of reduced cognition.

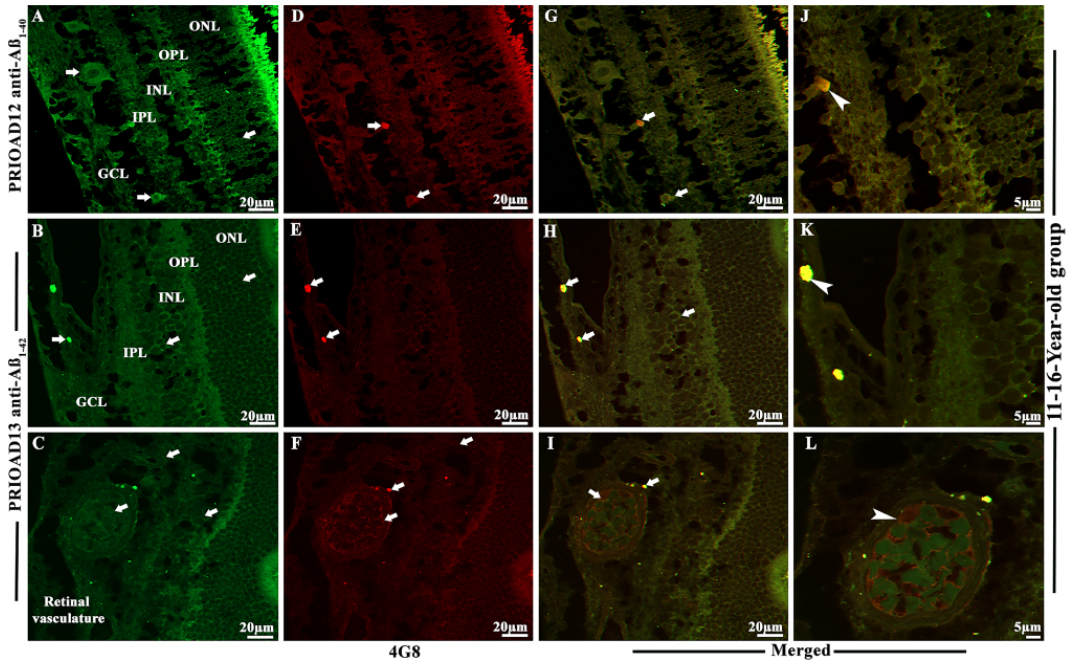

Figure 4. Immunofluorescence co-localization of retinal amyloid-beta oligomers and amyloid-beta plaques in dogs of 11-16-year-old group. Retinal co-staining with anti-$A\beta_{40}$ (PRIOAD 12) and anti-$A\beta_{42}$ (PRIOAD 13) camelid-derived single domain antibody (green) and 4G8 antibody (red) of a 12-year-old German shepherd dog (A-L). A large number of (A) $A\beta_{40}$ and (B) $A\beta_{42}$ oligomers were found in the GCL, INL, and ONL (white arrows, 40×). 4G8 positive Aβ plaque-like deposits were observed in the (D and E) GCL of the retina (white arrows, 40×). Widespread co-localization was observed in the (G and H) retinal layers (white arrows, 40×). Co-localization of 4G8 positive Aβ plaque with (J) $A\beta_{40}$ and (K) $A\beta_{42}$ depositions (white arrowhead) showed with higher magnification (100×) in the GCL of the same 12-year-old German shepherd dog retinal section. (C) Aβ oligomers and (F) 4G8 positive Aβ plaques were observed in the retinal vasculature (white arrows). (I and L) Co-localization of Aβ oligomers and 4G8 positive Aβ plaques were exhibited with 40× and also with higher 100× magnification in the retinal vessel wall, respectively (white arrowhead). The photomicrograph was derived from the peripheral region of the retina - away from the optic disc. Representative of 10 dogs examined from elder age group (11-16 years). GCL: ganglion cell layer; INL: inner nuclear layer; ONL: outer nuclear layer.

Despite the validation of the dog as a robust translational model for AD[24,30,69], only very limited studies investigated AD-related changes in the young and neurologically intact dogs. One study by Stylianaki and colleagues confirmed a similar pattern to that of humans; 61 dogs were subdivided into young (0-4 years old), middle-aged (4-8 years old), aged cognitively normal (8-20 years old), and aged cognitively impaired (8-17 years-old)[70]. The authors found that young dogs displayed the highest levels of total plasma $A\beta_{42}$ and $A\beta_{42}/A\beta_{40}$ ratio and the middle-aged dogs had the highest cerebrospinal fluid $A\beta_{40}$ and $A\beta_{42}$ when compared to neurologically intact aged dogs. Our first step was to investigate the distribution and morphological appearance of both $A\beta_{40}$ and $A\beta_{42}$ oligomers representing the canine lifetime, in the retinal layers of these neurologically intact 30 dogs. Previous studies have shown that A11 anti-oligomer antibody binds to different epitopes of the Aβo but also reacts with oligomeric aggregates of other proteins independent of their primary sequences. Of note, A11 cannot differentiate between $A\beta_{40}$ and $A\beta_{42}$. In contrast, PRIOAD12 and PRIOAD13 nanobodies bind to $A\beta_{40}$ and $A\beta_{42}$, respectively. Previous studies reported an inverse interrelationship between neurotoxicity and the size of Aβo, where the toxic effect of Aβo was shown to decrease with increased size. The general molecular weight of Aβo was found to range between 10-100 kDa in AD brain and included dimers to dodecamer[71]. A study by Lambert and colleagues first describes the cytotoxic effect of the small diffusible Aβo on the hippocampal neurons[72]. The small Aβo referred to as Aβ-derived diffusible ligands toxicity was tested in organotypic mouse brain slice cultures. The authors found that 17 and 22 kDa small oligomers killed hippocampal neurons at nanomolar concentration[72]. In addition, a study by Cizas and colleagues confirmed that oligomers larger than 30 KDa have a less toxic effect on the

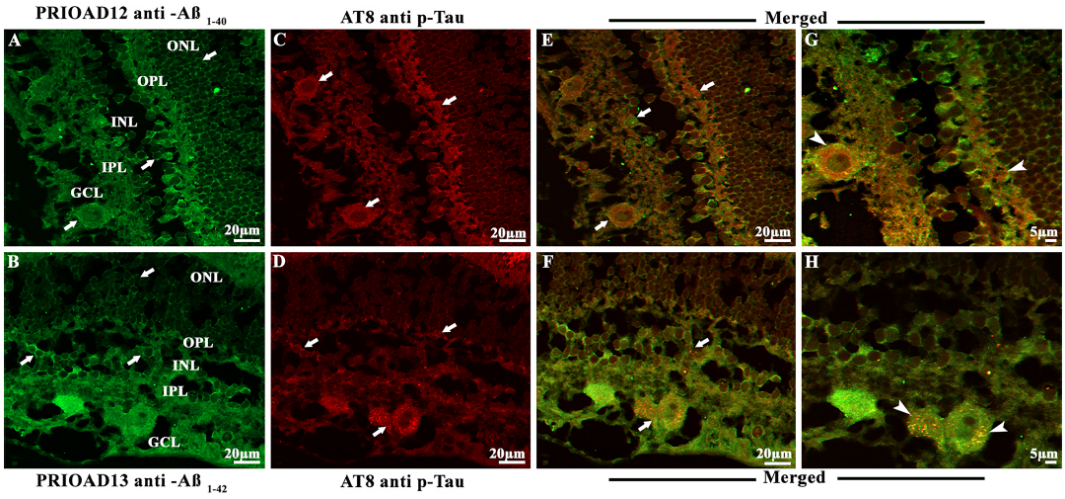

Figure 5. Immunofluorescence co-localization of retinal amyloid-beta oligomers and hyperphosphorylated tau in dogs of 11-16-year-old group. Retinal co-staining with anti-$A\beta_{40}$ (PRIOAD 12) and anti-$A\beta_{42}$ (PRIOAD 13) camelid-derived single domain antibody (green) and AT8 antibody (red) of a 12-year-old German shepherd dog. A large number of (A) $A\beta_{40}$ and (B) $A\beta_{42}$oligomers were found in the GCL, INL, and ONL (white arrows, 40×). AT8 positive diffuse p-Tau-like deposits were observed in the (C and D) GCL, IPL, INL, and OPL of the retina (white arrows, 40×). Widespread co-localization was observed in the (E and F) retinal layers (white arrows, 40×). Co-localization of AT8 positive p-Tau with (G) $A\beta_{40}$ and (H) $A\beta_{42}$ depositions (white arrowhead) showed with higher magnification (100×) in the GCL and OPL of the same 12-year-old German shepherd dog retinal section. The photomicrograph was derived from the peripheral region of the retina - away from the optic disc. Representative of 10 dogs examined from elder age group (≥ 11 years). GCL: Ganglion cell layer; IPL: inner plexiform layer; INL: inner nuclear layer; OPL: outer plexiform layer; ONL: outer nuclear layer.

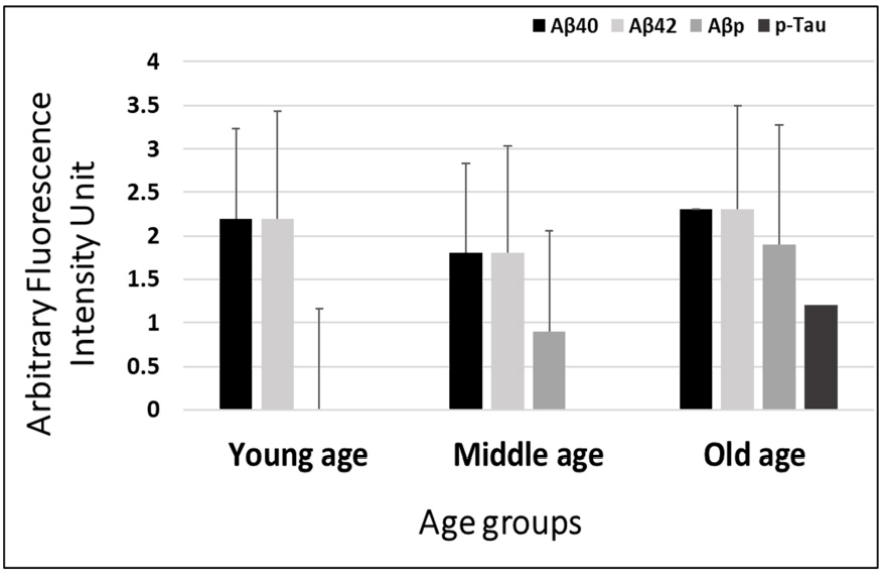

Figure 6. Semiquantitative analysis of $A\beta_{40}$ and $A\beta_{42}$ oligomers, Aβ plaques, and p-Tau in neurologically intact young (1-5-years), middle (6-10-years), and old (11-16-years) age groups of dogs. PRIOAD12 ($A\beta_{40}$ oligomers), PRIOAD13 ($A\beta_{42}$ oligomers), 4G8 (Aβp), and AT8 (p-Tau) fluorescence immunoreactivity and intensities were examined and quantified at 40× magnification under the fluorescence microscope. Semiquantitative analyses were compared with the three different age groups. A large amount of $A\beta_{40}$ and $A\beta_{42}$ oligomers were found in young dogs, which decreased in middle age group, then finally, an upward trend was noticed in older dogs. In comparison, Aβp were completely absent in young dogs, and then moderately found in middle, and large amounts in old age groups. Finally, p-Tau deposits were not found in young and middle age groups of dogs, whereas old dogs exhibited a considerable amount of p-Tau.

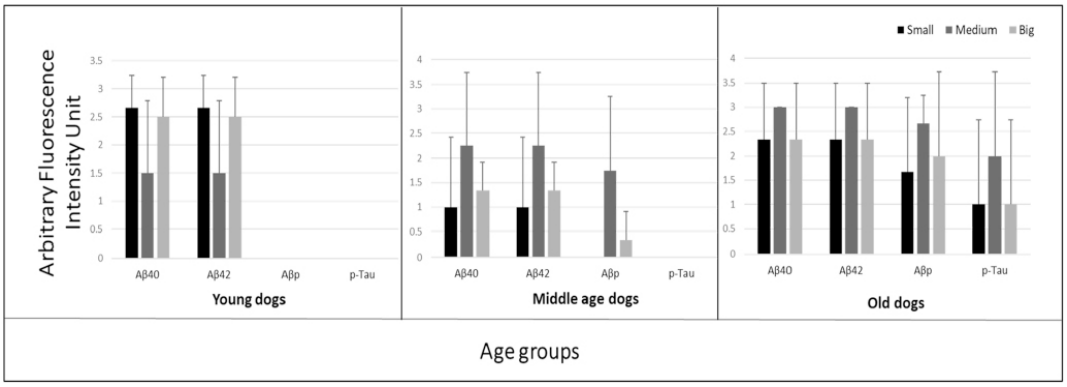

Figure 7. Influence of the size of dogs on the retinal deposition of amyloid-beta oligomers (Aβo), plaques (Aβp), and phosphorylated tau (p-Tau) in cognitively unimpaired young (1-5-years), middle (6-10-years) and old (11-16-years) age groups of dogs. PRIOAD12 ($Aβ_{40}$ oligomers), PRIOAD13 ($Aβ_{42}$ oligomers), 4G8 (Aβp), and AT8 (p-Tau) fluorescence immunoreactivity and intensities were examined and quantified at 40× magnification under the fluorescence microscope. In three different age groups, semiquantitative analyses were compared with the size of the dogs. In young dogs, a large number of oligomers were displayed by the small and big size dogs. The majority of medium-sized dogs displayed strong Aβo and Aβp staining intensity in the middle-aged dogs. Finally, among the different sizes of old dogs, medium-sized breeds displayed the highest amount of Aβo, Aβp, and p-Tau staining intensity.

inhibition of long-term potentiation[73]. They also suggested the transition of sizes from small to large correlate with the high to a low toxic effect of Aβo[73]. A11 specifically binds to the prefibrillar oligomers. However, studies suggested that the specificity of A11 to AD-related oligomers might vary as it recognized prefibrillar oligomers from various proteins that share a common structure including α-synuclein, islet amyloid polypeptide, polyglutamine (PolyQ), lysozyme, and prion peptide[36]. A study by Glabe and colleagues reported the ideal band size of prefibrillar oligomer-specific antibody A11 ranged from approximately tetrameric up to ~75 kDa[35]. In our study, we confirmed the presence of an A11-specific band at ~70KDa, confirming binding to prefibrillar oligomers in APP/PS1 mice. In comparison, camelid-derived single-domain nanobodies bind to ~15KDa band representing the small oligomers. In agreement with this current study, our previous report[55] also suggested that nanobodies were able to detect the toxic small diffusible oligomers specific to AD, whereas A11 binds to the larger oligomers believed to be less toxic to the neurons.

Studies suggested that in the canine brain, Aβo may be the toxic species responsible for cognitive decline and can potentially be an early biomarker for the detection of CCD[23,74]. Naaman and colleagues recently reported that $Aβ_{42}$ oligomers cause extensive retinal neurotoxicity in rats when compared to fibrillary $Aβ_{40}$ and $Aβ_{42}$[75]. Our findings demonstrated extensive deposition of $Aβ_{40}$ and $Aβ_{42}$ oligomers in the retinal layers, including GCL, INL, and ONL in 26/30 in the young, middle, and old age groups, except for a 1.4-year-old male Siberian husky, a 7-year-old neutered male Hound mixed, an 8-year-old spayed female Bedlington terrier, and an 11-year-old neutered male mixed breed. Moreover, we did not notice any difference in the intensity of immunofluorescence (graded - to +++), the pattern of deposition, or morphology between $Aβ_{40}$ and $Aβ_{42}$ oligomers in all age groups. This presentation was unlikely influenced by the breed of the animals; for instance, out of three Siberian Huskies, one dog failed to display $Aβ_{40}$ and $Aβ_{42}$ oligomers accumulation. Remarkably, the younger age group, with an age range of 1-5 years, equivalent to humans aged 15-40 years according to the American Kennel Club[76], has displayed extensive deposition of Aβ oligomers. Of interest, a 2013 brain study investigated the presence of three different types of Aβ oligomers, including Aβ trimers, Aβ*56, and Aβ dimers, in 75 cognitively unimpaired individuals aged 1 to 96 years[14]. Young children and adolescents were positive for Aβ oligomers; the authors found an age-related accumulation of Aβ oligomers where the level of the amyloid-β dimer was significantly higher in subjects in their 60s, and amyloid-β trimer

in their 70s, whereas Aβ*56 level was significantly higher in individuals in their 40s. The investigators proposed that Aβo, specifically Aβ*56, might trigger the pathological cascade in asymptomatic AD, a phase that may be identifiable two decades before the clinical onset[14].

Having found that the eyes of 26/30 dogs contained $A\beta_{40}$ and $A\beta_{42}$ oligomers, our next step was to demonstrate the presence/deposition of fibrillar Aβ in the canine retina of this same cohort. We show that none of the young dogs displays 4G8-positive Aβ fibrils and plaques (Aβp). However, Aβp were observed in some of the middle age group, where three dogs exhibited "low" staining intensity and two exhibited "strong" staining intensity in the GCL, IPL & INL. Aβp were also observed in the old age group, where five dogs showed "strong" signal intensity and two with "moderate" signal intensity in the GCL, IPL & INL. A pattern, not surprising, emerges; $A\beta_{40}$ and $A\beta_{42}$ oligomers are deposited in the retina following birth and subsequently, a fibrillar Aβ configuration, aggregated as plaques follow. Several studies have demonstrated the presence of Aβp in the canine brain and suggested only a weak correlation with the severity of cognitive dysfunction[77,78]. Schütt *et al.* investigated this question in further depth by studying dogs at differing ages, specifically aged 9-15 years, including neurologically intact dogs and dogs with CCD, and compared their amyloid burden with that of young dogs aged less than 6 years[69]. The authors reported that the levels of Aβ deposition strongly correlated with the age of the dog but not to their cognitive capacity. Asking the same questions regarding amyloid accretion in non-CNS neuronal populations, such as the retina, has not been investigated in the canine, but some recent reports confirmed their presence in the retina of AD[50,54,79]. In this study, we have demonstrated accumulation of retinal Aβp in the mature to an aged group of these 30 dogs which supports the hypothesis that Aβp might not influence the severity of cognitive deficits but can be a predictor of AD development[11,17]. Overall, our study revealed that the Aβ deposition pattern in the retina was such that Aβo was observed in all age groups, whereas Aβp accumulation was restricted to the middle and more intensely the old age group of dogs, regardless of demographic criteria, breed and gender. Interestingly, co-accumulation of both Aβo and Aβp were apparent in some middle and old dogs. This is in agreement with our report this year, where 17-18 months old APP/PS1 mice showed high levels of oligomers deposits in the retinal layers that co-localized with Aβp[55]. Previous neuropathological studies in AD have shown that cerebral Aβo is usually present in early disease stages and is the most cytotoxic of Aβ species, mostly responsible for neurotoxicity and synaptic dysfunction[34,80-83], whereas extracellular Aβp is believed to accumulate at later ages and may act as a reservoir for Aβo[84]. Moreover, the involvement of Aβo in retinal degeneration in AD has also been reported[85-87]. In the study reported herein, we noticed widespread distribution of Aβo in the retinal layers of dogs of all age groups, indicating potential involvement in retinal degeneration, perhaps leading to vision impairment in some dogs[88,89]. Of importance, a previous study by Ozawa and colleagues that focused on web and paper-based surveys of dogs aged ≥ 10 years to identify physical disturbances related to CCD showed that more than 90% of dogs affected with CCD had vision impairment[90]. In addition to the neural retina, we observed Aβ deposition s in the retinal microvasculature of young, middle, and old age groups, which might imitate CAA in AD[91-93]. Sharafi *et al.* suggested that retinal vasculature changes captured by hyperspectral imaging can differentiate cerebral amyloid status between cognitively impaired and unimpaired individuals[94].

Central to AD pathogenesis is the intraneuronal deposition of hyperphosphorylated tau (p-Tau) in granular form and eventual organization as NFTs, one of the cardinal neuropathological hallmarks[3,4]. In dogs with CCD, p-Tau, unlike NFTs, has been identified in the brain, but until recently, only in some cases. We speculate that, unlike human AD, p-Tau is only evident in pretangle granular form in dogs due to their shorter lifespan (Tayebi & Habiba, unpublished observation). p-Tau neuropathology was shown to develop about a decade before the formation of Aβp in AD brains and was hypothesized to trigger AD[95,96]. However, Aβo accumulation was shown to precede and drive p-Tau accumulation and transneuronal spread across synapses in the parietal cortex of AD[96].

In the retina of human AD patients, p-Tau displayed a diffuse pattern in the plexiform layers in the absence of NFTs[54]. Schön and colleagues reported the presence of AT8-positive intracellular NFTs and diffuse p-Tau signals in the retina of 5/6 deceased AD patients[97]. In this study, we investigated the presence of p-Tau Ser202/Thr205 to confirm the presence of retinal p-Tau in dogs. We revealed diffuse p-Tau distribution in the OPL, INL, IPL, and GCL in 4/10 dogs of the old age group, including a spayed female German shepherd and a neutered male Husky aged 12 years old, a neutered male Shih Tzu aged 12.8 years old, and a neutered male Border collie aged 13 years old. The same dogs also showed the widespread distribution of $A\beta_{40}$ and/or $A\beta_{42}$ oligomers and 4G8- positive Aβp. Similarly, in the brains of cognitively impaired, 14-17 years old dogs, Abey and colleagues have demonstrated the presence of p-Tau Ser202/Thr205 and p-Tau Ser396 in 1/6 and 6/6, respectively[40]. This pattern of deposition strongly supports a possible age-dependent progression as observed in AD mice models[49,55]. Previous studies have shown that breed variance does not determine the pathological outcome associated with CCD in aged dogs[98,99]. In agreement, our study did not reveal any breed-dependent pathological accumulation.

While previous studies have demonstrated the presence of Aβp and p-Tau in the aged dog brain[30,43], Pugleise *et al.* proposed that the acquisition of diffuse Aβp and p-Tau are unrelated and independent events of aged dogs[42]. Whether these two "ingredients" of AD dementia or CCD are closely linked (co-localized or at least act in concert) is likely crucial. In AD, it was shown that p-Tau and Aβo cause neuronal toxicity and may act synergistically to trigger synaptic dysfunction[36,37,100]. Manczak and colleagues showed that $A\beta_{40}$ or $A\beta_{42}$ oligomers co-localized with p-Tau in the brains of AD patients[101]. The authors also reported that the interaction between Aβo and p-Tau became more prominent with disease progression and was more pronounced at Braak stage V and VI compared to Braak stage III and IV[102,103]. The evidence from this canine retina study would support an interaction: we also show that p-Tau co-localized with $A\beta_{40}$ or $A\beta_{42}$ oligomers in the OPL, INL, IPL, and GCL of the retina of 4/10 dogs in the eldest age group. A recent PET brain imaging study by Lockhart *et al.*, which demonstrated the presence of both Aβ and Tau pathology in cognitively normal older adults, showed a significant spatial correlation with Aβ and Tau deposition[104]. Thus co-localization, while evident, does not itself necessarily imply neuronal cytotoxicity.

Several studies in the field of AD research highlighted the importance of diagnostic and therapeutic interventions in the asymptomatic phase while the individuals are cognitively intact[14,105]. However, it is challenging to first identify and then track disease progression in humans without sensitive, specific, and cost-effective early diagnostic approaches and a lack of robust natural translational models. In that context, dogs have the potential to be an effective natural model for the study of aging and AD. They share the same environment as humans[106,107]; there exists the option of brain CT and MRI imaging and intracranial biopsy, ease of cognitive testing which helps reduce physiological stress, and finally, a short lifespan[108]. Canine ophthalmology is a well-established clinical and investigative discipline (inherited retinopathies, for example). The current study provides strong impetus to track how this seemingly common process evolves, with potential consequences for aging, neurodegenerative disease, and also vision.

Lateralization in retinal and cerebral Aβ levels was previously investigated in an AD mouse model[109]. Some studies revealed left posterior brain-dominant lateralization in $A\beta_{42/40}$; however, no left or right brain hemisphere or retinal dominance lateralization was observed for $A\beta_{40}$ and $A\beta_{42}$. Although our current study does not provide information about left versus right retinal accumulation of Aβ, the significance of the lateralization in human Alzheimer's and CCD remains unknown. Moreover, previous reports have shown that Aβ accumulation was more prominent in the far-peripheral and mid-peripheral of the superior

temporal quadrant than in the central retina in AD patients[50,79]; however, in our study, no notable differences in Aβ and tau deposition have been observed in different parts of the retina.

The canine eye tissues used in this study had been surgically removed in the course of managing spontaneous disorders of the globe, eyelids, or structures within the orbit which necessitated enucleation. It could be asked whether any of these conditions played any part in Aβ and/or p-Tau deposition in the retina. We think this unlikely, given the diverse clinical conditions involved, which ranged from developmental abnormalities, inflammatory conditions, and proptosis to various neoplasms of differing grades of the eye, while other cases were disorders arising in the conjunctiva or orbit. The span of ages in these dogs (from juvenile to quite aged) would further make this seem unlikely and some evidence of human retinal Aβ and/or p-Tau exists, though such explorations are largely performed only at the end of life.

DECLARATIONS

Authors' contributions

Performed experiments and revised manuscript: Habiba U
Revised manuscript: Morley J, Krockenberger M
Was a major contributor in writing and revising the manuscript: Summers BA
Conceived and designed experiments and wrote manuscript: Tayebi M
All authors read and approved the final manuscript.

Availability of data and materials

Not applicable.

Financial support and sponsorship

None.

Conflicts of interest

All authors declared that there are no conflicts of interest.

Ethical approval and consent to participate

Not applicable.

Consent for publication

Not applicable.

REFERENCES

1. Clark CM, Karlawish JHT. Alzheimer disease: current concepts and emerging diagnostic and therapeutic strategies. *Ann Intern Med* 2003;138:400-10. DOI PubMed
2. Mott RT, Hulette CM. Neuropathology of Alzheimer's disease. *Neuroimaging Clinics* 2005;15:755-65. DOI PubMed
3. Perl DP. Neuropathology of Alzheimer's disease. *Mt Sinai J Med* 2010;77:32-42. DOI PubMed PMC
4. Serrano-Pozo A, Frosch MP, Masliah E, Hyman BT. Neuropathological alterations in Alzheimer disease. *Cold Spring Harb Perspect Med* 2011;1:a006189. DOI PubMed PMC
5. Hardy J, Selkoe DJ. The amyloid hypothesis of Alzheimer's disease: progress and problems on the road to therapeutics. *Science* 2002;297:353-6. DOI PubMed
6. Jack CR Jr, Wiste HJ, Weigand SD, et al. Age, sex, and APOE ε4 effects on memory, brain structure, and β-amyloid across the adult life span. *JAMA Neurol* 2015;72:511-9. DOI PubMed PMC
7. Rentz DM, Locascio JJ, Becker JA, et al. Cognition, reserve, and amyloid deposition in normal aging. *Ann Neurol* 2010;67:353-64.

DOI PubMed PMC

8. Rodrigue KM, Kennedy KM, Park DC. Beta-amyloid deposition and the aging brain. *Neuropsychol Rev* 2009;19:436-50. DOI PubMed PMC
9. Oh H, Mormino EC, Madison C, Hayenga A, Smiljic A, Jagust WJ. β-amyloid affects frontal and posterior brain networks in normal aging. *Neuroimage* 2011;54:1887-95. DOI PubMed PMC
10. Bourgeat P, Chételat G, Villemagne VL, et al; AIBL Research Group. Beta-amyloid burden in the temporal neocortex is related to hippocampal atrophy in elderly subjects without dementia. *Neurology* 2010;74:121-7. DOI PubMed
11. Rowe CC, Ellis KA, Rimajova M, et al. Amyloid imaging results from the Australian Imaging, Biomarkers and Lifestyle (AIBL) study of aging. *Neurobiol Aging* 2010;31:1275-83. DOI PubMed
12. Petersen RC, Aisen P, Boeve BF, et al. Mild cognitive impairment due to Alzheimer disease in the community. *Ann Neurol* 2013;74:199-208. DOI PubMed PMC
13. Erten-Lyons D, Woltjer RL, Dodge H, et al. Factors associated with resistance to dementia despite high Alzheimer disease pathology. *Neurology* 2009;72:354-60. DOI PubMed PMC
14. Lesné SE, Sherman MA, Grant M, et al. Brain amyloid-β oligomers in ageing and Alzheimer's disease. *Brain* 2013;136:1383-98. DOI PubMed PMC
15. Bischof GN, Rodrigue KM, Kennedy KM, Devous MD Sr, Park DC. Amyloid deposition in younger adults is linked to episodic memory performance. *Neurology* 2016;87:2562-6. DOI PubMed PMC
16. Hanseeuw BJ, Betensky RA, Jacobs HIL, et al. Association of amyloid and tau with cognition in preclinical alzheimer disease: a longitudinal study. *JAMA Neurol* 2019;76:915-24. DOI PubMed PMC
17. Rowe CC, Bourgeat P, Ellis KA, et al. Predicting Alzheimer disease with β-amyloid imaging: results from the Australian imaging, biomarkers, and lifestyle study of ageing. *Ann Neurol* 2013;74:905-13. DOI PubMed
18. Drummond E, Wisniewski T. Alzheimer's disease: experimental models and reality. *Acta Neuropathol* 2017;133:155-75. DOI PubMed PMC
19. Kitazawa M, Medeiros R, Laferla FM. Transgenic mouse models of Alzheimer disease: developing a better model as a tool for therapeutic interventions. *Curr Pharm Des* 2012;18:1131-47. DOI PubMed PMC
20. Cummings BJ, Head E, Ruehl W, Milgram NW, Cotman CW. The canine as an animal model of human aging and dementia. *Neurobiology of Aging* 1996;17:259-68. DOI PubMed
21. Head E, McCleary R, Hahn FF, Milgram NW, Cotman CW. Region-specific age at onset of β-amyloid in dogs. *Neurobiol Aging* 2000;21:89-96. DOI PubMed
22. Pugliese M, Gangitano C, Ceccariglia S, et al. Canine cognitive dysfunction and the cerebellum: acetylcholinesterase reduction, neuronal and glial changes. *Brain Res* 2007;1139:85-94. DOI PubMed
23. Head E, Pop V, Sarsoza F, et al. Amyloid-beta peptide and oligomers in the brain and cerebrospinal fluid of aged canines. *J Alzheimers Dis* 2010;20:637-46. DOI PubMed PMC
24. Youssef SA, Capucchio MT, Rofina JE, et al. Pathology of the aging brain in domestic and laboratory animals, and animal models of human neurodegenerative diseases. *Vet Pathol* 2016;53:327-48. DOI PubMed
25. Cummings BJ, Head E, Afagh AJ, Milgram NW, Cotman CW. Beta-amyloid accumulation correlates with cognitive dysfunction in the aged canine. *Neurobiol Learn Mem* 1996;66:11-23. DOI PubMed
26. Adams B, Chan A, Callahan H, Milgram NW. The canine as a model of human cognitive aging: recent developments. *Prog Neuropsychopharmacol Biol Psychiatry* 2000;24:675-92. DOI PubMed
27. Head E. A canine model of human aging and Alzheimer's disease. *Biochim Biophys Acta* 2013;1832:1384-9. DOI PubMed PMC
28. Rofina JE, van Ederen AM, Toussaint MJ, et al. Cognitive disturbances in old dogs suffering from the canine counterpart of Alzheimer's disease. *Brain Res* 2006;1069:216-26. DOI PubMed
29. Chow VW, Mattson MP, Wong PC, Gleichmann M. An overview of APP processing enzymes and products. *Neuromolecular Med* 2010;12:1-12. DOI PubMed PMC
30. Yu CH, Song GS, Yhee JY, et al. Histopathological and immunohistochemical comparison of the brain of human patients with Alzheimer's disease and the brain of aged dogs with cognitive dysfunction. *J Comp Pathol* 2011;145:45-58. DOI PubMed
31. Broersen K, Rousseau F, Schymkowitz J. The culprit behind amyloid beta peptide related neurotoxicity in Alzheimer's disease: oligomer size or conformation? *Alzheimers Res Ther* 2010;2:12. DOI PubMed PMC
32. Goure WF, Krafft GA, Jerecic J, Hefti F. Targeting the proper amyloid-beta neuronal toxins: a path forward for Alzheimer's disease immunotherapeutics. *Alzheimers Res Ther* 2014;6:42. DOI PubMed PMC
33. Morgado I, Fändrich M. Assembly of Alzheimer's Aβ peptide into nanostructured amyloid fibrils. *Current opinion in colloid & interface science* 2011;16:508-14. DOI
34. Sengupta U, Nilson AN, Kayed R. The role of amyloid-β oligomers in toxicity, propagation, and immunotherapy. *EBioMedicine* 2016;6:42-9. DOI PubMed PMC
35. Glabe CG. Structural classification of toxic amyloid oligomers. *J Biol Chem* 2008;283:29639-43. DOI PubMed PMC
36. Kayed R, Head E, Thompson JL, et al. Common structure of soluble amyloid oligomers implies common mechanism of pathogenesis. *Science* 2003;300:486-9. DOI PubMed
37. Haass C, Selkoe DJ. Soluble protein oligomers in neurodegeneration: lessons from the Alzheimer's amyloid beta-peptide. *Nat Rev Mol Cell Biol* 2007;8:101-12. DOI PubMed

38. Benilova I, Karran E, De Strooper B. The toxic Aβ oligomer and Alzheimer's disease: an emperor in need of clothes. *Nat Neurosci* 2012;15:349-57. DOI PubMed
39. Zhao LN, Long HW, Mu Y, Chew LY. The toxicity of amyloid β oligomers. *International journal of molecular sciences* 2012;13:7303-27. DOI
40. Abey A, Davies D, Goldsbury C, Buckland M, Valenzuela M, Duncan T. Distribution of tau hyperphosphorylation in canine dementia resembles early Alzheimer's disease and other tauopathies. *Brain Pathol* 2021;31:144-62. DOI PubMed PMC
41. Papaioannou N, Tooten PC, van Ederen AM, et al. Immunohistochemical investigation of the brain of aged dogs. I. Detection of neurofibrillary tangles and of 4-hydroxynonenal protein, an oxidative damage product, in senile plaques. *Amyloid* 2001;8:11-21. DOI PubMed
42. Pugliese M, Mascort J, Mahy N, Ferrer I. Diffuse beta-amyloid plaques and hyperphosphorylated tau are unrelated processes in aged dogs with behavioral deficits. *Acta Neuropathol* 2006;112:175-83. DOI PubMed
43. Schmidt F, Boltze J, Jäger C, et al. Detection and quantification of β-amyloid, pyroglutamyl Aβ, and tau in aged canines. *J Neuropathol Exp Neurol* 2015;74:912-23. DOI PubMed
44. Wegiel J, Wisniewski HM, Sołtysiak Z. Region- and cell-type-specific pattern of tau phosphorylation in dog brain. *Brain Research* 1998;802:259-66. DOI PubMed
45. Armstrong RA. Alzheimer's disease and the eye. *Journal of Optometry* 2009;2:103-11. Available from: https://doi.org/10.3921/joptom.2009.103.
46. Santos CY, Johnson LN, Sinoff SE, Festa EK, Heindel WC, Snyder PJ. Change in retinal structural anatomy during the preclinical stage of Alzheimer's disease. *Alzheimers Dement (Amst)* 2018;10:196-209. DOI PubMed PMC
47. Marquié M, Castilla-Martí M, Valero S, et al. Visual impairment in aging and cognitive decline: experience in a Memory Clinic. *Sci Rep* 2019;9:8698. DOI PubMed PMC
48. Lee ATC, Richards M, Chan WC, Chiu HFK, Lee RSY, Lam LCW. Higher dementia incidence in older adults with poor visual acuity. *J Gerontol A Biol Sci Med Sci* 2020;75:2162-8. DOI PubMed PMC
49. Habiba U, Merlin S, Lim JKH, et al. Age-specific retinal and cerebral immunodetection of amyloid-β plaques and oligomers in a rodent model of Alzheimer's disease. *J Alzheimers Dis* 2020;76:1135-50. DOI PubMed
50. Lee S, Jiang K, McIlmoyle B, et al. Amyloid Beta immunoreactivity in the retinal ganglion cell layer of the Alzheimer's eye. *Front Neurosci* 2020;14:758. DOI PubMed PMC
51. Koronyo-Hamaoui M, Koronyo Y, Ljubimov AV, et al. Identification of amyloid plaques in retinas from Alzheimer's patients and noninvasive in vivo optical imaging of retinal plaques in a mouse model. *Neuroimage* 2011;54 Suppl 1:S204-17. DOI PubMed PMC
52. Tsai Y, Lu B, Ljubimov AV, et al. Ocular changes in TgF344-AD rat model of Alzheimer's disease. *Invest Ophthalmol Vis Sci* 2014;55:523-34. DOI PubMed PMC
53. Jentsch S, Schweitzer D, Schmidtke KU, et al. Retinal fluorescence lifetime imaging ophthalmoscopy measures depend on the severity of Alzheimer's disease. *Acta Ophthalmol* 2015;93:e241-7. DOI PubMed
54. den Haan J, Morrema THJ, Verbraak FD, et al. Amyloid-beta and phosphorylated tau in post-mortem Alzheimer's disease retinas. *Acta Neuropathol Commun* 2018;6:147. DOI PubMed PMC
55. Habiba U, Descallar J, Kreilaus F, et al. Detection of retinal and blood Aβ oligomers with nanobodies. *Alzheimers Dement (Amst)* 2021;13:e12193. DOI PubMed PMC
56. Yi J, Chen B, Yao X, Lei Y, Ou F, Huang F. Upregulation of the lncRNA MEG3 improves cognitive impairment, alleviates neuronal damage, and inhibits activation of astrocytes in hippocampus tissues in Alzheimer's disease through inactivating the PI3K/Akt signaling pathway. *J Cell Biochem* 2019;120:18053-65. DOI PubMed
57. David MA, Jones DR, Tayebi M. Potential candidate camelid antibodies for the treatment of protein-misfolding diseases. *J Neuroimmunol* 2014;272:76-85. DOI PubMed
58. van Eersel J, Stevens CH, Przybyla M, et al. Early-onset axonal pathology in a novel P301S-Tau transgenic mouse model of frontotemporal lobar degeneration. *Neuropathol Appl Neurobiol* 2015;41:906-25. DOI PubMed
59. Radde R, Bolmont T, Kaeser SA, et al. Abeta42-driven cerebral amyloidosis in transgenic mice reveals early and robust pathology. *EMBO Rep* 2006;7:940-6. DOI PubMed PMC
60. Nakayama H, Uchida K, Doi K. A comparative study of age-related brain pathology - are neurodegenerative diseases present in nonhuman animals ? *Med Hypotheses* 2004;63:198-202. DOI PubMed
61. Cummings BJ, Pike CJ, Shankle R, Cotman CW. β-amyloid deposition and other measures of neuropathology predict cognitive status in Alzheimer's disease. *Neurobiology of Aging* 1996;17:921-33. DOI PubMed
62. Breydo L, Uversky VN. Structural, morphological, and functional diversity of amyloid oligomers. *FEBS Lett* 2015;589:2640-8. DOI PubMed
63. Silva EG, Dubielzig R, Zarfoss MK, Anibal A. Distinctive histopathologic features of canine optic nerve hypoplasia and aplasia: a retrospective review of 13 cases. *Vet Ophthalmol* 2008;11:23-9. DOI PubMed
64. Rüttimann G, Daicker B. Complex colobomas in the anterior eye segment in a beagle hound. *Zentralbl Veterinarmed A* 1982;29:528-37. PubMed
65. Williams DL. A comparative approach to anterior segment dysgenesis. *Eye (Lond)* 1993;7:607-16. DOI PubMed
66. Casaletto KB, Ward ME, Baker NS, et al. Retinal thinning is uniquely associated with medial temporal lobe atrophy in neurologically

normal older adults. *Neurobiol Aging* 2017;51:141-7. DOI PubMed PMC

67. Alonso-Caneiro D, Read SA, Collins MJ. Automatic segmentation of choroidal thickness in optical coherence tomography. *Biomed Opt Express* 2013;4:2795-812. DOI PubMed PMC
68. Ko F, Muthy ZA, Gallacher J, et al; UK Biobank Eye & Vision Consortium. Association of retinal nerve fiber layer thinning with current and future cognitive decline: a study using optical coherence tomography. *JAMA Neurol* 2018;75:1198-205. DOI PubMed PMC
69. Schütt T, Helboe L, Pedersen LØ, Waldemar G, Berendt M, Pedersen JT. Dogs with cognitive dysfunction as a spontaneous model for early Alzheimer's disease: a translational study of neuropathological and inflammatory markers. *J Alzheimers Dis* 2016;52:433-49. DOI PubMed
70. Stylianaki I, Polizopoulou ZS, Theodoridis A, Koutouzidou G, Baka R, Papaioannou NG. Amyloid-beta plasma and cerebrospinal fluid biomarkers in aged dogs with cognitive dysfunction syndrome. *J Vet Intern Med* 2020;34:1532-40. DOI PubMed PMC
71. Kuo YM, Emmerling MR, Vigo-Pelfrey C, et al. Water-soluble abeta (N-40, N-42) oligomers in normal and Alzheimer disease brains. *J Biol Chem* 1996;271:4077-81. DOI PubMed
72. Lambert MP, Barlow AK, Chromy BA, et al. Diffusible, nonfibrillar ligands derived from Abeta1-42 are potent central nervous system neurotoxins. *Proc Natl Acad Sci U S A* 1998;95:6448-53. DOI PubMed PMC
73. Cizas P, Budvytyte R, Morkuniene R, et al. Size-dependent neurotoxicity of beta-amyloid oligomers. *Arch Biochem Biophys* 2010;496:84-92. DOI PubMed PMC
74. Rusbridge C, Salguero FJ, David MA, et al. An aged canid with behavioral deficits exhibits blood and cerebrospinal fluid amyloid beta oligomers. *Front Aging Neurosci* 2018;10:7. DOI PubMed PMC
75. Naaman E, Ya'ari S, Itzkovich C, et al. The retinal toxicity profile towards assemblies of Amyloid-β indicate the predominant pathophysiological activity of oligomeric species. *Sci Rep* 2020;10:20954. DOI PubMed PMC
76. American Kennel Club. Dog years to human years 2018, January 02. Available from: https://www.akcpetinsurance.com/blog/year-of-the-dog [Last accessed on 23 May 2022].
77. Ozawa M, Chambers JK, Uchida K, Nakayama H. The relation between canine cognitive dysfunction and age-related brain lesions. *J Vet Med Sci* 2016;78:997-1006. DOI PubMed PMC
78. Kiatipattanasakul W, Nakamura S, Hossain MM, et al. Apoptosis in the aged dog brain. *Acta Neuropathol* 1996;92:242-8. DOI PubMed
79. Koronyo Y, Biggs D, Barron E, et al. Retinal amyloid pathology and proof-of-concept imaging trial in Alzheimer's disease. *JCI Insight* 2017;2:93621. DOI PubMed PMC
80. El-Agnaf OM, Salem SA, Paleologou KE, et al. Detection of oligomeric forms of alpha-synuclein protein in human plasma as a potential biomarker for Parkinson's disease. *FASEB J* 2006;20:419-25. DOI PubMed
81. El-agnaf OM, Walsh DM, Allsop D. Soluble oligomers for the diagnosis of neurodegenerative diseases. *The Lancet Neurology* 2003;2:461-2. DOI PubMed
82. Mucke L, Selkoe DJ. Neurotoxicity of amyloid β-protein: synaptic and network dysfunction. *Cold Spring Harb Perspect Med* 2012;2:a006338. DOI PubMed PMC
83. Kim HJ, Chae SC, Lee DK, et al. Selective neuronal degeneration induced by soluble oligomeric amyloid beta protein. *FASEB J* 2003;17:118-20. DOI PubMed
84. Mclean CA, Cherny RA, Fraser FW, et al. Soluble pool of A? *Ann Neurol* 1999;46:860-6. DOI PubMed
85. Lynn SA, Johnston DA, Scott JA, et al. Oligomeric $A\beta_{1-42}$ induces an AMD-like phenotype and accumulates in lysosomes to impair RPE function. *Cells* 2021;10:413. DOI PubMed PMC
86. Ratnayaka JA, Serpell LC, Lotery AJ. Dementia of the eye: the role of amyloid beta in retinal degeneration. *Eye (Lond)* 2015;29:1013-26. DOI PubMed PMC
87. Luibl V, Isas JM, Kayed R, Glabe CG, Langen R, Chen J. Drusen deposits associated with aging and age-related macular degeneration contain nonfibrillar amyloid oligomers. *J Clin Invest* 2006;116:378-85. DOI PubMed PMC
88. Denenberg S, Liebel F, Rose J. Behavioural and medical differentials of cognitive decline and dementia in dogs and cats. In: Landsberg G, Maďari A, Žilka N, editors. Canine and feline dementia. Cham: Springer International Publishing; 2017. p. 13-58. DOI
89. Acland G, Aguirre G. Retinal degenerations in the dog: IV. Early retinal degeneration (erd) in Norwegian elkhounds. *Exp Eye Res* 1987;44:491-521. DOI PubMed
90. Ozawa M, Inoue M, Uchida K, Chambers JK, Takeuch Y, Nakayama H. Physical signs of canine cognitive dysfunction. *J Vet Med Sci* 2019;81:1829-34. DOI PubMed PMC
91. Weber SA, Patel RK, Lutsep HL. Cerebral amyloid angiopathy: diagnosis and potential therapies. *Expert Rev Neurother* 2018;18:503-13. DOI PubMed
92. Patton N, Aslam T, Macgillivray T, Pattie A, Deary IJ, Dhillon B. Retinal vascular image analysis as a potential screening tool for cerebrovascular disease: a rationale based on homology between cerebral and retinal microvasculatures. *J Anat* 2005;206:319-48. DOI PubMed PMC
93. Shi H, Koronyo Y, Rentsendorj A, et al. Identification of early pericyte loss and vascular amyloidosis in Alzheimer's disease retina. *Acta Neuropathol* 2020;139:813-36. DOI PubMed PMC
94. Sharafi SM, Sylvestre JP, Chevrefils C, et al. Vascular retinal biomarkers improves the detection of the likely cerebral amyloid status from hyperspectral retinal images. *Alzheimers Dement (N Y)* 2019;5:610-7. DOI PubMed PMC

95. Arnsten AFT, Datta D, Del Tredici K, Braak H. Hypothesis: tau pathology is an initiating factor in sporadic Alzheimer's disease. *Alzheimers Dement* 2021;17:115-24. DOI PubMed PMC
96. Bilousova T, Miller CA, Poon WW, et al. Synaptic amyloid-β oligomers precede p-Tau and differentiate high pathology control cases. *Am J Pathol* 2016;186:185-98. DOI PubMed PMC
97. Schön C, Hoffmann NA, Ochs SM, et al. Long-term in vivo imaging of fibrillar tau in the retina of P301S transgenic mice. *PLoS One* 2012;7:e53547. DOI PubMed PMC
98. Rofina J, van Andel I, van Ederen AM, Papaioannou N, Yamaguchi H, Gruys E. Canine counterpart of senile dementia of the Alzheimer type: amyloid plaques near capillaries but lack of spatial relationship with activated microglia and macrophages. *Amyloid* 2003;10:86-96. DOI PubMed
99. Colle MA, Hauw JJ, Crespeau F, et al. Vascular and parenchymal abeta deposition in the aging dog: correlation with behavior. *Neurobiol Aging* 2000;21:695-704. DOI PubMed
100. De Felice FG, Wu D, Lambert MP, et al. Alzheimer's disease-type neuronal tau hyperphosphorylation induced by A beta oligomers. *Neurobiol Aging* 2008;29:1334-47. DOI PubMed PMC
101. Manczak M, Reddy PH. Abnormal interaction of oligomeric amyloid-β with phosphorylated tau: implications to synaptic dysfunction and neuronal damage. *J Alzheimers Dis* 2013;36:285-95. DOI PubMed PMC
102. Fein JA, Sokolow S, Miller CA, et al. Co-localization of amyloid beta and tau pathology in Alzheimer's disease synaptosomes. *Am J Pathol* 2008;172:1683-92. DOI PubMed PMC
103. Takahashi RH, Capetillo-Zarate E, Lin MT, Milner TA, Gouras GK. Co-occurrence of Alzheimer's disease β-amyloid and τ pathologies at synapses. *Neurobiol Aging* 2010;31:1145-52. DOI PubMed PMC
104. Lockhart SN, Schöll M, Baker SL, et al. Amyloid and tau PET demonstrate region-specific associations in normal older people. *Neuroimage* 2017;150:191-9. DOI PubMed PMC
105. Golde TE, Schneider LS, Koo EH. Anti-aβ therapeutics in Alzheimer's disease: the need for a paradigm shift. *Neuron* 2011;69:203-13. DOI PubMed PMC
106. Parker HG, Kim LV, Sutter NB, et al. Genetic structure of the purebred domestic dog. *Science* 2004;304:1160-4. DOI PubMed
107. Davis PR, Head E. Prevention approaches in a preclinical canine model of Alzheimer's disease: benefits and challenges. *Front Pharmacol* 2014;5:47. DOI PubMed PMC
108. Awano T, Johnson GS, Wade CM, et al. Genome-wide association analysis reveals a SOD1 mutation in canine degenerative myelopathy that resembles amyotrophic lateral sclerosis. *Proc Natl Acad Sci U S A* 2009;106:2794-9. DOI PubMed PMC
109. Doustar J, Rentsendorj A, Torbati T, et al. Parallels between retinal and brain pathology and response to immunotherapy in old, late-stage Alzheimer's disease mouse models. *Aging Cell* 2020;19:e13246. DOI PubMed PMC

Zou *et al. Ageing Neur Dis* 2022;2:8
DOI: 10.20517/and.2022.09

Ageing and Neurodegenerative Diseases

Clinical Observation

Open Access

Olfactory and gustatory dysfunctions in patients with COVID-19 in Wuhan, China

Li Zou[#], Ting Yu[#], Yangyang Zhang[#], Lijun Dai, Zhaohui Zhang, Zhentao Zhang

Department of Neurology, Renmin Hospital of Wuhan University, Wuhan 430060, Hubei, China.
[#]These authors contributed equally to this work.

Correspondence to: Prof. Zhentao Zhang, Department of Neurology, Renmin Hospital of Wuhan University, Wuhan 430060, Hubei, China. E-mail: zhentaozhang@whu.edu.cn

How to cite this article: Zou L, Yu T, Zhang Y, Dai L, Zhang Z, Zhang Z. Olfactory and gustatory dysfunctions in patients with COVID-19 in Wuhan, China. *Ageing Neur Dis* 2022;2:8. https://dx.doi.org/10.20517/and.2022.09

Received: 21 Mar 2022 **First Decision:** 22 Apr 2022 **Revised:** 6 May 2022 **Accepted:** 20 May 2022 **Published:** 30 May 2022

Academic Editor: Wei-dong Le **Copy Editor:** Peng-Juan Wen **Production Editor:** Peng-Juan Wen

Abstract

The coronavirus disease 2019 (COVID-19) is spreading all over the world. The main symptoms of COVID-19 include fever, cough, fatigue, and myalgia. However, there are few reports on olfactory and gustatory dysfunctions in patients with COVID-19. Our objective was to investigate the incidence of olfactory and gustatory dysfunctions in patients with COVID-19 infection in Wuhan, China. In this retrospective study, we collected 81 confirmed cases of COVID-19 from the Renmin Hospital of Wuhan University from February 2020 to March 2020, and analyzed the demographic characteristics, clinical manifestations (including olfactory and gustatory dysfunctions), laboratory findings, and comorbidities. In total, 81 confirmed COVID-19 patients were enrolled in this study (38 males and 43 females). The study showed that the most prevalent symptoms included cough, myalgia, and loss of appetite. On admission, 25 (30.9%) of all patients reported either olfactory dysfunction (OD) or gustatory dysfunction (GD), and 7 (8.6%) reported both OD and GD. Overall, 13.6% and 25.9% of all patients reported OD and GD, respectively. OD and GD were not associated with disease severity. Pearson correlation analysis identified some factors that are correlated with OD and GD, including headache or dizziness (r = 0.342, *P* = 0.002), dark urine (r = 0.256, *P* = 0.021), IgM titer (r = 0.305, *P* = 0.01), and diabetes (r = 0.275, *P* = 0.013). Multivariate adjusted logistic analysis showed that patients with headache or dizziness (OR = 7.382, 95%CI: 1.028-53.022) and diabetics (OR = 6.871, 95%CI: 1.096-43.086) were at higher risk of developing OD. In addition, patients with high IgM titers (OR = 1.006, 95%CI: 1.000-1.006) and diabetes (OR = 4.335, 95%CI: 1.098-17.287) were at high risk of developing GD. In 81.8% of the cases with OD and 28.6% of the cases with GD, the symptoms lasted for at least one month after

discharge. In addition, 3.6% of inpatients without OD developed OD after discharge. These findings suggest that OD and GD are common in COVID-19. These symptoms appear early during the course of the disease and may last for one month. The incidence of OD and GD is related to neurological manifestations, diabetics, and IgM titers.

Keywords: COVID-19, SARS-CoV-2, smell, taste, infection

INTRODUCTION

Coronavirus disease 2019 (COVID-19), an infectious disease caused by the acute respiratory syndrome coronavirus-2 (SARS-CoV-2), has spread globally. As of March 20, 2022, there have been more than 464 million confirmed cases of COVID-19 globally[1]. Early epidemiological investigations show that the basic reproduction number (R0) of SARS-CoV-2 is estimated to be about 2.2 (range, 1.4-6.5)[2]. The high spread and low fatality rate of COVID-19 made it a global pandemic. COVID-19 has become the largest pandemic since the H1N1 flu outbreak in 1918. Early genetic tests emphasized that the genome sequence identity of SARS-CoV-2 and SARS-CoV is 79.5%. Both viruses infect cells through angiotensin-converting enzyme 2 (ACE2)[3,4]. The similarity of the gene sequence and infection route suggests that SARS-CoV-2 and SARS-CoV have similar clinical manifestations. Similar to SARS, the most common symptoms of COVID-19 are fever, cough, sputum, fatigue, and myalgia[5-7]. Complications of COVID-19 involve multiple systems, such as the cardiovascular system, digestive system, and nervous system[8-10]. Current research mainly focuses on central nervous system complications such as cerebrovascular diseases and acute encephalopathy[10], while less is known about the peripheral nervous system complications. Symptoms in the head and neck such as dry eyes, tearing, and smell and taste disturbances were reported in COVID-19 patients and believed to be related to the neurophagy of the virus[11-12]. It is worth noting that SARS-CoV can be detected 60-66 h after infection and is most abundant in the olfactory bulb[13]. In addition, the virus may enter the brain through the olfactory bulb. Viral antigens can also be detected in brain areas connected to the olfactory bulb, such as the piriform nucleus and subliminal leather, basal ganglia, and midbrain[14,15].

The purpose of this study was to investigate the incidence of olfactory and taste disorders in confirmed COVID-19 cases and to analyze the risk factors related to olfactory and gustatory dysfunctions in order to provide clues for the clinical diagnosis and treatment of COVID-19.

METHODS

Patient enrollment and data collection

This descriptive study included 81 inpatients diagnosed with COVID-19 in the Renmin Hospital of Wuhan University, Wuhan, China. The diagnosis of COVID-19 was based on clinical symptoms, computed tomography (CT), real-time RT-PCR, and next-generation sequencing. The patient's admission date was from February 1 to March 3, 2020. All patients participating in this study lived in Wuhan during the COVID-19 outbreak. Two well-trained investigators collected the data including demographic characteristics, clinical characteristics (including medical history, comorbidities, and symptoms), preliminary laboratory findings, treatment, and clinical outcomes.

According to the SARS-CoV-2 diagnosis and treatment guidelines (Versions 3-7) issued by the National Health Commission of China, the severity of COVID-19 patients was defined. Severe cases were designated when the patients fit one of the following criteria: (1) respiratory distress with respiratory rate ≥ 30/min; (2) oxygen saturation ≤ 93% at rest; (3) arterial partial oxygen pressure (PaO_2)/oxygen absorption concentration (FiO_2) ≤ 300 mmHg; (4) respiratory failure that needs mechanical ventilation; or (5) shock or organ failure requiring ICU care.

Procedures

Two investigators collected the information on epidemiology, clinical symptoms, laboratory test results, treatment, and clinical outcomes. Laboratory tests included routine blood examination (including white blood cells, lymphocytes, and platelets), coagulation function, lactate dehydrogenation, and immune indicators (including lymphocyte differential counts and inflammatory factors). Participants were interviewed by telephone and were asked to report their olfactory and gustatory dysfunctions at the time of hospitalization and one month after discharge. Two years after discharge, those with olfactory and gustatory dysfunctions one month after discharge were re-interviewed to report their smell and taste status. Verbal informed consent was obtained from all participants or their legal guardians. The severity of symptoms was graded as totally normal, mild, moderate, and severe. Totally normal means that respondents rated smell and taste as "Good" or "Unaffected", mild dysfunction means the patient hardly noticed a smell and taste reduction, moderate dysfunction means there was a noticeable reduction, and severe dysfunction means the patient reported an almost complete loss of smell and taste. Patients with olfactory and gustatory dysfunctions before contracting COVID-19 were excluded, and so were patients with a diagnosis of chronic rhinitis, Alzheimer's disease (AD), or Parkinson's disease (PD) on admission. We also asked patients during the telephone interview whether they had a history of chronic rhinitis, AD, or PD. These patients might experience olfactory and gustatory dysfunctions, which could affect the study results. Cases with unsuccessful follow-ups were excluded.

Statistical analysis

Continuous variables were described as medians and interquartile range (IQR), and categorical variables were described as frequency rates and percentages. We used the chi-square (χ^2) test or the Fisher's exact test to compare categorical data. Mann-Whitney-Wilcoxon test was applied to compare non-normally continuous variables. Pearson correlation analysis was used to examine the correlations between olfactory/gustatory dysfunctions and all indicators (including epidemiology, clinical symptoms, laboratory test results, treatment, and disease severity). The sample size varied due to missing data, and missing data were not imputed. The analyses regarding different factors were based on non-missing data. Multivariate adjusted logistic regression models were adopted to analyze the factors influencing olfactory and gustatory dysfunction in patients with COVID-19. All statistical analyses were performed using SPSS software (V.23.0). Two-tailed *P* values were considered statistically significant at < 0.05. This study was approved by the Hospital Ethics Committee of the Renmin Hospital of Wuhan University (WDRY2020-K136).

RESULTS

Demographic characteristics in COVID-19

The demographic characteristics, clinical manifestations, and comorbidities are shown in Table 1. Of the 81 patients, 63 cases were diagnosed as non-severe and 18 cases were severe. The median age was 58 years (IQR, 50.0-68.5 years). The median age of the severe group was 11.5 years older than that of the non-severe group. Males accounted for 46.9% (38 of 81) of the total patients. However, males accounted for 66.7% (12 of 18) of patients in the severe group compared with 41.3% (26 of 63) of the non-severe group. These results suggest that males and older patients are more likely to develop into severe cases, which is consistent with other reports[16]. On admission, the most common clinical manifestations were fever (72.8%) and respiratory symptoms (70.4%), while chest pain, fatigue, gastrointestinal symptoms, dark urine, and headache or dizziness accounted for 27.2%, 37%, 27.2%, 19.8%, and 14.8% of the patients, respectively. Compared with the non-severe group, the severe group had a higher proportion of dark urine (17.5% *vs.* 27.8%), suggesting a potential relationship between urinary system dysfunction and disease severity. Among the 81 cases, 51.9% had at least one comorbidity, including hypertension, diabetes, coronary heart disease, stroke, cancers, and chronic pulmonary diseases. Compared with the non-severe group, more patients in the severe group had a history of stroke (0% *vs.* 5.6%) and coronary heart disease (1.6% *vs.* 11.1%), suggesting that patients with

Table 1. Demographic characteristics of the 81 patients with COVID-19

Clinical characteristics and symptoms	All patients (*n* = 81)	Disease severity	
		Non-severe (*n* = 63)	Severe (*n* = 18)
Age, median (IQR) - years	58 (50.00-68.50)	57 (49.00-67.00)	68.5 (56.25-77.25)
Age groups - No., %			
< 65	51 (63.0)	45 (71.4)	6 (33.3)
≥ 65	30 (37.0)	18 (28.6)	12 (66.7)
Gender - No., %			
Male	38 (46.9)	26 (41.3)	12 (66.7)
Female	43 (53.1)	37 (58.7)	6 (33.3)
Symptoms or signs - No., %			
Fever on admission	59 (72.8)	46 (73.0)	12 (72.2)
Chest distress	22 (27.2)	19 (30.2)	3 (16.7)
Fatigue	30 (37.0)	23 (36.5)	7 (38.9)
Headache or dizziness	12 (14.8)	9 (14.3)	3 (16.7)
Respiratory symptoms	57 (70.4)	45 (71.4)	12 (66.7)
Gastrointestinal symptoms	22 (27.2)	17 (27.0)	5 (27.8)
Dark urine	16 (19.8)	11 (17.5)	5 (27.8)
Coexisting disorders - No., %			
Any	42 (51.9)	30 (47.6)	12 (66.7)
Hypertension	23 (28.4)	17 (27.0)	6 (33.3)
Diabetes	15 (18.5)	12 (19.0)	3 (16.7)
Coronary heart disease	3 (3.7)	1 (1.6)	2 (11.1)
Stroke	1 (1.2)	0 (0.0)	1 (5.6)
Cancer*	6 (7.4)	4 (6.3)	2 (11.1)
Chronic pulmonary disease#	7 (8.6)	5 (7.9)	2 (11.1)

Data are presented as medians [interquartile ranges (IQR)] and n/N (%). *Cancers referred to any malignancy. All cases had stable disease. #Chronic pulmonary disease includes tuberculosis, chronic obstructive pulmonary disease, and bronchiectasis. All cases were stable and no obvious bacterial infections.

cardiovascular and cerebrovascular diseases are more likely to develop severe illness. The above findings are consistent with previous studies[17-19].

Olfactory and gustatory dysfunctions in COVID-19

Table 2 summarizes the incidence of olfactory dysfunction (OD) and gustatory dysfunction (GD) when the patients were admitted to the hospital. On admission, 30.9% of all patients reported an altered sense of smell or taste. Overall, 13.6% and 25.9% reported OD and GD, respectively, while 8.6% reported both OD and GD. The incidence of OD in the severe group (11.1%) was not significantly different from that in the non-severe group (14.3%). Compared with the non-severe group, the incidence of GD was lower in the severe group (28.6% *vs.* 16.7%). However, OD and GD do not seem to be related to the severity of the disease (Fisher's exact test, $P < 0.05$).

The factors related to OD and GD are summarized in Table 3. We considered general conditions, symptoms, comorbidities, and laboratory tests and calculated the Pearson correlation coefficient. Some factors were positively correlated with OD, including headache or dizziness ($r = 0.342$, $P = 0.002$), dark urine ($r = 0.256$, $P = 0.021$), IgM titer ($r = 0.305$, $P = 0.01$), and diabetes ($r = 0.275$, $P = 0.013$). These factors were also positively correlated to GD (all $r > 0.2$, $P < 0.05$). The IgG titers were not significantly related to patients with OD ($r = 0.083$, $P = 0.496$) or GD ($r = 0.164$, $P = 0.176$). However, IgG titers were associated with the

Table 2. The incidence of olfactory and gustatory dysfunctions in patients with different disease severity

Disease severity	Olfactory dysfunction				Gustatory dysfunction				OD and GD	Any
	Total	Mild	Moderate	Severe	Total	Mild	Moderate	Severe		
Non-severe - *n*/%	9 (14.3)*	5 (7.9)	1 (1.6)	3 (4.8)	18 (28.6)*	8 (12.7)	7 (11.1)	3 (4.8)	5 (7.9)*	22 (34.9)*
Severe	2 (11.1)	0 (0.0)	1 (5.6)	1 (5.6)	3 (16.7)	1 (5.6)	1 (5.6)	1 (5.6)	2 (11.1)	3 (16.7)
All patients	11 (13.6)	5 (6.2)	2 (2.5)	4 (4.9)	21 (25.9)	9 (11.1)	8 (9.9)	4 (4.9)	7 (8.6)	25 (30.9)

*Compared with the severe group, $P > 0.05$. OD: Olfactory dysfunction; GD: gustatory dysfunction.

Table 3. Factors associated with olfactory and gustatory dysfunctions in COVID-19

Factors	OD		GD		OD or GD	
	r	*P* value	r	*P* value	r	*P* value
Headache or dizziness	0.342	0.002	0.308	0.005	0.248	0.026
Dark urine	0.256	0.021	0.273	0.014	0.273	0.014
IgM	0.305	0.01	0.238	0.046	0.251	0.035
IgG	0.083	0.496	0.164	0.176	0.269	0.024
Diabetes	0.275	0.013	0.298	0.007	0.301	0.006

OD: Olfactory dysfunction; GD: gustatory dysfunction.

incidence of patients with either OD or GD (r = 0.269, $P < 0.05$).

The association between various factors and the risk of olfactory and gustatory dysfunction in patients with COVID-19 is shown in Table 4. In the multivariate adjusted logistic regression model, patients with headache and dizziness (adjusted OR = 7.382, 95%CI: 1.028-53.022) were more likely to have olfactory dysfunction than those without headache and dizziness. Patients with diabetes had a higher risk of olfactory dysfunction compared to those without diabetes (adjusted OR = 6.871, 95%CI: 1.096-43.086). In the logistic regression analysis of gustatory dysfunctions, patients with high IgM titers had a higher risk of developing gustatory dysfunctions compared to those with low IgM titers (adjusted OR = 1.003, 95%CI: 1.000-1.006). In addition, patients with diabetes had a higher risk of developing GD compared to patients without diabetes (adjusted OR = 4.335, 95%CI: 1.098-17.287). Similarly, when OD and GD were treated as one symptom, patients with diabetes (adjusted OR = 7.963, 95%CI: 1.557-37.515) and patients with higher IgM titers (adjusted OR = 1.006, 95%CI: 1.001-1.010) had a higher probability of developing this symptom.

Table 5 describes the incidence of OD and GD one month after the patients were discharged from the hospital. Six patients had residual GD, and eleven patients reported OD. Of patients with OD or GD during hospitalization, 48.0% still complained of OD or GD one month after discharge. In patients with no OD or GD during hospitalization, 3.6% developed OD or GD after discharge. Continued follow-up of these patients with OD or GD showed that, in 60% (6 of 10) of the cases with OD and 20% (1 of 5) of the cases with GD, the symptoms lasted for at least two years; in 20% (2 of 10) of the cases with OD, symptoms aggravated. One OD patient and one GD patient lost in follow-up were excluded. We also analyzed the relationship between treatment and the incidences of olfactory and urinary dysfunction after discharge [Supplementary Table 1] and found that treatments had no effect on the clinical outcomes of OD and GD after patients were discharged, suggesting that the OD and GD are most likely primary symptoms caused by SARS-CoV-2, rather than the side effects of drugs.

DISCUSSION

This retrospective descriptive study included 81 confirmed cases of COVID-19 and focused on the OD and

Table 4. Multivariate adjusted logistic regression of olfactory and gustatory dysfunctions

Variables	β	SE	Wald	Adjusted OR	95%CI	*P*
OD						
Headache or dizziness	1.999	1.006	3.949	7.382	1.028-53.022	0.047
Dark urine	0.656	1.040	0.397	1.927	0.251-14.796	0.528
IgM	0.002	0.002	1.867	1.002	0.999-1.006	0.172
IgG	-0.001	0.898	3.671	5.591	0.961-32.515	0.055
Diabetes	1.927	0.937	4.234	6.871	1.096-43.086	0.040
Constant	-3.258	0.759	18.412			
GD						
Headache or dizziness	1.358	0.789	2.963	3.890	0.828-18.263	0.085
Dark urine	0.432	0.806	0.287	1.540	0.317-7.472	0.592
IgM	0.003	0.002	4.058	1.003	1.000-1.006	0.044
IgG	0.001	0.002	0.480	1.001	0.998-1.004	0.488
Diabetes	1.471	0.703	4.387	4.335	1.098-17.287	0.036
Constant	-2.098	0.531	15.591			
OD or GD						
Headache or dizziness	1.297	0.841	2.387	3.659	0.704-19.026	0.123
Dark urine	0.338	0.868	0.151	1.402	0.256-7.684	0.697
IgM	0.006	0.002	6.961	1.006	1.001-1.010	0.008
IgG	0.003	0.002	2.526	1.003	0.999-1.007	0.112
Diabetes	2.040	0.714	6.369	7.963	1.557-37.515	0.012
Constant	-2.479	0.589	17.727			

OD: Olfactory dysfunction; GD: gustatory dysfunction.

Table 5. The clinical outcomes of olfactory and gustatory dysfunctions in COVID-19 patients

During hospitalization	After discharged*			
	OD (*n* = 11)	GD (*n* = 6)	OD and GD (*n* = 3)	OD or GD (*n* = 14)
None - *n*/%	2 (3.6)	0 (0.0)	0 (0.0)	2 (3.6)
OD	9 (81.8)	3 (27.3)	3 (27.3)	9 (81.8)
GD	6 (28.6)	6 (28.6)	3 (14.3)	9 (42.9)
OD and GD	6 (85.7)	3 (42.9)	3 (42.9)	6 (85.7)
Any	9 (36.0)	6 (24.0)	3 (12.0)	12 (48.0)

*All enrolled patients' chest CT scanning signs disappeared and permitted discharge. OD: Olfactory dysfunction; GD: gustatory dysfunction.

GD in COVID-19 patients in Wuhan. On admission or during hospitalization, patients self-reporting OD, GD, and both accounted for 13.6%, 25.9%, and 8.6% of all subjects, respectively. The incidence of OD and GD in the severe cases was not significantly different from the non-severe cases, suggesting OD and GD are not related to the severity of the disease. In addition, 48.0% of patients had persistent OD or GD after the other clinical manifestations of COVID-19 disappeared. Continued follow-up showed that, in 20% of the cases with OD, symptoms even aggravated two years after infection.

There are currently few studies on the incidence of OD and GD in patients with COVID-19[20]. One study found that 5.1% of COVID-19 patients reported hyposmia[21]. Compared with this study, we found a higher rate of hyposmia (13.6%). A multicenter European study reported that 85.6% and 88.0% of patients suffer from olfactory and gustatory dysfunctions, respectively[22]; this result indicates that, compared with Asian

patients, gustatory dysfunctions are more common in European patients. Notably, a recent study found that the prevalence of smell and taste dysfunction in COVID-19 patients has dropped significantly with the advent of the Omicron variant[23]. Thus, the different strains of the virus may have distinct effects on olfactory and gustatory dysfunction.

The reasons for the different incidences of OD and GD may be as follows: (1) Quantitative measurement is more sensitive than self-report. Studies have shown that only 35% of patients are aware of their olfactory deficits[24]. (2) The different affinity of the virus to different populations may lead to clinical differences among patients in different regions. A study showed that ACE2 mutations reduce the correlation between human ACE2 and SARS-CoV S-protein, thereby reducing the chance of infection[25]. ACE2 polymorphisms and the differences in expression levels between Asian and European populations may explain the difference in olfactory dysfunction between Asian and European populations[26]. (3) Different strains of the virus may cause different clinical manifestations.

Pearson correlation coefficient showed that headache or dizziness, dark urine, IgM, and diabetes all showed a positive correlation with OD and GD (all $P < 0.05$). We noted that chronic rhinitis and certain neurodegenerative diseases may directly lead to taste or smell disorders. In this study, such patients were excluded. Headache or dizziness are the most common symptoms of the nervous system. In a previous report, the incidence of headache and dizziness in COVID-19 patients were 13.1% and 16.8%, respectively[21]. OD and GD are positively related to dizziness and headache. It has been reported that ACE2 is highly expressed in the nasal goblet and ciliated cells[27]. The virus may infect the olfactory nerve early and cause OD before other neurological manifestations. OD and GD were also significantly related to dark urine. This may suggest that dark urine, similar to OD/GD, is a sign of early infection and damage to the urinary system. IgM is an early antibody produced by the immune system after infection. The interaction of infectivity, virulence, and immune response may explain the positive correlation between IgM and OD/GD. Consistent with other results, diabetes was significantly correlated with smell dysfunction[28]. The infection might exacerbate potential nerve damage in diabetic patients. In addition, multivariate adjusted logistic analysis showed that patients with headache or dizziness and diabetics were at higher risk of developing olfactory dysfunction, while patients with high IgM titers and diabetes were at high risk of developing gustatory dysfunction, which is consistent with the results of the above Pearson correlation coefficient.

One month or more after discharge, some patients still suffered from OD and GD. A few patients who did not have OD or GD during hospitalization developed these symptoms after discharge. Considering the damage caused by the virus to the olfactory or gustatory nerve, this may be one of the possible sequelae of COVID-19 patients. It is worth noting that SARS-CoV can be detected 60-66 h after infection and is most abundant in the olfactory bulb[29]. While the infection routes of SARS-CoV-2 and SARS-CoV are similar, OD may be an early symptom of COVID-19. Early screening of people with OG and GD, early detection of virus infections, and early isolation of COVID-19 patients can help prevent the spread of COVID-19.

In conclusion, we found that OD and GD are common symptoms of COVID-19. They appear early during the disease and may last from one month to even two years. Headache or dizziness, IgM titers, and diabetes are correlated with the occurrence of OD and GD. This retrospective study has some limitations. First, we collected self-reported data, which may lead to information bias. Second, the sample size was relatively small and geographically limited. We only recruited 81 confirmed cases of COVID-19 in our database since COVID-19 infectious was effectively controlled in Wuhan in early 2020. The cases reported here represent what happened to the first batch of patients in China. Third, grading bias might exist since we did not perform objective smell and taste tests. Fourth, as patients with other infectious diseases were not included

in the control group, it could not be determined whether COVID-19 had a more severe and longer-lasting impact on taste and smell than other infectious diseases.

DECLARATIONS

Authors' contributions

Full access to all of the data in the study, take responsibility for the integrity of the data and the accuracy of the data analysis, and wrote the manuscript: Zou L
The acquisition of data: Yu T, Zhang Y
Reviewed literature and gave technical support: Dai L
Conceived and supervised the project: Zhang Z, Zhang Z
All authors read and approved the submission of the manuscript.

Availability of data and materials

All analyzed data of this study are included within the article.

Financial support and sponsorship

This work was supported by grants from the National Natural Science Foundation of China (No. 81822016 and 81771382) and Medical Science Advancement Program of Wuhan University (No. TFLC2018001).

Conflicts of interest

All authors declared that there are no conflicts of interest.

Ethical approval and consent to participate

This study was approved by the Hospital Ethics Committee of the Renmin Hospital of Wuhan University [WDRY2020-K136].

Consent for publication

All patients agreed to participate in this study.

REFERENCES

1. WHO Coronavirus (COVID-19) Dashboard. Available from: https://www.who.int/redirect-pages/page/novel-coronavirus-(covid-19)-situation-dashboard [Last accessed on 26 May 2022].
2. Adhikari SP, Meng S, Wu YJ, et al. Epidemiology, causes, clinical manifestation and diagnosis, prevention and control of coronavirus disease (COVID-19) during the early outbreak period: a scoping review. *Infect Dis Poverty* 2020;9:29. DOI PubMed PMC
3. Zhou P, Yang XL, Wang XG, et al. A pneumonia outbreak associated with a new coronavirus of probable bat origin. *Nature* 2020;579:270-3. DOI PubMed PMC
4. Dutta K. Allosteric site of ACE-2 as a drug target for COVID-19. *ACS Pharmacol Transl Sci* 2022;5:179-82. DOI PubMed PMC
5. do Nascimento IJ, O'Mathúna DP, von Groote TC, et al; International Network of Coronavirus Disease 2019 (InterNetCOVID-19). Coronavirus disease (COVID-19) pandemic: an overview of systematic reviews. *BMC Infect Dis* 2021;21:525. DOI PubMed PMC
6. da Rosa Mesquita R, Francelino Silva Junior LC, Santos Santana FM, et al. Clinical manifestations of COVID-19 in the general population: systematic review. *Wien Klin Wochenschr* 2021;133:377-82. DOI PubMed PMC
7. Neto AR, Carvalho ARB, Oliveira EMN, Magalhães RLB, Moura MEB, Freitas DRJ. Symptomatic manifestations of the disease caused by coronavirus (COVID-19) in adults: systematic review. *Rev Gaucha Enferm* 2021;42:e20200205. DOI PubMed
8. Zheng YY, Ma YT, Zhang JY, Xie X. COVID-19 and the cardiovascular system. *Nat Rev Cardiol* 2020;17:25960. DOI PubMed PMC
9. Han C, Duan C, Zhang S, et al. Digestive symptoms in COVID-19 patients with mild disease severity: clinical presentation, stool viral RNA testing, and outcomes. *Am J Gastroenterol* 2020;115:916-23. DOI PubMed PMC
10. Portela-Sánchez S, Sánchez-Soblechero A, Melgarejo Otalora PJ, et al. Neurological complications of COVID-19 in hospitalized

patients: the registry of a neurology department in the first wave of the pandemic. *Eur J Neurol* 2021;28:3339-47. DOI PubMed PMC

11. Meduri A, Oliverio GW, Mancuso G, et al. Ocular surface manifestation of COVID-19 and tear film analysis. *Sci Rep* 2020;10:20178. DOI PubMed PMC
12. Freni F, Meduri A, Gazia F, et al. Symptomatology in head and neck district in coronavirus disease (COVID-19): a possible neuroinvasive action of SARS-CoV-2. *Am J Otolaryngol* 2020;41:102612. DOI PubMed PMC
13. Netland J, Meyerholz DK, Moore S, Cassell M, Perlman S. Severe acute respiratory syndrome coronavirus infection causes neuronal death in the absence of encephalitis in mice transgenic for human ACE2. *J Virol* 2008;82:7264-75. DOI PubMed PMC
14. Leyva-Grado VH, Churchill L, Wu M, et al. Influenza virus- and cytokine-immunoreactive cells in the murine olfactory and central autonomic nervous systems before and after illness onset. *J Neuroimmunol* 2009;211:73-83. DOI PubMed PMC
15. Wheeler DL, Athmer J, Meyerholz DK, Perlman S. Murine olfactory bulb interneurons survive infection with a neurotropic coronavirus. *J Virol* 2017;91:e01099-17. DOI PubMed PMC
16. Grasselli G, Zangrillo A, Zanella A, et al; COVID-19 Lombardy ICU Network. Baseline characteristics and outcomes of 1591 patients infected with SARS-CoV-2 admitted to ICUs of the lombardy region, Italy. *JAMA* 2020;323:1574-81. DOI PubMed PMC
17. Zhang JJ, Dong X, Cao YY, et al. Clinical characteristics of 140 patients infected with SARS-CoV-2 in Wuhan, China. *Allergy* 2020;75:1730-41. DOI PubMed
18. Guan WJ, Ni ZY, Hu Y, et al; China Medical Treatment Expert Group for Covid-19. Clinical characteristics of coronavirus disease 2019 in China. *N Engl J Med* 2020;382:1708-20. DOI PubMed PMC
19. Wang D, Hu B, Hu C, et al. Clinical characteristics of 138 hospitalized patients with 2019 novel coronavirus-infected pneumonia in Wuhan, China. *JAMA* 2020;323:1061-9. DOI PubMed PMC
20. Ghods K, Alaee A. Olfactory and taste disorders in patients suffering from Covid-19, a review of literature. *J Dent (Shiraz)* 2022;23:1-6. DOI PubMed PMC
21. Mao L, Jin H, Wang M, et al. Neurologic manifestations of hospitalized patients with coronavirus disease 2019 in Wuhan, China. *JAMA Neurol* 2020;77:683-90. DOI PubMed PMC
22. Lechien JR, Chiesa-Estomba CM, De Siati DR, et al. Olfactory and gustatory dysfunctions as a clinical presentation of mild-to-moderate forms of the coronavirus disease (COVID-19): a multicenter European study. *Eur Arch Otorhinolaryngol* 2020;277:2251-61. DOI PubMed PMC
23. Boscolo-Rizzo P, Tirelli G, Meloni P, et al. Coronavirus disease 2019 (COVID-19)-related smell and taste impairment with widespread diffusion of severe acute respiratory syndrome-coronavirus-2 (SARS-CoV-2) Omicron variant. *Int Forum Allergy Rhinol* 2022. DOI PubMed PMC
24. Giacomelli A, Pezzati L, Conti F, et al. Self-reported olfactory and taste disorders in patients with severe acute respiratory coronavirus 2 infection: a cross-sectional study. *Clin Infect Dis* 2020;71:889-90. DOI PubMed PMC
25. Li W, Zhang C, Sui J, et al. Receptor and viral determinants of SARS-coronavirus adaptation to human ACE2. *EMBO J* 2005;24:1634-43. DOI PubMed PMC
26. Cao Y, Li L, Feng Z, et al. Comparative genetic analysis of the novel coronavirus (2019-nCoV/SARS-CoV-2) receptor ACE2 in different populations. *Cell Discov* 2020;6:11. DOI PubMed PMC
27. Sungnak W, Huang N, Bécavin C, Berg M; HCA Lung Biological Network. SARS-CoV-2 entry genes are most highly expressed in nasal goblet and ciliated cells within human airways. *ArXiv* 2020;arXiv:2003.06122v1. PubMed PMC
28. Moein ST, Hashemian SM, Mansourafshar B, Khorram-Tousi A, Tabarsi P, Doty RL. Smell dysfunction: a biomarker for COVID-19. *Int Forum Allergy Rhinol* 2020;10:944-50. DOI PubMed PMC
29. Weiss SR, Navas-Martin S. Coronavirus pathogenesis and the emerging pathogen severe acute respiratory syndrome coronavirus. *Microbiol Mol Biol Rev* 2005;69:635-64. DOI PubMed PMC

Hu *et al. Ageing Neur Dis* 2022;2:9
DOI: 10.20517/and.2022.04

Ageing and Neurodegenerative Diseases

Review

Open Access

Electroneurography abnormality in Parkinson's disease: a potential biomarker to help diagnosis

Yiying Hu, Zhanhua Liang, Chunli Song

Department of Neurology, the First Affiliated Hospital of Dalian Medical University, Dalian 116011, Liaoning, China.

Correspondence to: Prof. Zhanhua Liang, Department of Neurology, the First Affiliated Hospital of Dalian Medical University, No. 222 Zhongshan Road, Xigang District, Dalian 116011, Liaoning, China. E-mail: liangzhanhua@dmu.edu.cn; Prof. Chunli Song, Department of Neurology, the First Affiliated Hospital of Dalian Medical University, No. 222 Zhongshan Road, Xigang District, Dalian 116011, Liaoning, China. E-mail: 510886190@qq.com

How to cite this article: Hu Y, Liang Z, Song C. Electroneurography abnormality in Parkinson's disease: a potential biomarker to help diagnosis. *Ageing Neur Dis* 2022;2:9. https://dx.doi.org/10.20517/and.2022.04

Received: 25 Jan 2022 **First Decision:** 4 Mar 2022 **Revised:** 3 May 2022 **Accepted:** 8 Jun 2022 **Published:** 13 Jun 2022

Academic Editor: Wei-Dong Le **Copy Editor:** Peng-Juan Wen **Production Editor:** Peng-Juan Wen

Abstract

Parkinson's disease (PD) is a common neurodegenerative disease, pathologically characterized by the progressive degeneration of dopaminergic neurons in the substantia nigra. Although various biomarkers and imaging criteria for PD have been established, objective and reliable evaluation methods are still lacking. Electroneurography, as an objective measurement of evoked compound muscle action potentials, is used to assess the integrity of the peripheral nerve and is important in the diagnosis and differential diagnosis of PD with neuromuscular injury. Moreover, it provides references for the evaluation and quantification of the motor function in PD. Here, we summarize recent advances in clinical research of electroneurography in PD, including the peripheral nerve conduction velocity, needle electromyography, surface electromyography, and motion unit number estimation. The potential values of electroneurography in PD diagnosis are also involved.

Keywords: Parkinson's disease, electroneurography, needle electromyography, surface electromyography, motor unit number estimation

INTRODUCTION

Parkinson's disease (PD) is a common neurodegenerative disease in middle-aged and elderly people. Currently, it is believed that the main pathological change of PD is the progressive degeneration of dopaminergic neurons in the substantia nigra. The prevalence rate of people over 65 years old in China is 1.7%, and the incidence increases with aging[1]. PD is clinically characterized by motor deficits including rest tremor, bradykinesia, myotonia, and postural balance disorders, as well as non-motor symptoms such as sensory disturbances, autonomic dysfunction, and mental and cognitive disorders. PD diagnosis is primarily based on history and physical examination[2]. In the early stage of the disease, there is still a lack of objective or reliable diagnostic measurements. Although several auxiliary examinations have been established including olfactory test[3], transcranial B-mode sonography of substantia nigra[4], positron emission tomography with 18-fluorodeoxyglucose examination[5], and autonomic nervous function examination such as ventricular variation rate detection[6], these methods lack sensitivity and specificity in the early stage of the disease. Meanwhile, with recent advances in the understanding of the non-motor symptoms of PD, increasing lines of evidence show that peripheral neuropathy (PN) caused by neuroinflammation, oxidative stress, environmental toxins, and apoptosis may play an important role in the pathophysiological process of PD. Axonal or myelin sheath injury caused by these factors often manifests as peripheral nerve conduction velocity, including the prolonged latency, decreased compound muscle action potential amplitude, altered conduction velocity, conduction block, or waveform dispersion.

As an objective examination method, electroneurography has been widely used in the diagnosis and differential diagnosis of PN, muscular diseases, neuromuscular junction, and other diseases. This article reviews the research progress in the clinical application of electroneurography in PD.

THE MECHANISM OF PERIPHERAL NEUROPATHY IN PD

Peripheral nerve conduction velocity (NCV) examination includes motor nerve conduction velocity, sensory nerve conduction velocity, and F-wave, which can objectively reflect the integrity of myelin sheath. According to the traditional view, PD lacks epidemiological correlation with PN, and it is limited to patients with rare gene mutations such as PARK2, FMR1, ATXN3, and ATP13A2[7] or mitochondrial disease. In recent years, it has been demonstrated that PN can also be found in idiopathic PD. Damage affecting medium to large fibers was found in PD in lower limbs, which can be confirmed by NCV as a new clinical fact, and the most common nerve found was the superficial fibular nerve, followed by the sural[8].

Axonopathy in PD, as shown by the decreased amplitude of sural nerve[9,10], may also be due to long-term treatment with levodopa. Levodopa is methylated by catechol-O-methyltransferase to produce S-adenosyl homocysteine in central and peripheral tissues, which is immediately cleaved to form homocysteine (HCY). Folate and vitamin B12 as cofactors are required to convert HCY back to S-adenosylmethionine (SMA). Therefore, with the increase of levodopa, vitamin B12 consumption increases, and PN associated with vitamin B12 deficiency occurs[11]. On the other hand, HCY induces inflammatory responses by increasing brittleness to mitochondrial toxins and increasing free radicals, impinging on DNA repair mechanisms[12,13] and RNA methylation[14], leading to terminal degeneration of sural nerve axon. The incidence rate of large fibrous lesions in PD is 16.3%, and in small fibers, confirmed by biopsy is 56.9%[15]. However, the literature does not exclude the possible influence of other factors such as diabetes and age-related factors on peripheral nerve damage. Levodopa is not the initial factor of PD with peripheral neuropathy, but the treatment exacerbates the progression of neuropathy.

A third mechanism of the causal relationship between PN and PD is the massive accumulation of α-synuclein in peripheral nerve terminal and damaged axon transport, resulting in small fibers[16]. Pathological changes have also been demonstrated in animal models, i.e., the spreading of α-synuclein is associated with sensory nerve degeneration and defective nociception. α-synuclein aggregates in the afferent sensory system, including sensory neurons, axons from the dorsal roots, and spinal dorsal horn neurons, and can reduce NCV through the ultrastructural damaged small and medium myelinated fibers. Meanwhile, α-synuclein, immunoreactive in lamina I of the dorsal horn, modulates pain processing, which is related to the pain of PD[17,18]. PN is a frequent yet underestimated feature of PD. PD patients with PN are older, have a higher levodopa dose, have worse axial motor features, and are independently associated with cognitive impairment. NCV examination can provide an objective diagnostic basis for PD with peripheral nerve damage. PN may be an independent peripheral marker of PD, indicating that there is a long course of disease accompanied by worse axial motion and impairment[19].

NEEDLE ELECTROMYOGRAPHY

Needle electromyography (NEMG) is a method to record various electrical characteristics of muscle resting or voluntary contraction by using a concentric needle electrode to determine the localization and type of neuromuscular disease. NEMG inspection is conducted in three parts. The first is the spontaneous activity in the muscle resting state. The second is the contraction [motor unit action potential (MUAP)], which is the sum of synchronous discharges of a group of muscle fibers dominated by one anterior horn cell. The third is the electrical activity during vigorous muscle contraction (recruitment pattern). NEMG is often used in PD with camptocormia and anal electromyography.

The NEMG in PD with camptocormia

Abnormal postures are common in PD, mainly including camptocormia, antecollis, Pisa syndrome, scoliosis, and striatal deformity[20]. According to epidemiological statistics, the incidence of PD with camptocormia is about 22.5%, also with multiple system atrophy (MSA), dementia with Lewy bodies, frontotemporal lobar degeneration, progressive supranuclear palsy, and Alzheimer's disease[21]. While the exact mechanism underlying the pathogenesis of camptocormia is unknown, it has been recognized that both central and peripheral mechanisms may be involved, including abnormal motor function of basal ganglia-thalamic-cortical circuits[22], sensory afferent dysfunction, muscle and joint proprioception abnormalities[23], acetylcholine-dopamine transmitter imbalance[24], and inflammatory infiltration in paraspinal muscles. The possible pathogenesis can be divided into the following four types[25]: those caused by the progression of PD, manifested in the form of PD with dystonia, secondary to paraspinal muscle myogenic diseases, and antipsychotics caused by treatment.

Myopathy, myositis, neurogenic changes, and dystonia can be seen in NEMG in PD with camptocormia[26]. NEMG of paravertebral muscles can suggest myopathy-like manifestations, with a narrow duration of multiphase potential and low amplitude, or accompanied by a small amount of spontaneous potential[27], as well as dorsal and ventral trunk muscles (mainly about rectus abdominis, iliopsoas, internal oblique, and external oblique muscles)[28]. Distal and proximal limb muscles may also be involved[29].

In some patients, burst discharges were observed in the responsible muscles under electromyography, which usually suggests pathogenesis caused by dystonia. The camptocormia in PD is aggravated when walking or exercising and relieved by standing against a wall. Similar to the "sensory trick" of dystonia, camptocormia can be caused by the strong contraction of abnormal muscles[30]. NEMG can be used to guide the treatment of botulinum toxin A when the pathogenesis suggests dystonia to identify the target muscles with the more active potentials. When botulinum toxin A was injected into rectus abdominis muscle and external oblique

muscle for treatment, the abnormal posture and abdominal pain were significantly improved 7-8 weeks after injection[31,32].

The external anal sphincter electromyography in PD

External anal sphincter electromyography (EAS-EMG) is widely used in the differential diagnosis of neurological dysfunction of lumbosacral segment related diseases, such as lumbosacral radiculopathy, tethered cord syndrome, neurodegenerative diseases, and intraoperative monitoring of lumbosacral related operations. In the 1960s, Graham and Oppenheimer[33] proposed that Onuf's nucleus, located in 1/3 of the ventral gray matter of S2-S3 sacral medullary, is a motor nucleus which sends out the pudendal nerve to innervate the external urethral sphincter, anal sphincter, and pelvic floor striated muscle.

Both PD and MSA are associated with the impairment of autonomic nerve function, and their pathological mechanisms are different. Since MSA may be associated with the motor neuron degeneration of Onuf's nucleus, EAS-EMG (including duration, phase, and satellite potential) could efficiently make a differentiation between MSA and PD with a sensitivity of 100% and specificity of 86%[34]. The prolonged motor unit potentials (MUPs) duration and polyphasic MUPs usually indicate collateral reinnervation, which can be seen in early PD and MSA[35]. Compared with PD, MSA is mainly characterized by a more prolonged mean duration and decreased amplitude during vigorous contraction[36]. Most studies show that the abnormal rate of MSA is about 70%; muscular denervation such as fibrillation potential, positive sharp wave, and the duration of the action potential are widened; and the amplitude and polyphase wave are increased, as can be seen under the electromyography[37].

Based on EAS-EMG, using the test of the bulbocavernosus reflex (BCR) by stimulating the pudendal nerve can also reflect the degree of damage to the autonomic nerve. The amplitude of BCR in PD is lower than in MSA. It is confirmed that PD can be accompanied with functional impairment of the autonomic nervous, but the degree is less than in MSA. Patients with MSA have a longer latent period and higher amplitude. In some cases, BCR can be used to distinguish MSA from PD[38]. However, it is well known that the amplitude is greatly affected by the individual; thus, latency is more accurate in reflecting the degree of autonomic nerve damage, which is not mentioned in the literature above.

APPLICATION OF SURFACE ELECTROMYOGRAPHY IN PD

Surface electromyography (sEMG) is a non-invasive method to record the movement of motor units through the skin surface with electrodes[39]. The characteristics of the signals mainly include linear (amplitude and frequency) and nonlinear (complexity and orderly) indices. It is usually used to evaluate the activity and quantify the function of neuromuscular objectively. Motor neurons are activated when muscles contract autonomously or receive an external stimulus; all recruited motor units produce continuous MUAP, which is transmitted through fat and subcutaneous tissues and finally recorded by surface electrodes[40]. Many researchers have used sEMG technology for gait disorder evaluation, fatigue status detection, tremor analysis, central motor control, and acoustic kinematics in PD.

Application of sEMG in the assessment of gait disorder in PD

Gait disorder is a common feature of PD with the main characteristics of reduced shuffling, reduced step length and speed, difficult starting, increased rigidity, and freezing. It is one of the important factors of falls in PD. Some gait disturbances, such as bradykinesia and rigidity, have proven to be due to the decreased output of cortical motor caused by the imbalance of basal ganglia loop or supplementary motor area, as well as the changes in cortical and subcortical connectivity[41]. Some abnormal gait with instability is not only caused by the central factor but also peripheral factors, such as the greater contraction of agonist/antagonist

muscle groups and less effective recruitment of individual muscles[42]. sEMG can describe the walking characteristics of the patient to evaluate the motor function and formulate the next treatment and rehabilitation plan[43] by analyzing the way different muscles in the lower body are recruited. Gait analysis by sEMG should include the phase of stance and swing, two-limb support, and one-limb support[44]. Anterior tibial (TA) is the most frequently assessed muscle as it can receive more projections from the cortex with other limb muscles. Patients with PD always have reduced TA activity during the stance phase[45]. Some patients with freezing have a higher activity of bilateral TA during the swing phase[46], which reflects the impairment in motor control with the step length. The activity of medial gastrocnemius (MG) in PD is lower than in healthy controls, suggesting the defective function of proprioceptive[47]. MG plays an important role in supporting the body in the vertical direction and stabilizing the ankle joint to maintain the balance of walking speed and posture[48]. The asymmetric activities of TA-MG in PD are higher, which is an early feature of PD, as they have reduced muscle activity[49]. The increased EMG variability usually indicates a high risk of falls in PD[50], and it is an important trigger factor with frozen gait. Different walking modes, such as straight walk, U-turn, and point turn, require high energy consumption and therefore limit walking speed and flexibility[51]. Kugler *et al.* used a classification algorithm based on data collected from sEMG and accelerometers for step segmentation[52]. The proposed step detection method reached 98.9% sensitivity and 99.3% specificity for the classification accuracy of distinguishing between PD and healthy subjects. The reduced step length seems to be a specific feature of PD gait that can be detected early in the disease and can be a useful marker of disease progression. Co-activation is another feature of gait in PD, which can stabilize the joints and increase rigidity[53]. Interventions for gait disorders must modify the activities and patterns of individual muscles, changing the coordinated contraction on the basis of gait impairment in PD.

Fatigue evaluation of sEMG in PD

Patients with PD often have unexplained fatigue as a sense of overwhelming tiredness, which is different from apathy, depression, dementia, or sleepiness, and it has two forms: subjective fatigue and objective fatigue[54]. The incidence rate ranges from 33% to 50%[55]. Some studies have demonstrated that this figure is as high as 70%. Fatigue can be observed in some but not all patients with good motor function, as well as in patients with depression, sleep disturbance, and autonomic symptoms[56]. Basal ganglia dysfunction, such as the extrastriatal dopaminergic projections or frontal striato-thalamo-cortical loops, has been suggested as the pathophysiology, and the reduced blood perfusion in the frontal lobes can also be a contributor to fatigue[57]. Some potential biomarkers such as C-reactive protein, cytokines, and interleukin-6 may be correlated to fatigue. Other researchers have suggested pathophysiological mechanisms including dysfunction of the hypothalamic-pituitary-adrenal system[58]. The demographic characteristics indicate that the patients with fatigue are 1.4 years older on average, more likely to be female, and have a longer disease duration, higher UPDRS motor scores and levodopa dose, worse cognitive performances, and depression[59]. Fatigue is usually measured through scales with no specific biomarkers. The scales are suitable for subjective fatigue. Subjective fatigue and objective fatigue are distinct and independent concepts. sEMG can detect bioelectrical activities associated with muscle contraction and reveal neural changes in objective fatigue. It can be measured based on changes during sustained muscle contraction. Longer periods of vigorous contraction indicate that more activities are required to initiate movement, leading to bradykinesia[60]. Some researchers have indicated that the sEMG pattern of fatigue in PD is not different from that in healthy controls[61], which might be due to the impacts from patients with subjective fatigue. sEMG can be used as a viable clinical assessment tool to detect the muscle pattern of fatigue and identify the risk during the onset.

The potential mechanism in tremor with PD by sEMG

With the development of the sEMG technology, many researchers have recently used acceleration measurement combined with sEMG to explore the tremor pattern of PD. The diagnosis of PD is

challenging; to date, sEMG is the gold standard for the analysis and diagnosis of tremors[62]. The movement during tremor and different burst modes of a pair of antagonistic muscles can be recorded by sEMG. The frequency of most pathological tremors is 4-8 Hz, some palatal tremors are below 4 Hz, and orthostatic tremors are 13-18 Hz[63]. Tremor generators are often classified as central or peripheral in origin[64]. An abnormal rhythm of tremor exists in the basal ganglia of PD, while the network of ET is in the lower olive nucleus. The tremor harmonics as a valuable biomarker for tremor is important[65].

The rest tremor as a typical and unique feature of PD has been considered for a long time, but recent studies have shown that rest tremor is also present in 15% of patients with ET[66], causing misdiagnosis. For tremor analysis based on sEMG, parkinsonian rest tremor differs from ET as the tremor amplitude is suppressed during initiation of voluntary and target movements[67]. The suppressed rest tremor may have delayed re-emergence when a new posture is sustained (re-emergent tremor), and the rest tremor in PD is usually unilateral in onset with 4-6 Hz[63]. The rest tremor suppression test has demonstrated a very good sensitivity of ≥ 0.92 and a specificity of ≥ 0.69 for identifying rest tremor of PD[67].

Thirty-nine percent of CBD patients have tremors during the disease course, including rest tremor, postural tremor, and action tremor. They are similar to low amplitude action myoclonus and differ from the typical rest tremor of PD[68].

Shaikh *et al.*[69] applied sEMG to differentiate PD from drug-induced secondary parkinsonian syndrome (dopamine receptor blockers such as antiemetic drugs and antipsychotics and DRBA-induced parkinsonism). Intentional tremor amplitude increased significantly in DRBA-induced parkinsonism, and the amplitude of tremor in resting and postural is similar. It may be due to the irregularity in the oscillation waveforms and the disturbance of central oscillator output. Tremor analysis is particularly useful in the diagnosis of various tremors.

The application of sEMG in central motor control of PD

Determinism (%DET), sample entropy (SampEn), and intermuscular coherence provide estimates of the signals of sEMG structure as nonlinear patterns. Higher %DET, lower SampEn, and higher theta, alpha, and beta band intermuscular coherences are observed in PD, which is correlated with MDS-UPDRS scores[70]. This may reflect the oscillatory synchronization between the central nervous system and motor neurons, resulting in the enhancement of motor unit synchronization. The enhanced theta (4-6 Hz) and alpha (8-12 Hz) band coherences contribute to PD tremor. The amplified alpha-band drive in PD is involved in reticulospinal pathways, cortex and corticospinal output to muscles, and cerebello-thalamo-cortical circuit[71]. The above signal analysis process is complex and requires specific mathematical models or analysis software. Further research is needed to verify the reliability and validity of the analysis method.

The use of sEMG in acoustic kinematics

The output of speech includes the cognitive, neuromotor cortex, neuromuscular, and musculoskeletal components. Gómez *et al.*[72] used sEMG to differentiate the speech kinematic behavior by absolute velocities (dynamic and acoustic) of the joint jaw-tongue in PD, and their amplitude distributions can be used as potential biomarkers. They showed the characteristics of the interaction between the orofacial muscles by sEMG, which suggest that the facial nucleus and perioral muscles are well-preserved in PD. The lower amplitude ratio is consistent with thalamocortical activation, is limited by motor cortex activity, and contributes to bradykinesia and hypokinesia of orofacial muscles[73].

CLINICAL APPLICATION OF MOTOR UNIT NUMBER ESTIMATION IN PD

The axon of an anterior horn motor cell and all muscle fibers it dominates are called a motor unit. Motor unit number estimation (MUNE) is a non-invasive electrophysiological test for estimating the signs of degeneration of anterior horn cells. Mes found MUNE measurements were smaller in PD with different muscles, suggesting a slight degeneration[74]. Changes in MUNE are also associated with age, due to the degeneration of motor neurons due to physiological aging. It was also confirmed in the model of rats[75] that the threshold of MUAP was lower and recruited less. Neurofibrodegeneration and Lewy body appeared in large- and medium-sized motor neurons of spinal cord anterior horn cells, while small motor neurons were not found.

Some studies showed the increased motor unit amplitude and duration, which means reinnervation of motor units in PD[76]. Asymptomatic motor neuron degeneration may be one of the pathological manifestations of PD, and MUNE has a certain standard deviation which needs to be confirmed by further studies with other electroneurography techniques.

CONCLUSION

PD is a common neurodegenerative disease, the diagnosis of which is based on clinical criteria only due to the lack of biomarkers. Thus, it has become important to detect the disease early. NEMG is an invasive method and poorly accepted by patients, but EAS-EMG is sensitive and specific for PD and MSA. NEMG is necessary for the auxiliary diagnosis of PD with camptocormia and striatal deformity; it can also be used as a guide for the therapy with botulinum toxin A to identify the target muscles for more precise treatment. sEMG is non-invasive with significant value in PD gait analysis and tremor. Especially, tremor analysis technology is simple and reliable in separating PD from other diseases. It may be a choice to be included in the diagnosis criteria. The application of sEMG in central motor control and acoustic kinematics is not widely used in clinical practice, but it is irreplaceable in the research on the development of quantitative biomarkers such as optimized neuromuscular performance and motor neuron activity. Electroneurogram has localization significance in PD with the diagnosis of the damage in peripheral nerve and anterior horn cells, and it needs further research. Therefore, electroneurography plays a certain role in the clinical diagnosis of PD and needs large samples to be further confirmed.

DECLARATIONS

Authors' contributions

Prepared the first draft: Hu Y
Made substantial contributions to conception and revised manuscript: Song C
Gave critical comments: Liang Z

Availability of data and materials

Not applicable.

Financial support and sponsorship

None.

Conflicts of interest

All authors declared that there are no conflicts of interest.

Ethical approval and consent to participate

Not applicable.

Consent for publication

Not applicable.

REFERENCES

1. Chinese Society of Parkinson's Disease and Movement Disorders. Diagnosis and treatment of Parkinson disease: a review. 4th ed. *Chin J Neurol* 2020;53:973-86. (in Chinese)
2. Armstrong MJ, Okun MS. Diagnosis and treatment of Parkinson disease: a review. *JAMA* 2020;323:548-60. DOI PubMed
3. Berendse HW, Ponsen MM. Detection of preclinical Parkinson's disease along the olfactory trac(t). *J Neural Transm Suppl* 2006;70:321-5. DOI PubMed
4. Yilmaz R, Berg D. Transcranial B-mode sonography in movement disorders. *Int Rev Neurobiol* 2018;143:179-212. DOI PubMed
5. Hilker R, Voges J, Weisenbach S, et al. Subthalamic nucleus stimulation restores glucose metabolism in associative and limbic cortices and in cerebellum: evidence from a FDG-PET study in advanced Parkinson's disease. *J Cereb Blood Flow Metab* 2004;24:7-16. DOI PubMed
6. Potashkin J, Huang X, Becker C, Chen H, Foltynie T, Marras C. Understanding the links between cardiovascular disease and Parkinson's disease. *Mov Disord* 2020;35:55-74. DOI PubMed PMC
7. Vital A, Lepreux S, Vital C. Peripheral neuropathy and parkinsonism: a large clinical and pathogenic spectrum. *J Peripher Nerv Syst* 2014;19:333-42. DOI PubMed
8. Hernandez Fustes OJ, Hernandez Fustes OJ. Sensory neuropathy in Parkinson disease: electrodiagnostic evaluation. *Neurodiagn J* 2020;60:177-84. DOI PubMed
9. Müller T, Renger K, Kuhn W. Levodopa-associated increase of homocysteine levels and sural axonal neurodegeneration. *Arch Neurol* 2004;61:657-60. DOI PubMed
10. Toth C, Breithaupt K, Ge S, et al. Levodopa, methylmalonic acid, and neuropathy in idiopathic Parkinson disease. *Ann Neurol* 2010;68:28-36. DOI PubMed
11. Zis P, Grünewald RA, Chaudhuri RK, Hadjivassiliou M. Peripheral neuropathy in idiopathic Parkinson's disease: a systematic review. *J Neurol Sci* 2017;378:204-9. DOI PubMed
12. Manca D, Cossu G, Murgia D, et al. Reversible encephalopathy and axonal neuropathy in Parkinson's disease during duodopa therapy. *Mov Disord* 2009;24:2293-4. DOI PubMed
13. Paul DA, Qureshi ARM, Rana AQ. Peripheral neuropathy in Parkinson's disease. *Neurol Sci* 2020;41:2691-701. DOI PubMed
14. Lee JJ, Baik JS. Peripheral neuropathy in de novo patients with Parkinson's disease. *Yonsei Med J* 2020;61:1050-3. DOI PubMed PMC
15. Themistocleous AC, Ramirez JD, Serra J, Bennett DL. The clinical approach to small fibre neuropathy and painful channelopathy. *Pract Neurol* 2014;14:368-79. DOI PubMed PMC
16. Cossu G, Melis M. The peripheral nerve involvement in Parkinson disease: a multifaceted phenomenon. *Parkinsonism Relat Disord* 2016;25:17-20. DOI PubMed
17. Ferreira N, Gonçalves NP, Jan A, et al. Trans-synaptic spreading of alpha-synuclein pathology through sensory afferents leads to sensory nerve degeneration and neuropathic pain. *Acta Neuropathol Commun* 2021;9:31. DOI PubMed PMC
18. La Vitola P, Balducci C, Baroni M, et al. Peripheral inflammation exacerbates α-synuclein toxicity and neuropathology in Parkinson's models. *Neuropathol Appl Neurobiol* 2021;47:43-60. DOI PubMed
19. Merola A, Rosso M, Romagnolo A, et al. Peripheral neuropathy as marker of severe Parkinson's disease phenotype. *Mov Disord* 2017;32:1256-8. DOI PubMed
20. Doherty KM, van de Warrenburg BP, Peralta MC, et al. Postural deformities in Parkinson's disease. *Lancet Neurol* 2011;10:538-49. DOI PubMed
21. Ali F, Matsumoto JY, Hassan A. Camptocormia: etiology, diagnosis, and treatment response. *Neurol Clin Pract* 2018;8:240-8. DOI PubMed PMC
22. Ashour R, Tintner R, Jankovic J. Striatal deformities of the hand and foot in Parkinson's disease. *Lancet Neurol* 2005;4:423-31. DOI PubMed
23. Barra J, Marquer A, Joassin R, et al. Humans use internal models to construct and update a sense of verticality. *Brain* 2010;133:3552-63. DOI PubMed
24. Pandey S, Kumar H. Assessment of striatal & postural deformities in patients with Parkinson's disease. *Indian J Med Res* 2016;144:682-8. DOI PubMed PMC
25. Srivanitchapoom P, Hallett M. Camptocormia in Parkinson's disease: definition, epidemiology, pathogenesis and treatment modalities.

J Neurol Neurosurg Psychiatry 2016;87:75-85. DOI PubMed PMC
26. Ruttiman R, Eltorai AEM, Daniels AH. Etiology and management of spinal deformity in patients with Parkinson's disease. *Int J Spine Surg* 2018;12:15-21. DOI PubMed PMC
27. Margraf NG, Wrede A, Rohr A, et al. Camptocormia in idiopathic Parkinson's disease: a focal myopathy of the paravertebral muscles. *Mov Disord* 2010;25:542-51. DOI PubMed
28. Tatu L, Bogousslavsky J. Camptocormia: new signs in an old syndrome. *Front Neurol Neurosci* 2018;42:87-95. DOI PubMed
29. Margraf NG, Wrede A, Deuschl G, Schulz-Schaeffer WJ. Pathophysiological concepts and treatment of camptocormia. *J Parkinsons Dis* 2016;6:485-501. DOI PubMed PMC
30. Wijemanne S, Jimenez-Shahed J. Improvement in dystonic camptocormia following botulinum toxin injection to the external oblique muscle. *Parkinsonism Relat Disord* 2014;20:1106-7. DOI PubMed
31. Jocson A, Lew M. Use of botulinum toxin in Parkinson's disease. *Parkinsonism Relat Disord* 2019;59:57-64. DOI PubMed
32. Bertram KL, Stirpe P, Colosimo C. Treatment of camptocormia with botulinum toxin. *Toxicon* 2015;107:148-53. DOI PubMed
33. Graham JG, Oppenheimer DR. Orthostatic hypotension and nicotine sensitivity in a case of multiple system atrophy. *J Neurol Neurosurg Psychiatry* 1969;32:28-34. DOI PubMed PMC
34. Cao Z, Wu Y, Liu G, et al. Differential diagnosis of multiple system atrophy-Parkinsonism and Parkinson's disease using α-synuclein and external anal sphincter electromyography. *Front Neurol* 2020;11:1043. DOI PubMed PMC
35. Linder J, Libelius R, Nordh E, Holmberg B, Stenlund H, Forsgren L. Anal sphincter electromyography in patients with newly diagnosed idiopathic parkinsonism. *Acta Neurol Scand* 2012;126:248-55. DOI PubMed
36. Vodusek DB. Sphincter EMG and differential diagnosis of multiple system atrophy. *Mov Disord* 2001;16:600-7. DOI PubMed
37. Huang HJ, Zhu XY, Wang X, et al. The bulbocavernosus reflex in the differential diagnosis of multiple system atrophy with predominant Parkinsonism and Parkinson's disease. *Front Neurol* 2017;8:697. DOI PubMed PMC
38. Papagiannis GI, Triantafyllou AI, Roumpelakis IM, et al. Methodology of surface electromyography in gait analysis: review of the literature. *J Med Eng Technol* 2019;43:59-65. DOI PubMed
39. Chowdhury RH, Reaz MB, Ali MA, Bakar AA, Chellappan K, Chang TG. Surface electromyography signal processing and classification techniques. *Sensors (Basel)* 2013;13:12431-66. DOI PubMed PMC
40. Rissanen SM, Koivu M, Hartikainen P, Pekkonen E. Ambulatory surface electromyography with accelerometry for evaluating daily motor fluctuations in Parkinson's disease. *Clin Neurophysiol* 2021;132:469-79. DOI PubMed
41. Warabi T, Furuyama H, Sugai E, Kato M, Yanagisawa N. Gait bradykinesia in Parkinson's disease: a change in the motor program which controls the synergy of gait. *Exp Brain Res* 2018;236:43-57. DOI PubMed
42. Baradaran N, Tan SN, Liu A, et al. Parkinson's disease rigidity: relation to brain connectivity and motor performance. *Front Neurol* 2013;4:67. DOI PubMed PMC
43. Volpe D, Spolaor F, Sawacha Z, et al. Muscular activation changes in lower limbs after underwater gait training in Parkinson's disease: a surface emg pilot study. *Gait Posture* 2020;80:185-91. DOI PubMed
44. Islam A, Alcock L, Nazarpour K, Rochester L, Pantall A. Effect of Parkinson's disease and two therapeutic interventions on muscle activity during walking: a systematic review. *NPJ Parkinsons Dis* 2020;6:22. DOI PubMed PMC
45. Dietz V, Zijlstra W, Prokop T, Berger W. Leg muscle activation during gait in Parkinson's disease: adaptation and interlimb coordination. *Electroencephalogr Clin Neurophysiol* 1995;97:408-15. DOI PubMed
46. Albani G, Sandrini G, Künig G, et al. Differences in the EMG pattern of leg muscle activation during locomotion in Parkinson's disease. *Funct Neurol* 2003;18:165-70. PubMed
47. Miller RA, Thaut MH, Mcintosh GC, Rice RR. Components of EMG symmetry and variability in parkinsonian and healthy elderly gait. *Electroencephalogr Clin Neurophysiol* 1996;101:1-7. DOI PubMed
48. Francis CA, Lenz AL, Lenhart RL, Thelen DG. The modulation of forward propulsion, vertical support, and center of pressure by the plantarflexors during human walking. *Gait Posture* 2013;38:993-7. DOI PubMed PMC
49. Keloth SM, Arjunan SP, Raghav S, Kumar DK. Muscle activation strategies of people with early-stage Parkinson's during walking. *J Neuroeng Rehabil* 2021;18:133. DOI PubMed PMC
50. Bailey CA, Corona F, Murgia M, Pili R, Pau M, Côté JN. Electromyographical gait characteristics in Parkinson's disease: effects of combined physical therapy and rhythmic auditory stimulation. *Front Neurol* 2018;9:211. DOI PubMed PMC
51. Lang KC, Hackney ME, Ting LH, McKay JL. Antagonist muscle activity during reactive balance responses is elevated in Parkinson's disease and in balance impairment. *PLoS One* 2019;14:e0211137. DOI PubMed PMC
52. Kugler P, Jaremenko C, Schlachetzki J, Winkler J, Klucken J, Eskofier B. Automatic recognition of Parkinson's disease using surface electromyography during standardized gait tests. *Annu Int Conf IEEE Eng Med Biol Soc* 2013;2013:5781-4. DOI PubMed
53. Lamontagne A, Richards CL, Malouin F. Coactivation during gait as an adaptive behavior after stroke. *J Electromyogr Kinesiol* 2000;10:407-15. DOI PubMed
54. Kluger BM, Herlofson K, Chou KL, et al. Parkinson's disease-related fatigue: a case definition and recommendations for clinical research. *Mov Disord* 2016;31:625-31. DOI PubMed PMC
55. Prell T, Witte OW, Grosskreutz J. Biomarkers for dementia, fatigue, and depression in Parkinson's disease. *Front Neurol* 2019;10:195. DOI PubMed PMC
56. Schapira AHV, Chaudhuri KR, Jenner P. Non-motor features of Parkinson disease. *Nat Rev Neurosci* 2017;18:435-50. DOI PubMed
57. Lazcano-Ocampo C, Wan YM, van Wamelen DJ, et al. Identifying and responding to fatigue and apathy in Parkinson's disease: a

review of current practice. *Expert Rev Neurother* 2020;20:477-95. DOI PubMed

58. Nassif DV, Pereira JS. Fatigue in Parkinson's disease: concepts and clinical approach. *Psychogeriatrics* 2018;18:143-50. DOI PubMed
59. Siciliano M, Trojano L, Santangelo G, De Micco R, Tedeschi G, Tessitore A. Fatigue in Parkinson's disease: a systematic review and meta-analysis. *Mov Disord* 2018;33:1712-23. DOI PubMed
60. Roland KP, Jones GR, Jakobi JM. Daily electromyography in females with Parkinson's disease: a potential indicator of frailty. *Arch Gerontol Geriatr* 2014;58:80-7. DOI PubMed
61. Fundarò C, Gazzoni M, Pinna GD, Dallocchio C, Rainoldi A, Casale R. Is fatigue a muscular phenomenon in Parkinson's disease? *Eur J Phys Rehabil Med* 2021;57:691-700. DOI PubMed
62. Vescio B, Quattrone A, Nisticò R, Crasà M, Quattrone A. Wearable devices for assessment of tremor. *Front Neurol* 2021;12:680011. DOI PubMed PMC
63. Bhatia KP, Bain P, Bajaj N, et al; Tremor Task Force of the International Parkinson and Movement Disorder Society. Consensus statement on the classification of tremors. from the task force on tremor of the International Parkinson and Movement Disorder Society. *Mov Disord* 2018;33:75-87. DOI PubMed PMC
64. Chen KS, Chen R. Principles of electrophysiological assessments for movement disorders. *J Mov Disord* 2020;13:27-38. DOI PubMed PMC
65. Dideriksen JL, Gallego JA, Holobar A, Rocon E, Pons JL, Farina D. One central oscillatory drive is compatible with experimental motor unit behaviour in essential and Parkinsonian tremor. *J Neural Eng* 2015;12:046019. DOI PubMed
66. Lorenz D, Poremba C, Papengut F, Schreiber S, Deuschl G. The psychosocial burden of essential tremor in an outpatient- and a community-based cohort. *Eur J Neurol* 2011;18:972-9. DOI PubMed
67. Papengut F, Raethjen J, Binder A, Deuschl G. Rest tremor suppression may separate essential from parkinsonian rest tremor. *Parkinsonism Relat Disord* 2013;19:693-7. DOI PubMed
68. Armstrong MJ, Litvan I, Lang AE, et al. Criteria for the diagnosis of corticobasal degeneration. *Neurology* 2013;80:496-503. DOI PubMed PMC
69. Shaikh AG. Tremor analysis separates Parkinson's disease and dopamine receptor blockers induced parkinsonism. *Neurol Sci* 2017;38:855-63. DOI PubMed
70. Flood MW, Jensen BR, Malling AS, Lowery MM. Increased EMG intermuscular coherence and reduced signal complexity in Parkinson's disease. *Clin Neurophysiol* 2019;130:259-69. DOI PubMed
71. Laine CM, Valero-Cuevas FJ. Parkinson's disease exhibits amplified intermuscular coherence during dynamic voluntary action. *Front Neurol* 2020;11:204. DOI PubMed PMC
72. Gómez A, Gómez P, Palacios D, et al. A neuromotor to acoustical jaw-tongue projection model with application in Parkinson's disease hypokinetic dysarthria. *Front Hum Neurosci* 2021;15:622825. DOI PubMed PMC
73. Chu SY, Barlow SM, Lee J, Wang J. Polar-phase indices of perioral muscle reciprocity during syllable production in Parkinson's disease. *Int J Speech Lang Pathol* 2017;19:616-27. DOI PubMed
74. Mes M, Janik P, Zalewska E, Gawel M. Motor neurons loss in Parkinson disease: an electrophysiological study (MUNE). *J Electromyogr Kinesiol* 2021;61:102606. DOI PubMed
75. Barghi E, Gladden M. Motor unit number estimation in normal and parkinsonism model of medial gastrocnemius muscle in rats. *Int J Mol Cell Med* 2013;2:72-9. PubMed PMC
76. Caviness J, Smith B, Clarke Stevens J, et al. Motor unit number estimates in idiopathic Parkinson's disease. *Parkinsonism Relat Disord* 2002;8:161-4. DOI PubMed

AUTHOR INSTRUCTIONS

1. Submission Overview

Before you decide to publish with *Ageing and Neurodegenerative Diseases* (*AND*), please read the following items carefully and make sure that you are well aware of Editorial Policies and the following requirements.

1.1 Topic Suitability

The topic of the manuscript must fit the scope of the journal. Please refer to Aims and Scope for more information.

1.2 Open Access and Copyright

The journal adopts Gold Open Access publishing model and distributes content under the Creative Commons Attribution 4.0 International License. Copyright is retained by authors. Please make sure that you are well aware of these policies.

1.3 Publication Fees

AND is an open access journal. When a paper is accepted for publication, authors are required to pay Article Processing Charges (APCs) to cover its editorial and production costs. The APC for each submission is $600. There are no additional charges based on color, length, figures, or other elements. For more details, please refer to OAE Publication Fees.

1.4 Language Editing

All submissions are required to be presented clearly and cohesively in good English. Authors whose first language is not English are advised to have their manuscripts checked or edited by a native English speaker before submission to ensure the high quality of expression. A well-organized manuscript in good English would make the peer review even the whole editorial handling more smoothly and efficiently.

If needed, authors are recommended to consider the language editing services provided by Charlesworth to ensure that the manuscript is written in correct scientific English before submission. Authors who publish with OAE journals enjoy a special discount for the services of Charlesworth via the following two ways.

Submit your manuscripts directly at http://www.charlesworthauthorservices.com/~OAE;

Open the link http://www.charlesworthauthorservices.com/, and enter Promotion Code “OAE” when you submit.

1.5 Work Funded by the National Institutes of Health

If an accepted manuscript was funded by National Institutes of Health (NIH), the authors may inform Editors of the NIH funding number. The Editors are able to deposit the paper to the NIH Manuscript Submission System on behalf of the authors.

2. Submission Preparation

2.1 Cover Letter

A cover letter is required to be submitted accompanying each manuscript. It should be concise and explain why the study is significant, why it fits the scope of the journal, and why it would be attractive to readers, etc.

Here is a guideline of a cover letter for authors’ consideration:

In the first paragraph: include the title and type (e.g., Original Article, Review, Case Report, etc.) of the manuscript, a brief on the background of the study, the question the author sought out to answer and why;

In the second paragraph: concisely explain what was done, the main findings and why they are significant;

In the third paragraph: indicate why the manuscript fits the Aims and Scope of the journal, and why it would be attractive to readers;

In the fourth paragraph: confirm that the manuscript has not been published elsewhere and not under consideration of any other journal. All authors have approved the manuscript and agreed on its submission to the journal. Journal’s specific requirements have been met if any.

If the manuscript is contributed to a Special Issue, please also mention it in the cover letter.

If the manuscript was presented partly or entirely in a conference, the author should clearly state the background information of the event, including the conference name, time and place in the cover letter.

2.2 Types of Manuscripts

There is no restriction on the length of manuscripts, number of figures, tables and references, provided that the manuscript is concise and comprehensive. The journal publishes Original Article, Review, Meta-Analysis, Case Report, Commentary, *etc.* For more details about paper type, please refer to the following table.

Manuscript Type	Definition	Abstract	Keywords	Main Text Structure
Original Article	An Original Article describes detailed results from novel research. All findings are extensively discussed.	Structured abstract including Aim, Methods, Results and Conclusion. No more than 250 words.	3-8 keywords	The main content should include four sections: Introduction, Methods, Results and Discussion.
Review	A Review paper summarizes the literature on previous studies. It usually does not present any new information on a subject.	Unstructured abstract. No more than 250 words.	3-8 keywords	The main text may consist of several sections with unfixed section titles. We suggest that the author includes an "Introduction" section at the beginning, several sections with unfixed titles in the middle part, and a "Conclusion" section in the end.
Case Report	A Case Report details symptoms, signs, diagnosis, treatment, and follows up an individual patient. The goal of a Case Report is to make other researchers aware of the possibility that a specific phenomenon might occur.	Unstructured abstract. No more than 150 words.	3-8 keywords	The main text consists of three sections with fixed section titles: Introduction, Case Report, and Discussion.
Meta-Analysis	A Meta-Analysis is a statistical analysis combining the results of multiple scientific studies. It is often an overview of clinical trials.	Structured abstract including Aim, Methods, Results and Conclusion. No more than 250 words.	3-8 keywords	The main content should include four sections: Introduction, Methods, Results and Discussion.
Systematic Review	A Systematic Review collects and critically analyzes multiple research studies, using methods selected before one or more research questions are formulated, and then finding and analyzing related studies and answering those questions in a structured methodology.	Structured abstract including Aim, Methods, Results and Conclusion. No more than 250 words.	3-8 keywords	The main content should include four sections: Introduction, Methods, Results and Discussion.
Technical Note	A Technical Note is a short article giving a brief description of a specific development, technique or procedure, or it may describe a modification of an existing technique, procedure or device applied in research.	Unstructured abstract. No more than 250 words.	3-8 keywords	/
Commentary	A Commentary is to provide comments on a newly published article or an alternative viewpoint on a certain topic.	Unstructured abstract. No more than 250 words.	3-8 keywords	/
Editorial	An Editorial is a short article describing news about the journal or opinions of senior editors or the publisher.	None required	None required	/
Letter to Editor	A Letter to Editor is usually an open post-publication review of a paper from its readers, often critical of some aspect of a published paper. Controversial papers often attract numerous Letters to Editor	Unstructured abstract (optional). No more than 250 words.	3-8 keywords (optional)	/
Opinion	An Opinion usually presents personal thoughts, beliefs, or feelings on a topic.	Unstructured abstract (optional). No more than 250 words.	3-8 keywords	/
Perspective	A Perspective provides personal points of view on the state-of-the-art of a specific area of knowledge and its future prospects. Links to areas of intense current research focus can also be made. The emphasis should be on a personal assessment rather than a comprehensive, critical review. However, comments should be put into the context of existing literature. Perspectives are usually invited by the Editors.	Unstructured abstract. No more than 150 words.	3-8 keywords	/

Clinical Observation	Clinical observation refers to records of the effects of treatment on hospitalized patients. It details symptoms, diagnosis and treatment of the disease to be reported. The characteristics of clinical reports include new or rare, complex adverse reactions, confusing symptoms or signs, examples of new theories, etc.	Unstructured abstract. No more than 250 words.	3-8 keywords	The main content should include four sections: Introduction, Methods, Results and Discussion.

2.3 Manuscript Structure

2.3.1 Front Matter

2.3.1.1 Title

The title of the manuscript should be concise, specific and relevant, with no more than 16 words if possible. When gene or protein names are included, the abbreviated name rather than full name should be used.

2.3.1.2 Authors and Affiliations

Authors' full names should be listed. The initials of middle names can be provided. Institutional addresses and email addresses for all authors should be listed. At least one author should be designated as corresponding author. In addition, corresponding authors are suggested to provide their Open Researcher and Contributor ID upon submission. Please note that any change to authorship is not allowed after manuscript acceptance.

2.3.1.3 Abstract

The abstract should be a single paragraph with word limitation and specific structure requirements (for more details please refer to Types of Manuscripts). It usually describes the main objective(s) of the study, explains how the study was done, including any model organisms used, without methodological detail, and summarizes the most important results and their significance. The abstract must be an objective representation of the study: it is not allowed to contain results which are not presented and substantiated in the manuscript or exaggerate the main conclusions. Citations should not be included in the abstract.

2.3.1.4 Keywords

Three to eight keywords should be provided, which are specific to the article, yet reasonably common within the subject discipline.

2.3.2 Main Text

Manuscripts of different types are structured with different sections of content. Please refer to Types of Manuscripts to make sure which sections should be included in the manuscripts.

2.3.2.1 Introduction

The introduction should contain background that puts the manuscript into context, allow readers to understand why the study is important, include a brief review of key literature, and conclude with a brief statement of the overall aim of the work and a comment about whether the aim was achieved. Relevant controversies or disagreements in the field should be introduced as well.

2.3.2.2 Methods

Methods should contain sufficient details to allow others to fully replicate the study. New methods and protocols should be described in detail while well-established methods can be briefly described or appropriately cited. Experimental participants selected, the drugs and chemicals used, the statistical methods taken, and the computer software used should be identified precisely. Statistical terms, abbreviations, and all symbols used should be defined clearly. Protocol documents for clinical trials, observational studies, and other non-laboratory investigations may be uploaded as supplementary materials.

2.3.2.3 Results

This section contains the findings of the study. Results of statistical analysis should also be included either as text or as tables or figures if appropriate. Authors should emphasize and summarize only the most important observations. Data on all primary and secondary outcomes identified in the section Methods should also be provided. Extra or supplementary materials and technical details can be placed in supplementary documents.

2.3.2.4 Discussion

This section should discuss the implications of the findings in context of existing research and highlight limitations of the study. Future research directions may also be mentioned.

2.3.2.5 Conclusion

It should state clearly the main conclusions and include the explanation of their relevance or importance to the field.

2.3.3 Back Matter

2.3.3.1 Acknowledgments

Anyone who contributed towards the article but does not meet the criteria for authorship, including those who provided professional writing services or materials, should be acknowledged. Authors should obtain permission to acknowledge from all those mentioned in the Acknowledgments section. This section is not added if the author does not have anyone to acknowledge.

2.3.3.2 Authors' Contributions

Each author is expected to have made substantial contributions to the conception or design of the work, or the acquisition, analysis, or interpretation of data, or the creation of new software used in the work, or have drafted the work or substantively revised it.

Please use Surname and Initial of Forename to refer to an author's contribution. For example: made substantial contributions to conception and design of the study and performed data analysis and interpretation: Salas H, Castaneda WV; performed data acquisition, as well as provided administrative, technical, and material support: Castillo N, Young V.

If an article is single-authored, please include "The author contributed solely to the article." in this section.

2.3.3.3 Availability of Data and Materials

In order to maintain the integrity, transparency and reproducibility of research records, authors should include this section in their manuscripts, detailing where the data supporting their findings can be found. Data can be deposited into data repositories or published as supplementary information in the journal. Authors who cannot share their data should state that the data will not be shared and explain it. If a manuscript does not involve such issue, please state "Not applicable." in this section.

2.3.3.4 Financial Support and Sponsorship

All sources of funding for the study reported should be declared. The role of the funding body in the experiment design, collection, analysis and interpretation of data, and writing of the manuscript should be declared. Any relevant grant numbers and the link of funder's website should be provided if any. If the study is not involved with this issue, state "None." in this section.

2.3.3.5 Conflicts of Interest

Authors must declare any potential conflicts of interest that may be perceived as inappropriately influencing the representation or interpretation of reported research results. If there are no conflicts of interest, please state "All authors declared that there are no conflicts of interest." in this section. Some authors may be bound by confidentiality agreements. In such cases, in place of itemized disclosures, we will require authors to state "All authors declare that they are bound by confidentiality agreements that prevent them from disclosing their conflicts of interest in this work.". If authors are unsure whether conflicts of interest exist, please refer to the "Conflicts of Interest" of *AND* Editorial Policies for a full explanation.

2.3.3.6 Ethical Approval and Consent to Participate

Research involving human subjects, human material or human data must be performed in accordance with the Declaration of Helsinki and approved by an appropriate ethics committee. An informed consent to participate in the study should also be obtained from participants, or their parents or legal guardians for children under 16. A statement detailing the name of the ethics committee (including the reference number where appropriate) and the informed consent obtained must appear in the manuscripts reporting such research.

Studies involving animals and cell lines must include a statement on ethical approval. More information is available at Editorial Policies.

If the manuscript does not involve such issue, please state "Not applicable." in this section.

2.3.3.7 Consent for Publication

Manuscripts containing individual details, images or videos, must obtain consent for publication from that person, or in the case of children, their parents or legal guardians. If the person has died, consent for publication must be obtained from the next of kin of the participant. Manuscripts must include a statement that a written informed consent for publication was obtained. Authors do not have to submit such content accompanying the manuscript. However, these documents must be available if requested. If the manuscript does not involve this issue, state "Not applicable." in this section.

2.3.3.8 Copyright

Authors retain copyright of their works through a Creative Commons Attribution 4.0 International License that clearly states how readers can copy, distribute, and use their attributed research, free of charge. A declaration "© The Author(s) 2022." will be added to each article. Authors are required to sign License to Publish before formal publication.

2.3.3.9 References

References should be numbered in order of appearance at the end of manuscripts. In the text, reference numbers should be placed in square brackets and the corresponding references are cited thereafter. If the number of authors is less than or equal

to six, we require to list all authors' names. If the number of authors is more than six, only the first three authors' names are required to be listed in the references, other authors' names should be omitted and replaced with "et al.". Abbreviations of the journals should be provided on the basis of Index Medicus. Information from manuscripts accepted but not published should be cited in the text as "Unpublished material" with written permission from the source.
References should be described as follows, depending on the types of works:

Types	Examples
Journal articles by individual authors	Weaver DL, Ashikaga T, Krag DN, et al. Effect of occult metastases on survival in node-negative breast cancer. *N Engl J Med* 2011;364:412-21. [PMID: 21247310 DOI: 10.1056/NEJMoa1008108]
Organization as author	Diabetes Prevention Program Research Group. Hypertension, insulin, and proinsulin in participants with impaired glucose tolerance. *Hypertension* 2002;40:679-86. [PMID: 12411462]
Both personal authors and organization as author	Vallancien G, Emberton M, Harving N, van Moorselaar RJ; Alf-One Study Group. Sexual dysfunction in 1,274 European men suffering from lower urinary tract symptoms. *J Urol* 2003;169:2257-61. [PMID: 12771764 DOI: 10.1097/01.ju.0000067940.76090.73]
Journal articles not in English	Zhang X, Xiong H, Ji TY, Zhang YH, Wang Y. Case report of anti-N-methyl-D-aspartate receptor encephalitis in child. *J Appl Clin Pediatr* 2012;27:1903-7. (in Chinese)
Journal articles ahead of print	Odibo AO. Falling stillbirth and neonatal mortality rates in twin gestation: not a reason for complacency. BJOG 2018; Epub ahead of print [PMID: 30461178 DOI: 10.1111/1471-0528.15541]
Books	Sherlock S, Dooley J. Diseases of the liver and billiary system. 9th ed. Oxford: Blackwell Sci Pub; 1993. pp. 258-96.
Book chapters	Meltzer PS, Kallioniemi A, Trent JM. Chromosome alterations in human solid tumors. In: Vogelstein B, Kinzler KW, editors. The genetic basis of human cancer. New York: McGraw-Hill; 2002. pp. 93-113.
Online resource	FDA News Release. FDA approval brings first gene therapy to the United States. Available from: https://www.fda.gov/NewsEvents/Newsroom/PressAnnouncements/ucm574058.htm. [Last accessed on 30 Oct 2017]
Conference proceedings	Harnden P, Joffe JK, Jones WG, editors. Germ cell tumours V. Proceedings of the 5th Germ Cell Tumour Conference; 2001 Sep 13-15; Leeds, UK. New York: Springer; 2002.
Conference paper	Christensen S, Oppacher F. An analysis of Koza's computational effort statistic for genetic programming. In: Foster JA, Lutton E, Miller J, Ryan C, Tettamanzi AG, editors. Genetic programming. EuroGP 2002: Proceedings of the 5th European Conference on Genetic Programming; 2002 Apr 3-5; Kinsdale, Ireland. Berlin: Springer; 2002. pp. 182-91.
Unpublished material	Tian D, Araki H, Stahl E, Bergelson J, Kreitman M. Signature of balancing selection in Arabidopsis. *Proc Natl Acad Sci U S A*. Forthcoming 2002.

For other types of references, please refer to U.S. National Library of Medicine.
The journal also recommends that authors prepare references with a bibliography software package, such as EndNote to avoid typing mistakes and duplicated references.

2.3.3.10 Supplementary Materials

Additional data and information can be uploaded as Supplementary Materials to accompany the manuscripts. The supplementary materials will also be available to the referees as part of the peer-review process. Any file format is acceptable, such as data sheet (word, excel, csv, cdx, fasta, pdf or zip files), presentation (powerpoint, pdf or zip files), image (cdx, eps, jpeg, pdf, png or tiff), table (word, excel, csv or pdf), audio (mp3, wav or wma) or video (avi, divx, flv, mov, mp4, mpeg, mpg or wmv). All information should be clearly presented. Supplementary materials should be cited in the main text in numeric order (e.g., Supplementary Figure 1, Supplementary Figure 2, Supplementary Table 1, Supplementary Table 2, etc.). The style of supplementary figures or tables complies with the same requirements on figures or tables in main text. Videos and audios should be prepared in English and limited to a size of 500 MB.

2.4 Manuscript Format

2.4.1 File Format

Manuscript files can be in DOC and DOCX formats and should not be locked or protected.

2.4.2 Length

There are no restrictions on paper length, number of figures, or amount of supporting documents. Authors are encouraged to present and discuss their findings concisely.

2.4.3 Language

Manuscripts must be written in English.

2.4.4 Multimedia Files

The journal supports manuscripts with multimedia files. The requirements are listed as follows:
Videos or audio files are only acceptable in English. The presentation and introduction should be easy to understand. The

frames should be clear, and the speech speed should be moderate.
A brief overview of the video or audio files should be given in the manuscript text.
The video or audio files should be limited to a size of up to 500 MB.
Please use professional software to produce high-quality video files, to facilitate acceptance and publication along with the submitted article. Upload the videos in mp4, wmv, or rm format (preferably mp4) and audio files in mp3 or wav format.

2.4.5 Figures

Figures should be cited in numeric order (e.g., Figure 1, Figure 2) and placed after the paragraph where it is first cited;
Figures can be submitted in format of tiff, psd, AI or jpeg, with resolution of 300-600 dpi;
Figure caption is placed under the Figure;
Diagrams with describing words (including, flow chart, coordinate diagram, bar chart, line chart, and scatter diagram, *etc.*) should be editable in word, excel or powerpoint format. Non-English information should be avoided;
Labels, numbers, letters, arrows, and symbols in figure should be clear, of uniform size, and contrast with the background;
Symbols, arrows, numbers, or letters used to identify parts of the illustrations must be identified and explained in the legend;
Internal scale (magnification) should be explained and the staining method in photomicrographs should be identified;
All non-standard abbreviations should be explained in the legend;
Permission for use of copyrighted materials from other sources, including re-published, adapted, modified, or partial figures and images from the internet, must be obtained. It is authors' responsibility to acquire the licenses, to follow any citation instruction requested by third-party rights holders, and cover any supplementary charges.

2.4.6 Tables

Tables should be cited in numeric order and placed after the paragraph where it is first cited;
The table caption should be placed above the table and labeled sequentially (e.g., Table 1, Table 2);
Tables should be provided in editable form like DOC or DOCX format (picture is not allowed);
Abbreviations and symbols used in table should be explained in footnote;
Explanatory matter should also be placed in footnotes;
Permission for use of copyrighted materials from other sources, including re-published, adapted, modified, or partial tables from the internet, must be obtained. It is authors' responsibility to acquire the licenses, to follow any citation instruction requested by third-party rights holders, and cover any supplementary charges.

2.4.7 Abbreviations

Abbreviations should be defined upon first appearance in the abstract, main text, and in figure or table captions and used consistently thereafter. Non-standard abbreviations are not allowed unless they appear at least three times in the text. Commonly-used abbreviations, such as DNA, RNA, ATP, *etc*., can be used directly without definition. Abbreviations in titles and keywords should be avoided, except for the ones which are widely used.

2.4.8 Italics

General italic words like *vs*., *et al., etc*., *in vivo*, *in vitro*; *t* test, *F* test, *U* test; related coefficient as *r*, sample number as *n*, and probability as *P*; names of genes; names of bacteria and biology species in Latin.

2.4.9 Units

SI Units should be used. Imperial, US customary and other units should be converted to SI units whenever possible. There is a space between the number and the unit (i.e., 23 mL). Hour, minute, second should be written as h, min, s.

2.4.10 Numbers

Numbers appearing at the beginning of sentences should be expressed in English. When there are two or more numbers in a paragraph, they should be expressed as Arabic numerals; when there is only one number in a paragraph, number < 10 should be expressed in English and number > 10 should be expressed as Arabic numerals. 12345678 should be written as 12,345,678.

2.4.11 Equations

Equations should be editable and not appear in a picture format. Authors are advised to use either the Microsoft Equation Editor or the MathType for display and inline equations.

2.5 Submission Link

Submit an article via https://oaemesas.com/login?JournalId=and.

3. Research and Publication Ethics

3.1 Research Involving Human Subjects

All studies involving human subjects must be in accordance with the Helsinki Declaration and seek approval to conduct the study from an independent local, regional, or national review body (e.g., ethics committee, institutional review board, etc.).

Such approval, including the names of the ethics committee, institutional review board, etc., must be listed in a declaration statement of Ethical Approval and Consent to Participate in the manuscript. If the study is judged exempt from ethics approval, related information (e.g., name of the ethics committee granting the exemption and the reason for the exemption) must be listed. Further documentation on ethics should also be prepared, as Editors may request more detailed information. Manuscripts with suspected ethical problems will be investigated according to COPE Guidelines.

3.1.1 Consent to Participate

For all studies involving human subjects, informed consent to participate in the studies must be obtained from participants, or their parents or legal guardians for children under 16. Statements regarding consent to participate should be included in a declaration statement of Ethical Approval and Consent to Participate in the manuscript. If informed consent is not required, the name of the ethics committee granting the exemption and the reason for the exemption must be listed. If any ethical violation is found at any stage of publication, the issue will be investigated seriously based on COPE Guidelines.

3.1.2 Consent for Publication

All articles published by *AND* are freely available on the Internet. All manuscripts that include individual participants' data in any form (i.e., details, images, videos, etc.) will not be published without Consent for Publication obtained from that person(s), or for children, their parents or legal guardians. If the person has died, Consent for Publication must be obtained from the next of kin. Authors must add a declaration statement of Consent for Publication in the manuscript, specifying written informed consent for publication has been obtained.

3.1.3 Trial Registration

AND requires all authors to register all relevant clinical trials that are reported in manuscripts submitted. *AND* follows the World Health Organization (WHO)'s definition of clinical trials: "A clinical trial is any research study that prospectively assigns human participants or groups of humans to one or more health-related interventions to evaluate the effects on health outcomes. Interventions include but are not restricted to drugs, cells, other biological products, surgical procedures, radiologic procedures, devices, behavioral treatments, process-of-care changes, preventive care, etc.".

In line with International Committee of Medical Journal Editors (ICMJE) recommendation, *AND* requires the registration of clinical trials in a public trial registry at or before the time of first patient enrollment. *AND* accepts publicly accessible registration in any registry that is a primary register of the WHO International Clinical Trials Registry Platform or in ClinicalTrials.gov. The trial registration number should be listed at the end of the Abstract section.

Secondary data analyses of primary (parent) clinical trials should not be registered as a new clinical trial, but rather reference the trial registration number of the primary trial.

Editors of *AND* will consider carefully whether studies failed to register or had an incomplete trial registration. Because of the importance of prospective trial registration, if there is an exception to this policy, trials must be registered and the authors should indicate in the publication when registration was completed and why it was delayed. Editors will publish a statement indicating why an exception was allowed. Please note such exceptions should be rare, and authors failing to prospectively register a trial risk its inadmissibility to *AND*.

Authors who are not sure whether they need trial registration may refer to ICMJE FAQs for further information.

3.2 Research Involving Animals

Experimental research on animals should be approved by an appropriate ethics committee and must comply with institutional, national, or international guidelines. *AND* encourages authors to comply with the AALAS Guidelines, the ARRIVE Guidelines, and/or the ICLAS Guidelines, and obtain prior approval from the relevant ethics committee. Manuscripts must include a statement indicating that the study has been approved by the relevant ethical committee and the whole research process complies with ethical guidelines. If a study is granted an exemption from requiring ethics approval, the name of the ethics committee granting the exemption and the reason(s) for the exemption should be detailed. Editors will take account of animal welfare issues and reserve the right to reject a manuscript, especially if the research involves protocols that are inconsistent with commonly accepted norms of animal research.

3.3 Research Involving Cell Lines

Authors must describe what cell lines are used and their origin so that the research can be reproduced. For established cell lines, the provenance should be stated and references must also be given to either a published paper or to a commercial source. For de novo cell lines derived from human tissue, appropriate approval from an institutional review board or equivalent ethical committee, and consent from the donor or next of kin, should be obtained. Such statements should be listed on the Declaration section of Ethical Approval and Consent to Participate in the manuscript.

Further information is available from the International Cell Line Authentication Committee (ICLAC). *AND* recommends that authors check the NCBI database for misidentification and contamination of human cell lines.

3.4 Research Involving Plants

Experimental research on plants (either cultivated or wild), including collection of plant material, must comply with institutional, national, or international guidelines. Field studies should be conducted in accordance with local legislation, and the manuscript should include a statement specifying the appropriate permissions and/or licenses. *AND* recommends that authors comply with the IUCN Policy Statement on Research Involving Species at Risk of Extinction and the Convention on the Trade in Endangered Species of Wild Fauna and Flora.

For each submitted manuscript, supporting genetic information and origin must be provided for plants that were utilized. For research manuscripts involving rare and non-model plants (other than, e.g., Arabidopsis thaliana, Nicotiana benthamiana, Oriza sativa, or many other typical model plants), voucher specimens must be deposited in a public herbarium or other public collections providing access to deposited materials.

3.5 Publication Ethics Statement

OAE is a member of the Committee on Publication Ethics (COPE). We fully adhere to its Code of Conduct and to its Best Practice Guidelines.

The Editors of *AND* enforce a rigorous peer-review process together with strict ethical policies and standards to guarantee to add high-quality scientific works to the field of scholarly publication. Unfortunately, cases of plagiarism, data falsification, image manipulation, inappropriate authorship credit, and the like, do arise. The Editors of *AND* take such publishing ethics issues very seriously and are trained to proceed in such cases with zero tolerance policy.

Authors wishing to publish their papers in *AND* must abide to the following:
The author(s) must disclose any possibility of a conflict of interest in the paper prior to submission.
The authors should declare that there is no academic misconduct in their manuscript in the cover letter.
Authors should accurately present their research findings and include an objective discussion of the significance of their findings.
Data and methods used in the research need to be presented in sufficient detail in the manuscript so that other researchers can replicate the work.
Authors should provide raw data if referees and the Editors of the journal request.
Simultaneous submission of manuscripts to more than one journal is not tolerated.
Republishing content that is not novel is not tolerated (for example, an English translation of a paper that is already published in another language will not be accepted).
The manuscript should not contain any information that has already been published. If you include already published figures or images, please get the necessary permission from the copyright holder to publish under the CC-BY license.
Plagiarism, data fabrication and image manipulation are not tolerated.
Plagiarism is not acceptable in *AND*.
Plagiarism involves the inclusion of large sections of unaltered or minimally altered text from an existing source without appropriate and unambiguous attribution, and/or an attempt to misattribute original authorship regarding ideas or results, and copying text, images, or data from another source, even from your own publications, without giving credit to the source.

As to reusing the text that is copied from another source, it must be between quotation marks and the source must be cited. If a study's design or the manuscript's structure or language has been inspired by previous studies, these studies must be cited explicitly.

If plagiarism is detected during the peer-review process, the manuscript may be rejected. If plagiarism is detected after publication, we may publish a Correction or retract the paper.

Falsification is manipulating research materials, equipment, or processes, or changing or omitting data or results so that the findings are not accurately represented in the research record.

Image files must not be manipulated or adjusted in any way that could lead to misinterpretation of the information provided by the original image.

Irregular manipulation includes introduction, enhancement, moving, or removing features from the original image; grouping of images that should be presented separately, or modifying the contrast, brightness, or color balance to obscure, eliminate, or enhance some information.

If irregular image manipulation is identified and confirmed during the peer-review process, we will reject the manuscript. If irregular image manipulation is identified and confirmed after publication, we may publish a Retraction or retract the paper.

AND reserves the right to contact the authors' institution(s) to investigate possible publication misconduct if the Editors find conclusive evidence of misconduct before or after publication. OAE has a partnership with iThenticate, which is the most trusted similarity checker. It is used to analyze received manuscripts to avoid plagiarism to the greatest extent possible.

When plagiarism becomes evident after publication, we will retract the original publication or require modifications, depending on the degree of plagiarism, context within the published article, and its impact on the overall integrity of the published study. Journal Editors will act under the relevant COPE Guidelines.

4. Authorship

Authorship credit of *AND* should be solely based on substantial contributions to a published study, as specified in the following four criteria:
1. Substantial contributions to the conception or design of the work, or the acquisition, analysis, or interpretation of data for the work;
2. Drafting the work or revising it critically for important intellectual content;
3. Final approval of the version to be published;
4. Agreement to be accountable for all aspects of the work in ensuring that questions related to the accuracy or integrity of any part of the work are appropriately investigated and resolved.

All those who meet these criteria should be identified as authors. Authors must specify their contributions in the section Authors' Contributions of their manuscripts. Contributors who do not meet all the four criteria (like only involved in acquisition of funding, general supervision of a research group, general administrative support, writing assistance, technical editing, language editing, proofreading, etc.) should be acknowledged in the section of Acknowledgement in the manuscript rather than being listed as authors.

If a large multiple-author group has conducted the work, the group ideally should decide who will be authors before the work starts and confirm authors before submission. All authors of the group named as authors must meet all the four criteria for authorship.

5. Reviewers Exclusions

You are welcome to exclude a limited number of researchers as potential Editors or reviewers of your manuscript. To ensure a fair and rigorous peer review process, we ask that you keep your exclusions to a maximum of three people. If you wish to exclude additional referees, please explain or justify your concerns—this information will be helpful for Editors when deciding whether to honor your request.

6. Editors and Journal Staff as Authors

Editorial independence is extremely important and *AND* does not interfere with editorial decisions. Editorial staff or Editors shall not be involved in the processing their own academic work. Submissions authored by editorial staff/Editors will be assigned to at least two independent outside reviewers. Decisions will be made by other Editorial Board members who do not have conflict of interests with the author. Journal staffs are not involved in the processing of their own work submitted to any OAE journals.

7. Conflict of Interests

AND require authors to declare any possible financial and/or non-financial conflicts of interest at the end of their manuscript and in the cover letter, as well as confirm this point when submitting their manuscript in the submission system. If no conflicts of interest exist, authors need to state "The authors declare no conflicts of interest". We also recognize that some authors may be bound by confidentiality agreements, in which cases authors need to sate "The authors declare that they are bound by confidentiality agreements that prevent them from disclosing their competing interests in this work".

8. Editorial Process

8.1 Initial check

8.1.1 Initial manuscript check

New submissions are initially checked by the Managing Editor from the perspectives of originality, suitability, structure and formatting, conflicts of interest, background of authors, etc. Poorly-prepared manuscripts may be rejected at this stage. If your manuscript does not meet one or more of these requirements, we will return it for further revisions.

8.1.2 Publishing ethics

All manuscripts submitted to *AND* are screened using iThenticate powered by CrossCheck to identify any plagiarized content. Your study must also meet all ethical requirements as outlined in our Editorial Policies. If the manuscript does not pass any of these checks, we may return it to you for further revisions or decline to consider your study for publication.

8.2 Editorial assessment

Once your manuscript has passed the initial manuscript check, it will be assigned to an Assistant Editor, and then the Editor-in-Chief, or an Associate Editor in the case of a conflict of interest, will be notified of the submission and invited to review. Regarding Special Issue paper, after passing the initial check, the manuscript will be successively assigned to an

Assistant Editor, Guest Editor, and then to the Editor-in-Chief, or an Associate Editor in the case of conflict of interest for the Editor-in-Chief to review. The Editor-in-Chief, or the Associate Editor may reject manuscripts that they deem highly unlikely to pass peer review without further consultation. Once your manuscript has passed the editorial assessment, the Assistant Editor will start to organize peer-review.

8.3 Process

AND operates a single-blind review process. The technical quality of the research described in the manuscript is assessed by a minimum of two independent expert reviewers. The Editor-in-Chief is responsible for the final decision regarding acceptance or rejection of the manuscript. For controversial manuscripts, the Editor-in-Chief is responsible for making the final decision.

8.4 Decisions

Your research will be judged on technical soundness only, not on its perceived impact as judged by Editors or referees. There are three possible decisions: Accept (your study satisfies all publication criteria), Invitation to Revise (more work is required to satisfy all criteria), and Reject (your study fails to satisfy key criteria and it is highly unlikely that further work can address its shortcomings).

9. Contact Us

Journal Contact

Ageing and Neurodegenerative Diseases Editorial Office
Suite 1504, Plaza A, Xi'an National Digital Publishing Base, No. 996 Tiangu 7th Road, Gaoxin District, Xi'an 710077, Shaanxi, China.
Tel: +86 (0)29 8954 0089

Monica Wang
Managing Editor
editorialoffice@ageneudisjournal.com

www.oaepublish.com

Ageing and Neurodegenerative Diseases
(*AND*)
Los Angeles Office
245 E Main Street ste122, Alhambra,
CA 91801, USA
E-mail: editorialoffice@ageneudisjournal.com
Website: www.ageneudisjournal.com